Characterizing Dynamic Protein Interactions That Mediate mTOR Signaling in Shank3-deficient Neurons during Homeostatic Scaling

Devin Taylor Wehle

A dissertation submitted in partial fulfillment of the requirements for the degree of

Doctor of Philosophy

University of Washington

2024

Reading Committee:

Stephen E.P. Smith, Chair

Kathleen Millen

Franck Kalume

Program Authorized to Offer Degree:

Neuroscience

University of Washington

Abstract

Characterizing Dynamic Protein Interactions That Mediate mTOR Signaling in Shank3-deficient Neurons during Homeostatic Scaling

Devin Taylor Wehle

Chair of the Supervisory Committee:

Stephen E.P. Smith

Department of Pediatrics

The mTOR signaling cascade is a central signaling pathway that has been implicated in autism spectrum disorder (ASD). We have developed a Quantitative Multiplex Immunoprecipitation (QMI) panel to analyze changes in the mTOR protein interaction network (PIN). We observed extensive PIN one hour after the addition of fresh media despite phosphorylation changes occurring after five minutes. Various mTOR/ERK inhibitors acted on subsets of the PIN, referred to as modules, that responded differently to each inhibitor. Homeostatic scaling, induced by TTX or BIC treatment in cultured neurons, caused dissociations in different combinations of modules depending on scaling direction. In Shank3B$^{-/-}$ neurons, the scaling-responsive modules were pre-active at baseline and their response range was warped during scaling. Shank3B$^{-/-}$ neurons also produced an exaggerated response to treatment with the mTOR inhibitor Rapalink-1. These data provide the basis for understanding the relationship between mTOR signaling, synaptic scaling, and autism spectrum disorder.

Acknowledgements

I must first express my gratitude to my advisor, Dr. Stephen E.P Smith, for his guidance and mentorship during my graduate training. He has been an enthusiastic, patient, and insightful advisor who has encouraged and steered me through countless challenges. I truly appreciate his dedication to my education and development as an independent scientist. I am thankful that I have had the opportunity to train under his mentorship.

I would also like to thank my committee members: Dr. Sharona Gordon, Dr. Smita Yadav, Dr. Kathleen Millen, and Dr. Franck Kalume. I would also like to thank my former committee members Dr. Bertil Hille and Dr. Raphe Bernier. They have all provided invaluable scientific insight as well as personal advice that has helped me complete this work. I am truly grateful for the effort they put into my training.

I also want to thank my colleagues in the Smith lab, both former and current. They have also been incredibly supportive during my time there and many have continued to provide support even after leaving. I am truly grateful to have been able to work with such an intelligent and kind group of people.

Finally, I would like to thank my mother Colette and my brother Dylan. I cannot imagine getting through this without their support. My mother has always been incredibly supportive, and my brother is who inspired me to pursue neuroscience. I am truly grateful for them and all they have done.

Table of Contents

Figures and Tables

Chapter 1:

ASD-linked genes are components of phase-separated synaptic protein interaction networks

ASD-risk genes converge on the synaptic protein interaction network

Autism spectrum disorder (ASD) is a complex neurodevelopmental disorder characterized by deficits in various social behaviors that include compromised social interactions, reduced verbal communication, stereotyped behaviors, and restricted interests (American Psychiatric Association, 2013). Genetically, ASD is a heterogenous group of disorders that converge upon a shared set of behavioral phenotypes. Large scale sequencing studies have identified over one hundred ASD-associated genes, and the most frequently disrupted genes are those involved in either gene expression or neuronal signaling (Heavner and Smith, 2020; Satterstrom et al., 2020). Additionally, ASD risk genes enriched for synaptic functions are more likely to encode proteins that interact with one another and form a protein-protein interaction network (Cirnigliaro et al., 2023). The fact that ASD risk genes are interconnected at the synapse indicates that disruption of the synaptic protein interaction network is a convergent feature of ASD. The most frequently affected genes include SynGAP1, SCN2A, GRIN2B, and Shank3; all of which participate in synaptic signaling or scaffolding (Satterstrom et al., 2020). The postsynaptic scaffolding protein PSD95 and the proteins that interact with it have been identified as a mechanistic hub for ASD (Farahani et al., 2022). Dysfunction in synaptic signaling and synaptic protein assembly are key characteristics in ASD. Determining how different autism-related mutations disrupt the synaptic proteome has been a crucial route of research to achieve this end.

Many ASD-linked mutations in synaptic genes affect their ability to bind to other proteins. Mutations in the C-terminal region of Shank3 affect binding to proteins like Homer and cortactin (Durand et al., 2007). C-terminal mutations in the Shank3 gene

have also been implicated in ASD patients and the loss of the C-terminus is the basis of the Shank3Δ ex21 mouse model (Boccuto et al., 2013; Yang et al., 2012). Many ASD-associated mutations in SynGAP alter its interactions with PSD-95, affecting SynGAP localization (Zeng et al., 2017). Mutations in the C-terminal region of GRIN2B are associated with protein binding and ASD (Hu et al., 2016). ASD mutations congregate around the architecture of the synapse and signaling through the synaptic interaction network. Elucidating how ASD affects the assembly of synaptic protein-protein interactions is important for understanding autism-related disruptions at the synapse.

Protein interaction domains regulate the assembly of protein complexes

When characterizing protein-protein interactions, considerable attention has been given to protein interaction domains (Pawson 1995). Protein interaction domains provide a mechanism for controlling protein localization, post-translational modification, protein conformation, and substrate specificity (Pawson and Nash 2000; Pawson and Nash 2003). Protein interaction domains are foundational in understanding the organization of complex protein assemblies and the synapse protein network. Discussion of protein interaction domains is necessary before reviewing the synaptic proteome and how ASD-related mutations dysregulate its architecture and function. Here we will discuss protein interaction domains common in synaptic proteins, their relevance to ASD, and how they shape the behavior of protein interaction networks.

SH3 Domains

The Src-homology domain 3 (SH3) domain is about sixty amino acids in length and was discovered during the cloning of the Crk oncogene. The domain structure is comprised

of five to eight beta-strands that are arranged into two antiparallel beta-sheets or as a beta-barrel (Kurochkina and Guha, 2012). SH3 domains can be located adjacent to and within intrinsically disordered regions (Arbesu and Pons, 2019). The site that SH3 domains bind to are short proline rich motifs with a PXXP sequence at the center (Ren et al., 1993). Individual SH3 interactions tend to be weak, typically in the 10 μM range, but multiple domains can act cooperatively to strengthen and stabilize an interaction (Yu et al., 1994; Sipeki et al., 2021). It is common for proteins with SH3 binding sites to contain more than one proline rich sequence and stable binding can require the cooperation between multiple binding sites and SH3 domains (Wunderlich et al., 1999).

Cooperativity increases avidity, which refers to the accumulated strength of multiple interactions between two or more partners. Interaction avidity is crucial to the formation and function of protein complexes - like those found between the scaffolding proteins at the post-synaptic density - by regulating the localization, configuration, and concentration of proteins (Erlendsson and Teilum 2021). The cooperative nature of SH3 binding increases an interaction's avidity, stabilizing the resulting protein complex. Additionally, one study revealed that almost half of SH3 domains exhibit non-canonical binding outside of the proline binding site and lacked PXXP motif binding specificity (Teyra et al., 2017). SH3 domains can therefore be multitopic and the multiple possible binding sites increase an SH3 domains' contribution to a protein complexes avidity.

The proteins that contain the SH3 domain are often structural proteins or molecular signaling proteins. SH3 domains are present in tyrosine kinases like Fyn and PI3KR1, both of which are associated with ASD (Rickles et al., 1994; Lombardo et al., 2020; Chen et al., 2014; Stemenkovic et al., 2024). Additionally, several synaptic proteins

contain SH3 domains such as Shank3, SynGAP, and PSD95 (Kursula 2019; Gamche et al., 2020; Sturgill et al., 2009). Mutations near the SH3 domain of Shank3 have been reported in both ASD and schizophrenia patients (Gauthier et al., 2010; Ivashko-Pachima et al., 2022). SynGAP and PSD95 related intellectual disability are also associated with mutations in their SH3 domain (Holder et al., 2019; Shao et al., 2021).

PH Domains

The pleckstrin homology (PH) domain is the eleventh most common domain in the human proteome (Mistry et al., 2011). The structure of the PH domain is described as two perpendicular anti-parallel beta sheets capped on one end by a C-terminal amphipathic helix (Powis et al., 2021). One of the first reported properties of the PH domain is binding to phosphoinositide lipids that are phosphorylated at different inositol rings (PIPs) and this property is present in 49% of PH domains (Singh et al., 2021). These interactions are important in trafficking PH domain proteins to their necessary subcellular locations. Once there, they bind to other PH domain proteins to form a network of signal transduction and cytoskeletal proteins (Lenoir et al., 2015).

SynGAP's N-terminus contains a PH domain that is truncated in some individuals with intellectual disability. (Gamache et al., 2020; Li et al., 2023). The synaptic regulator Kalirin is a Rho-guanosine nucleotide exchange factor that is important for synaptic development and has been implicated in several neurodevelopmental disorders (Parnell et al., 2021). Kalirin contains a PH domain that interacts with GluN2B subunit of the NMDA receptor (Kilary et al., 2011; Paskus et al., 2020). Additionally, the PH domain's role in trafficking and regulating signaling proteins like AKT is critical to the regulation and response of the synapse to stimuli (Chen et al., 2014).

PDZ Domains

The PDZ domain is a ~90 amino acid long motif that occurs an estimated 270 times in the human proteome. (Luck et al., 2012). PDZ domains can form large protein complexes through mediating protein-protein interactions. The typical structure of a PDZ domain is comprised of two alpha helices with six beta sheets between them. Binding specificity is determined by the interaction between the first residue of the αB helix and the second residue of the C-terminal ligand (Songyang et al., 1997). PDZ domain containing proteins often have multiple PDZ domains that facilitate interactions with multiple binding partners at once to create large complexes. This allows proteins like PSD95 and the other MAGUKs at the synapse to organize other proteins for local signaling. Additionally, the ability for PDZ containing proteins to form oligomers with protein interaction domains may increase the avidity between binding partners (Pascoe et al., 2015).

The PDZ domain can mediate protein self-assembly and form long multimers that cluster protein binding partners at specific cell locations like the post-synaptic density (PSD) (Kim and Sheng, 2004). PDZ domain interactions have high off rates and weak affinities, making their interactions very dynamic. Around 40% of PDZ interactions in the mouse proteome exhibited a low affinity, with a dissociation constant between 20-100 μM (Stiffler et al., 2007). However, PDZ domain interactions with an affinity as low as 600 μM have been shown to be physiologically important (Cushing et al., 2008). The multivalent and promiscuous nature of PDZ domains make them central to the dynamic organization of signaling complexes and therefore a therapeutic target for a variety of disorders and diseases (Amacher et al., 2020).

The synaptic protein PSD95 was one of the first three PDZ proteins discovered and is abundant in the glutamatergic synapse (Kennedy 1997). PSD95 contains three PDZ domains and mutations at these sites underlay various instances of intellectual disabilities and ASD (Tumer et al., 1993). The synaptic adapter protein GRIP (glutamate receptor interacting protein) contains seven PDZ domains and is involved in the regulation of AMPARs and synaptic plasticity (Tan et al 2020). The synapse is host to a wide range of PDZ containing proteins: the glutamate receptor subunits NR2A-D, the voltage gated potassium channel Kv1, the synaptic adhesion protein Nueroligin, Kalirin, and Shank proteins are all examples (Kim and Sheng, 2004).

PDZ domains are also present in non-synaptic proteins that are involved in ASD. The phosphatase and tensin homolog (PTEN), a negative regulator of the PI3K/Akt/mTOR pathway and prominent ASD-related gene, contains a PDZ domain at the C-terminal that is crucial for protein-protein interactions (Sotelo et al., 2015). PTEN is recruited to the synapse after activation of the NMDA receptor by its PDZ domain (Jurado et al., 2010). Structured protein interaction domains such as the PDZ, PH, and SH3 domain are crucial for managing the interactions between proteins at the synapse. However, protein-protein interactions do not necessarily involve a structured interaction domain.

Intrinsically Disordered Regions

Traditional analysis of proteins, their functions, and their interactions have focused on their structured regions. However, there is increasing recognition of the importance disordered proteins and regions have in cell physiology. Intrinsically disordered regions (IDRs) are amino acid sequences that form dynamic peptide chains that do not form fixed tertiary structures (van der Lee et al., 2014). Intrinsically disordered regions can

function as dynamic linkers and tunable binding interfaces for multiple, simultaneous interacting proteins and drive subcellular organization. IDRs exist as rapidly shifting confirmations called ensembles and have a wide range of possible lengths, from ten amino acid residues to 1000+ long tails. Around 70% of proteins in the human proteome have at least a single IDR of at least 30 residues (Holehouse and Kragelund., 2024).

IDRs binding occurs through three main mechanisms: coupled folding, fuzzy binding, and fully disordered. Coupled folding/binding refers to when an IDR or its sub-section folds after binding to a partner (Wright and Dyson 2015). This mechanism can involve an IDR with many possible interacting partners, including proteins, DNA, and RNA. Fuzzy binding involves a variety of structurally distinct states that comprise a bound complex. Fuzzy binding may involve static or dynamic disorder. Static disorder refers to the scenario where individual binding events yield a distinct structural state that remains stable for its lifetime (Tompa and Fuxreiter, 2008). Dynamic disorder refers to a handful of distinct states that interconvert. The third mechanism, fully disordered complexes, is driven by a distribution of complementary chemical interactions that undergo fast confirmational rearrangements that produce a dynamic and heterogeneous bound-state ensemble (Schuler et al., 2020). Due to the nature of this mechanism, study of dynamic disorder involves the combination of single molecule Förster resonance energy transfer (smFRET), nuclear magnetic resonance (NMR), and molecular simulations (Milles et al., 2015; Wu et al., 2017; Schuler at al., 2020).

These three mechanisms are not mutually exclusive, and an IDR binding event often involves multiple modes of binding. IDRs can also achieve dynamic binding specificity through the combination of IDRs or the availability of its various ligands. Different

intrinsically disordered proteins (IDPs) have also demonstrated biases in the types of structures and ensembles formed in the cell (Das et al., 2015). These structural biases affect the function of disordered proteins and are sensitive to both the amino acid sequence of the protein and the conditions of the solution such as osmotic pressure and temperature (Moses et al., 2024).

Intrinsically disordered domains are important to interaction hub proteins by enabling a single protein to bind to many proteins or the binding of multiple proteins to a common target (Cortese et al., 2008). Additionally, structured protein domains like SH2, SH3, and the PDZ domain can participate in IDR binding. For example, the PDZ domain of PSD95 binds to Kv channels through the intrinsically disordered domain of the Kv channels C-terminus (Magidovich et al., 2006). IDR's have also been shown to modulate protein-protein interactions by increasing the rate of associations. This is due to IDRs providing weak non-specific interactions that serve to hold partners in an 'encounter complex' until later conditions allow for direct binding (Pontius 1993).

IDRs have been noted to be common in the general proteome and among synaptic proteins. According to the UniProt database, a disordered region is present in Shank1, Shank3, Homer1, PSD95, SynGAP, and SCN2A. The subunits of the NMDA receptor have a long-disordered C-terminal tail that interacts with many synaptic proteins like PSD95, CaMK2, and calmodulin to regulate downstream signaling (Warnet et al., 2021). The prevalence of IDRs among synaptic proteins indicates that the formation of complex protein ensembles is an important feature of synaptic proteins. Disorders that affect the ensembles formed by disordered regions/proteins may cause cascading cellular deficiencies (Moses et al., 2024).

The preponderance of synaptic ASD-linked proteins that contain an IDR suggests that the dysregulation of IDR ensembles is convergent pathological feature. ASD related deficiencies in IDR ensemble formation may extend beyond synaptic proteins. The fragile x messenger ribonucleoprotein (FMRP), the genetic cause of fragile X syndrome and a common syndromic form of ASD, contains a disordered C-terminal domain that can be post-translationally modified to its ability to regulate translation (Tsang et al., 2019). PTEN contains an IDR at the C-terminal that is crucial for its protein-protein interactions (Malaney et al., 2013). This suggests that IDRs are important in regulating protein interaction hubs that ASD converge upon. Disruption of these hubs for protein interaction networks may cause complex neurological deficits because they affect the formation of and signaling between membraneless compartments that control cell function.

Phase Separation and the formation of membraneless organelles

Maintaining proper localization and organization of biomolecules is critical during cell signaling. The components of a signaling pathway must be present at the right place and time to ensure proper cell function. To achieve this spatiotemporal control, the components of a signaling pathway must be localized to regulate their biochemical reactions. Aggregating or segregating biochemical components can hasten or inhibit such reactions. Membrane bound organelles can concentrate and segregate biomolecules through a lipid bilayer. However, many subcellular compartments lack a bound membrane, such as RNA-protein granules. Such structures concentrate their associated proteins and biomolecules without a physical barrier.

These membraneless compartments exist in the nucleus, cytosol, and on membrane surfaces in almost all eukaryotic cells. They form through liquid-liquid phase separation, a process where macromolecules in solution condense into a dense liquid-like phase that coexists with a dilute phase. Observations of P granules utilizing fluorescence recovery after photobleaching (FRAP) revealed the protein/RNA mixture that make up P granules exchange components with the cytoplasm, fuse together when flow is induced, and otherwise display liquid like properties (Brangwynne et al., 2009). Additionally, the proteins in the nucleus are highly mobile and the behavior of the compartments are indicative of proteins associating and dissociating at a steady state (Phair and Misteli 2000). This raised the possibility that protein complexes emerging from stochastic processes form membraneless compartments.

Phase separation can be understood through classical thermodynamics. In a mixture of soluble macromolecules in water, the macromolecules exhibit weak intermolecular interactions with one another and the water. The soluble macromolecules will exhibit stronger interactions with each other rather than the water. Phase separation occurs when such attraction can overcome the entropic tendency to remain homogenous in solution. One phase is a large volume, low concentration dilute phase while the other is a small volume, high concentration solute. The chemical potential is at equilibrium, preventing diffusive flux but allowing for exchange of individual molecules (Chen et al., 2020; Hyman et al., 2014).

In biomolecular condensates, there is an enrichment of molecules that have many domains that regulate inter- and intra-molecular interactions. This multivalency allows for the proteins to assemble into polymers. This promotes phase separation by

decreasing solubility (Banjade and Rosen, 2014). Molecules with such behavior include proteins with multiple modular interaction domains or intrinsically disordered regions, along with DNA and RNA molecules.

SH3 domains often employ liquid-liquid phase separation as a compartmentalization mechanism (Ghosh et al., 2019). The SH3 domain of Fyn kinase is also involved in phase separation (Amaya et al., 2018). The PDZ domain also plays a role in phase separation at the synapse. SynGAP has been reported to recruit PSD95 into SynGAP condensates through its PDZ domain (Acharya et al., 2023). Phosphorylation of PSD95's PDZ domains regulates its ability to phase separate with different synaptic proteins (Vistrup-Parry et al., 2021).

While IDRs are not necessary or sufficient for phase separation, their multivalency provides a medium that can enable a dynamic network of interactions that is necessary for liquid-liquid phase separation (Borcherds et al., 2021). IDRs can drive and tune the formation of condensates, determine the condensates material properties, and regulate the condensate through post-translational modifications (Bhattarai and Emerson 2020). IDRs can also influence the inclusion or exclusion of other molecules into the condensate. One IDR that drives condensate formation is the DDX4 region. Condensates formed from the DDX4 N-terminal IDR reduce the stability of duplexed nucleic acids. This potentially enhances RNA folding and enzyme catalysis (Nott et al., 2015).

Interaction domains are important players in the assembly of protein condensates and provide specificity. Condensate assemblies can be driven by i) modular domain-mediated, and specific stoichiometric interactions; ii) intrinsic disordered region driven

and nonspecific interactions; iii) combination of specific and promiscuous interactions (Feng et al., 2021). This indicates that a phase-separation based approach for understanding protein complex assembly is not a distinct or competing model to the interaction domain approach. Rather, phase separation is a natural extension of the preceding interaction domain approach.

The properties of phase separated condensates reflect their physiological function. Condensates can increase the local concentration of chemical species and thus accelerate reactions. This can only occur if all members of a reaction are present in the structure, however. The rate of mRNA histone processing is reduced if a component is not present in the histone locus body. Actin polymerization rates increase by concentrating relevant proteins into droplets (Li et al., 2012). However, molecular crowding can inhibit reactions by decreasing the accessible volume due to higher concentrations. The ability for molecules to move through condensates will also be influenced by its components. A condensate made up of small molecules will slow the movement of everything within. However, a large polymer matrix may form openings due to the large free volume between scaffold components (Cai et al 2011). Small proteins and other molecules may move freely through, but large molecules will be unable to permeate or move slowly through the condensate.

Phase separated condensates could also serve as a mechanism to regulate specificity. Condensates concentrate enzymes, substrates, and various binding partners together while excluding other molecules (Banani et al., 2017). An example of this has been observed during T-cell receptor (TCR) activation. TCR phosphorylation caused the formation of liquid-like clusters that concentrated kinases, excluded phosphatases, and

enhanced signaling outputs and actin filament assembly (Su et al., 2016). Phase separation concentrated the proteins necessary to promote signaling and segregated away inhibitory proteins. This shows how signal specificity can be achieved through the structural organization of proteins, a crucial characteristic for sub-cellular compartments like the synapse.

Additionally, signaling pathways regulate the formation of downstream biological condensates and promote different physiological outcomes. For example, the protein complex mTORC1 phosphorylates the P-granule component PGL-1/3, which promotes phase separation of P-granules and confers embryonic heat resistance (Zhang et al., 2018). Phase separated condensates can recruit specific signaling proteins that then influence the formation of downstream granules, linking membraneless compartments together.

Phase separated granules have also been speculated to provide a mechanism to store spatial information. Protein droplets have been shown to persist long after the stimuli that established the droplet has ended. Additionally, protein phase separation can amplify weak stimuli (Dine et al., 2018). Proteins that adopt self-perpetuating assemblies also have the properties necessary to encode information (Lau et al., 2020). The ability to encode and store information in response to stimuli is the defining role of the synapse. Many synaptic proteins form self-assembled protein complexes and granules in response to synaptic activity. The structure of synapse, synaptic signaling, and memory storage may be intertwined with the phase separation. Analysis of organization of synaptic proteins is crucial to understanding how the synapse achieves molecular memory storage.

The organization of synaptic proteins mediates neuronal signaling and plasticity.

The PSD displays several features expected of membraneless condensates. The proteins that compose the PSD are highly concentrated and mobile, moving between the PSD and cytoplasm. The PSD itself can change in size due to the changes in its component proteins (Chen et al., 2020). An even mixture of PSD scaffolding proteins PSD95, GKAP, Shank, and Homer underwent phase separation and all four components co-condensed (Zeng et al., 2016). This condensate could also co-condense the NR2B tail and SynGAP, indicating that phase separation can mediate synaptic signaling. For example, stimulated emission depletion microscopy (STED) experiments indicate that synaptic spines contain aligned nanomodules of pre- and postsynaptic proteins. Chemical long-term potentiation induces an increase in the number of synaptic nanodomains at the spine and an increase in nanodomain mobility (Hruska et al., 2018). Plasticity induces parallel modifications to the pre- and post-synaptic architecture. The increased movement of NMDAR nanodomains is linked with the increase in nanodomains at the synapse that align with anchoring proteins and pre-synaptic proteins following plasticity (Hruska et al., 2018). The reorganization of synaptic proteins and their associated condensates is a key feature of neuronal signaling and plasticity.

The role of glutamate receptors in synaptic architecture.

In excitatory glutamatergic synapses, several types of glutamate receptors mediate neuronal signaling. Ionotropic glutamate receptors consist of AMPA, NMDA and kainite type receptors (Scheefhals and MacGillavry 2018). AMPA and NMDA are the principle ionotropic GLURs and act on a millisecond timescale to facilitate fast transmission.

Metabotropic glutamate receptors, such as mGLUR1 and mGLUR5, have a much slower timescale with longer lasting physiological effects. The ionotropic and metabotropic receptors are spatially segregated at the synapse. Ionotropic receptors are enriched at the core of the PSD so that they are opposing the presynaptic vesicle release site (Nusser et al., 1994). mGLURs are excluded from the PSD and enriched in the peri-synaptic domain (Baude et al., 1993). The organization of glutamate receptors has functional implications that are related to each receptor's physiology.

AMPA receptor nanodomains and their function at the synapse

The organization of AMPA receptors in the synapse is informed by their electrophysiological properties. Due to their affinity for glutamate and the rate of desensitization when binding, AMPARs have the highest probability of opening near vesicle release sites (Scheefhals and MacGillavry, 2018). AMPARs form high-density nanodomains within individual synapses that are mirrored by opposing presynaptic nanodomains that are enriched in vesicle proteins. These spatially aligned nanodomains create a transsynaptic nano-column that provides a mechanism for efficient transmission. A typical synapse was shown to have one to three nanodomains, containing about 20 AMPARs, which can freely diffuse in and out of the domain (Nair et al., 2013). The mechanisms that regulate the organization of AMPA receptors into nanodomains directly inform their electrophysiological properties.

Scaffolding proteins regulate AMPA receptor localization and function

Scaffolding proteins form a laminated structure at the PSD for the positioning of receptors (Harris and Weinberg 2012). The AMPARs interact with scaffolding proteins

like PSD95 through the AMPAR's PDZ ligand in the C-terminal domain (CTD). AMPA nanodomains are often colocalized with clusters of PSD95, immobilizing AMPA receptors to form nanodomains (Nair et al., 2013). A reduction of AMPA receptor clustering through GluA C-tail expression reduces the size of the PSD95 clusters. Conversely, tetrodotoxin treatment increases both AMPA receptor number and PSD95 cluster size (MacGillavry et al., 2013). AMPA and PSD95 clusters are functionally interlinked, and their association plays a key role in the management of synaptic architecture.

The CTD of the AMPAR subunits is also responsible for binding additional synaptic scaffolding proteins like SAP97, PICK1, and GRIP (Barry and Ziff 2002). The αSAP97 isoform is anchored within the PSD, regulates the number of binding sites for GLUA1, and increase synaptic currents. βSAP97 regulates the cluster size and density of GLUA1 at the periphery of the PSD and decreases synaptic currents (Waites et al., 2009). The C-terminal domain regulates AMPA receptor clustering with scaffolding proteins that support AMPA receptor nanodomains. The architecture of AMPA receptors and supporting scaffolding proteins both responds to and shapes synaptic activity.

Phase separation plays an important role in AMPA receptor organization at the synapse. The immediate early gene Arc regulates synaptic plasticity through the removal of AMPA receptors (Chowdhury et al., 2006). Arc disperses the transmembrane AMPA receptor regulating proteins (TARPs) from the PSD condensate in a concentration dependent manner. Phosphorylation of TARPs prevents this dispersal, but enhancing ARC-TARP binding weakens synapses further (Chen et al., 2022). Mutations in TARP_CT Arg-rich motif that cause charge neutralization weaken TARP's condensation with PSD95 and

impair AMPA receptor synaptic transmission in mouse hippocampal neurons (Zeng et al., 2019). This indicates regulation of phase separation at the synapse directly affects AMPAR function, which is directly tied to the nanodomains AMPARs that form through protein-protein interactions.

Additionally, SynGAP forms a homotrimer and binds to multiple copies of PSD95 and the resulting multivalent complex is critical for the resulting phase separation (Zeng et al., 2016). Recently, SynGAPs role in long term potentiation has been shown to be driven by its ability to form condensates with PSD95 at the synapse. SynGAP condensates compete with TARPs for binding to PSD95. LTP induction causes SynGAP phosphorylation, which disperses it from PSD95 and allows the formation of PSD95-TARP-AMPAR condensate that enables LTP (Araki et al., 2024). The structure of AMPA receptor nanodomains and phase separated condensates mediate synaptic plasticity.

Dysregulation of the PSD condensate and its control of AMPAR synaptic transmission may be a crucial part of neurodevelopmental disorders. Arc has been implicated in several neurodevelopmental disorders including ASD (Alhowikan 2016). Mutations in the GRIA2 subunit have been identified in individuals with various neurodevelopmental disorders including ASD (Salpeitro et al., 2019). Additionally, the Shank3 and SynGAP models of ASD have displayed deficits in AMPA receptor synaptic function (Jimenez-Gomez et al., 2024). Regulation of the structure of AMPA nanodomains and their associated function is important for neurotypical synaptic activity and the disruption of AMPARs appears to be a shared molecular node in the pathology of ASD.

The organization of NMDA receptor nanodomains and their role in synaptic plasticity

The NMDA receptor also forms distinct nanodomains in the glutamatergic synapse. NMDAR nanodomains tend to localize at the center of the PSD, while AMPAR nanodomains are located more peripherally around NMDAR domains (Zhang and Diamond, 2006; Goncalves et al., 2020). A synapse will typically contain one to four nanodomains and nanodomains vary by subunit composition. GluN2A and GluN2B containing receptors will segregate into different nanodomains that are differentially regulated by PSD95 binding to the NMDAR's CTD (Kellermayer et al., 2018).

NMDARs' CTD is intrinsically disordered, is the largest single domain in the protein, and has been implicated in patients with ASD (Liu et al., 2017). Additionally, phase separation plays an important role in the regulation of NMDA receptors. The C-terminal of the GluN2B subunit readily undergoes phase separation with PSD95 and SynGAP while the GluN2A subunit does not support phase separation with PSD95 and SynGAP (Basak et al., 2023). However, the GluN2A binding protein Rabphilin-3A (Rph3A) demonstrates phase separation and the formation of the Rph3A-PSD95-GluN2A protein complex promotes Rph3A phase separation. Disrupting Rph3A phase separation suppresses GluN2A's synaptic localization, surface clustering, and synaptic responses (Yang et al., 2023). This indicates that variation in the NMDAR subunit ratio may have a strong effect on the organization of synaptic proteins into dynamic condensates.

Phase separation is also a crucial element of NMDAR and Ca2+/calmodulin-dependent protein kinase II (CaMKII) interactions. The interaction between the NMDAR CTD and CaMKII is greatly associated with synaptic plasticity. After an influx of calcium, CaMKII

binds to the CTD of GluN2B, and the two proteins undergo phase separation. This causes co-segregation of AMPA receptors and the adhesion protein neuroligin into a phase-in-phase assembly (Hosokawa et al., 2021). The subsequent partitioning of AMPARs and neuroligin may enrich AMPARs near pre-synaptic release sites to form previously mentioned AMPA receptor nanodomains and enhance synaptic signaling. In support of this hypothesis, the clustering of neuroligins can induce clustering of the pre-synaptic neurexin and subsequent recruitment of vesicle release machinery (Dean et al., 2003). GluN2B-CAMKII binding mediates synaptic rearrangement that is crucial to synaptic plasticity through phase separation.

While CaMKII has a well-recognized role in synaptic plasticity, the assumption was this function dependent on its kinase activity. However, a CaMKII mutation that blocked GluN2B binding while preserving enzymatic activity failed to induce glutamate and glycine driven chemical long-term potentiation (cLTP). Additionally, treatment with a CAMKII inhibitor that only targeted enzymatic activity and preserved GluN2B binding did not prevent cLTP induction (Tullis et al., 2023). This work demonstrated that CAMKII's enzymatic activity is not necessary to induce long term depression. Rather, CAMKII's structural role at the synapse appears to be the critical factor in synaptic plasticity. The observation that expression of a CAMKII mutant protein that is unable to phase separate with GluN2B fails to rescue synaptic transmission and LTP deficits in CaMKII deficient mice further supports this hypothesis (Cai et al., 2023). CAMKII's ability to form dynamic membraneless compartments through its interaction with GluNR2B's disordered CTD appears to drive synaptic plasticity.

Metabotropic glutamate receptors

Group I mGLURs are g-protein coupled receptors with many effectors and whose ultimate effects are the increase of postsynaptic excitability by modulating ion channels and the regulation of NMDAR currents (Niswender and Conn 2010). mGLUR activity has been linked to several types of plasticity. mGLUR5 participates in long term potentiation, which seems to reflect a priming effect where prior mGLUR activation primes the induction of LTP by increasing excitability or prolongs LTP expression via local protein synthesis (Cohen et al., 1999; Raymond et al., 2000). mGLUR activation is also sufficient to cause long term depression mediated by protein synthesis dependent endocytosis of AMPARs (Huber et al., 2000). mGluR5-dependent LTD is dependent on activation of the mTOR pathway and mTORC2 by mGLUR5 (Zhu et al., 2018; Hou and Klann 2004).

The CTD of mGLURs is intrinsically disordered and interacts with many binding partners that include kinases, ion channels, and scaffolding proteins (Enz 2012). The CTD has recently been implicated in the assembly of mGLUR5 nanodomains at the perisynapse. mGluR5 is transiently trapped in these perisynaptic nanodomains and rapidly shift between diffusive states (Scheefhals et al., 2023). The mGLURs are bound to other receptors indirectly, including NMDARs, through the CTD binding to synaptic scaffolding proteins (Shiraishi-Yamaguchi and Furuichi, 2007; Tu et al., 1999). The CTD of mGLURs has a PDZ ligand that interacts with Shanks and Tamalin and seems to be involved in surface trafficking (Kitano et al., 2002). Additionally, the position of mGLURs at the synapse is regulated by its interaction with the Homer protein family (Aloisi et al., 2017).

The Homer-mGluR interaction mediates synaptic plasticity and mGluR activity

The Homer proteins are dendritic proteins that bind to C-terminus region of phosphoinositide-linked mGLURs (Brakeman et al., 1997). The Homer1 gene produces two constitutively expressed long form Homer1 isoforms (Homer1b and Homer1c) and a short isoform known as Homer1a whose expression is inducible (de Bartolomeis et al., 2022). Homer proteins interact with the binding motif of mGLURs through their EVH1 domain (Fagni et al 2002). The EVH1 domain has been shown to be essential for the PSD condensate-induced actin bundle formation and spine growth. This actin-bundling formation can only occur when Homers form a condensate with other scaffolding proteins like Shank or SAPAP and is regulated by CaMKII and Homer1a (Chen et al., 2023). Phase separation between synaptic proteins and actin has been proposed as a mechanism to facilitate communication between the PSD and the spine cytoskeleton proteins (Chen et al., 2023). Homer1's role in phase separation indicates that phase separation can facilitate cell communication by mediating the formation of nearby condensates. The formation of one condensate will affect the concentration of proteins in the surrounding area. The change in local protein concentration will affect how subsequent nearby condensates form. This may produce cycles of condensate formation and regulation that occur in response to stimuli.

Additionally, Homer binding to mGluRs regulates the receptors' activity and disrupting the interaction between mGluRs and Homer1b/c induces constitutive mGluR activity (Ango et al 2001). Homer1a interrupts the binding of long-form Homer with mGluRs to cause agonist independent mGluR activity. The activity of mGluRs is explicitly tied to the interactions formed in the mGluRs nanodomains. Homer1 dissociation from mGluR5

and Shank3 follows depolarization, and it has been suggested that Homer's preeminent function is linking Shanks and mGluR5 to regulated synaptic activity (Stillman et al., 2022). Homeostatic scaling also requires Homer1a-mediated activation of mGluRs (Hu et al., 2010; Chokshi et al., 2019). Homer1 deficient mice have shown a range of behavioral and physiological deficits including poor motor coordination, sensory reactivity, learning deficits, and increased aggression in social interactions (Jaubert et al., 2007). Homer1 interactions have an indispensable role in managing mGluR nanodomains and mGluR mediated plasticity.

mGLUR signaling has a crucial role in synaptic plasticity and neurodevelopmental disorders

Deficiencies in mGluR5-dependent LTD are most notably present in the fragile X messenger ribonucleoprotein 1 (FMR1) knockout mouse (Huber et al., 2002). mGluR5 is less associated with the long Homer isoforms in FMRP-deficient mice, which contributes to mGLUR5 dysfunction (Ronesi et al., 2012). FMRP deficiency decreases the number of mRNA granules due to exaggerated mGluR5 signaling (Aschrafi et al., 2005). The disruption of Homer-mGluR5 scaffolding increases mGLUR5 mobility and mGluR5/NMDA co-clustering, which reduces NMDAR currents (Aloisi et al., 2017). Genetic mutation of the Homer binding site on mGLUR5 replicates FMR1 knockout phenotypes such as GLUR5 association to the PSD, enhanced mGLUR5 signaling, and plasticity deficits (Guo et al., 2016).

Analysis of the mGluR5-FMRP signaling axis may hint to how different phase-separated condensates can affect one another through signal transduction. Synaptic activity mediated through mGluR5 regulates the assembly of the synaptic condensate and the

FMRP/RNA condensate. mGluRs directly participate in the assembly of the PSD condensate during neuronal signaling. The mGluR5 condensate then recruits mTOR and ERK signaling proteins. FMRP phosphorylation is downstream of mGLUR5 signaling through the ERK and mTOR pathway (Narayanan et al., 2008). Post translational modification of FMRP's IDR regulates its ability to form condensates and regulate translation (Starke et al 2022; Tsang et al., 2019). In support of this model, induction of LTP has been shown to produce an increase in 'disassembled' FMRP granules and a decrease in 'assembled' granules, indicating translational activation (Narayanan et al., 2008). The activity dependent regulation of the synaptic condensate recruits signaling cascades that regulate the FMRP/RNA condensate downstream. mGluRs are an important biological nexus due to their ability to recruit signaling proteins and interactions with synaptic scaffolding proteins the regulate the organization of the synapse and the FMRP granule.

Shank family proteins are central mediators of the synaptic protein interaction network

Shank3 and the remaining Shank family proteins are important scaffolding proteins at the synapse. Shank family proteins were first identified as binding partners of PSD95 and other MAGUK family kinases. The three Shank genes consist of seven ankyrin repeats near the N terminus, an SH3 domain, a PDZ domain, a long proline rich region, and a SAM domain at the C-terminus (Naisbitt et al, 1999). The PDZ domain at the C terminus binds to the MAGUK family proteins and the GKAP protein localizes the Shanks to the synapse and forms a complex with the NMDA receptor (Naisbitt et al,

1999). Shank family proteins, through their proline rich motif, also bind to Homer proteins at their EVH1 domain at the synapse (Lin et al., 2021).

The Shanks mediate a quaternary complex with PSD95 and Homer, providing a link between Homer and the NMDA receptor. Homer-Shank complexes result in mGLUR5 and Shank co-clustering (Tu et al., 1999). The Shank3 isoform binds to the C-terminal of mGluR5 through its PDZ domain (Tu et al., 1999). Shank proteins multimerize through their SAM domain, allowing crosslinking of multiple protein complexes at the synapse. Shank3 also binds to the GRIP scaffolding protein, providing a link to AMPA receptors (Sheng and Kim, 2011). Shank3 is also a binding partner for autoinhibited CaMKII. Shank3 and GluN2B reciprocally bind to CaMKII through calcium and phosphatase actions. Phase separation mediates CaMKII recruitment to the Shank3 sub-compartment of the PSD (Cai et al., 2023). Shank3 interactions at the synapse link the various glutamate receptor condensates and their activity together.

The deletion of Shank3 is responsible for 22q13.3 deletion syndrome, commonly known as Phelan-McDermid syndrome. Additionally, individuals with idiopathic ASD carry mutations in the Shank3 gene. This led to the creation of several ASD mouse models that are deficient in Shank3 (Peca et al., 2011). The loss of Shank3 expression prevents synaptic plasticity (Tatavarty et al., 2020). Shank3 haploinsufficiency in dogs produces morphological and functional deficiencies in pre-frontal cortex pyramidal neurons. Synaptic transmission was impaired, dendric complexity and spine density was reduced, and PSD structures were impaired in Shank3 mutant neurons (Zhu et al., 2024). Shank3 is a critical mediator of synaptic organization and the PSD condensate. The wide array of synaptic deficits caused by the loss of Shank3 is due to the

dysregulation of scaffolding assemblies at the postsynaptic density. This further indicates that the activity of the synapse is managed through protein-protein interaction networks that operate together as membraneless organelles and disrupting these networks may underlie the pathology of many neurodevelopmental disorders.

Conclusions

Growing research into the synaptic interactome is producing novel insights into the mechanisms of synaptic signaling and neurodevelopmental disorders like ASD. Dynamic protein interactions that manage phase separated condensates are an important mechanism for synaptic functioning. Proteins that function as interaction hubs or protein domains that facilitate multivalent interactions are at the heart of signaling at the synapse. Furthermore, it is increasingly evident that the liquid-like qualities of these proteins are critical to regulating synaptic activity. The ability of these proteins to properly assemble and disassemble into condensates has been shown to directly affect the functioning of the synapse. Furthermore, we have highlighted how several ASD-linked genes products undergo phase separation during neurotypical functioning. Disruptions in the formation or regulation of protein condensates at the synapse and RNA granules have also been directly linked to ASD.

We believe that these insights into the synaptic interactome indicate that protein interactions and phase separation may drive signal specificity, synaptic functioning, and the neuronal deficits observed in ASD. Neuronal signaling occurs through modules of protein interactions that assemble or disassemble functional membranelles organelles in response to stimuli. At the synapse, a potentiating signal will cause synaptic proteins to form condensates that are conducive for LTP. This is exemplified by SynGAP

condensates dispersing from AMPARs after LTP-mediated phosphorylation and allowing the formation of PSD95-TARP-AMPAR condensates that enable LTP (Araki et al., 2024). CaMKII's role in phase separation with NMDA receptors directly enables LTP (Tullis et al., 2023). The structure of the condensate at the post synaptic density will influence other condensates and signaling pathways. Homer1's role in linking the formation of actin condensates and PSD scaffold condensates is a prime example of this phenomenon (Chen et al., 2023).

The state of the synaptic condensate may also influence the recruitment and activity of different signaling pathways in response to neuronal activity. PTEN is both capable of phase separation at the membrane and recruited to the synapse after NMDAR activation (Gamba et al., 2005). This makes PTEN an obvious target of study to elucidate the role that synaptic phase separation has in the regulation of signaling pathways. Regulation of signaling pathways will also influence the structure of downstream condensates. Condensate-regulated signal transduction may provide a mechanism that links compartments together. It is also possible that ASD linked mutations affect neurons by dysregulating the structure of membraneless compartments or signaling between them. Mutations that affect synaptic scaffolding proteins' interactions will have far reaching consequences for neuron physiology. These mutations would cause deficits in the recruitment of other proteins to their targets, dysregulating their functions. This would have cascading effects beyond the PSD condensate, as abnormal protein recruitment and signaling would affect downstream compartments.

Protein interactions are critical to understanding molecular and neuronal signaling as they are the means through which biological activity occurs. As proteins must physically interact with its targets to influence the cell's physiology, characterizing how their interactions change between various states can elucidate crucial biological insights. It should not be surprising that shared patterns in protein interaction modules between different modes of ASD confer to shared pathology. Future work will have to continue to elucidate the mechanisms that link protein condensates together. Understanding cell signaling through their membraneless compartments may be the key to signal specificity.

In this dissertation, we focus on a signaling pathway that is crucial to several cellular and neuronal functions as well as several biological condensates. The mammalian target of rapamycin (mTOR) is a serine-threonine kinase that acts as a central regulator of translation and is involved in many physiological processes like cell growth/survival, autophagy, and plasticity (Hoeffer and Klann 2011). Canonical mTOR signaling begins with signal induced translocation of phosphoinositide 3-kinase (PI3K) to the membrane. PI3K phosphorylates membrane inositol PIP2 to PIP3, leading to AKT phosphorylation by PDK1 and mTOR complex 2 (mTORC2) (Liu and Sabatini 2020). PIP3 is de-phosphorylated by PTEN to negatively regulate the pathway (Vazques and Devreotes 2006). Phosphorylated AKT then phosphorylates TSC2, disrupting the TSC1-TSC2 complex and leading to TSC2 degradation, disinhibiting the GTPase Rheb. Rheb activates mTOR complex 1 (mTORC1) by binding to the mTOR protein and inducing a confirmation change to an active state (Inoki et al., 2002). Active mTORC1 promotes translation through the phosphorylation of p70S6K and 4EBP. P70S6K then

phosphorylates the ribosomal protein S6 (RPS6) and phosphorylated 4EBP unbinds EIF4E, leading to the formation of the ribosomal complex. mTORC1 regulates transcription and autophagy through its effects on sterol-response binding proteins (SREBPs) and the ULK1 complex respectively (Lipton and Sahin 2014).

Several members of the mTOR cascade, such as PTEN and FMRP, play an important role in phase separation and have been previously discussed. Several mTOR proteins are also implicated in both idiopathic and syndromic forms of ASD (Chen et al., 2014; Hoeffer and Klann, 2010; Winden et al., 2018). Additionally, the mTOR signaling cascade plays a crucial role in synaptic plasticity. Specifically, mTOR signaling is involved in form of plasticity known as homeostatic scaling (Srinivasan et al., 2021; Hou et al. 2008; Wang et al., 2023). Homeostatic scaling is a form of plasticity that maintains a neurons baseline level of activity through adjusting the levels of AMPARs at the synapse (Turrigiano 2012). Various mouse models of autism, including FMR1, Homer1, and Shank3 display deficits in homeostatic scaling (Hu et al., 2010; Soden and Chen 2010; Tatavarty et al., 2020). This makes both mTOR signaling and homeostatic scaling attractive points of interest to better understand ASD and the functional role of signaling through protein interactions. This dissertation seeks to understand mTOR signaling through its protein interaction network, its role in homeostatic scaling, and how ASD disrupts both mTOR signaling and homeostatic scaling.

References:

Acharya, S., Tsunoyama, T. A., Hoffmann, C., Aguilar, G., Meshcheryakova, I., Nemoto, Y. L., Nakamura-Norimoto, A., Fujiwara, T., Milovanovic, D., & Kusumi, A. (2023). Syngap LLPS condensates as the basic platform for recruiting PSD95 and receptor oligomers for generating neuronal excitatory synapses. Biophysical Journal, 122(3, Supplement 1), 417a. https://doi.org/10.1016/j.bpj.2022.11.2263

Alhowikan, A. M. (2016). Activity-Regulated Cytoskeleton-Associated Protein Dysfunction May Contribute to Memory Disorder and Earlier Detection of Autism Spectrum Disorders. Medical Principles and Practice: International Journal of the Kuwait University, Health Science Centre, 25(4), 350–354. https://doi.org/10.1159/000445351

Aloisi, E., Corf, K. L., Dupuis, J., Zhang, P., Ginger, M., Labrousse, V., Spatuzza, M., Haberl, M. G., Costa, L., Shigemoto, R., Tappe-Theodor, A., Drago, F., Piazza, P. V., Mulle, C., Groc, L., Ciranna, L., Catania, M. V., & Frick, A. (2017). Altered surface mGluR5 dynamics provoke synaptic NMDAR dysfunction and cognitive defects in Fmr1 knockout mice. Nature Communications, 8. https://doi.org/10.1038/s41467-017-01191-2

Amacher, J. F., Brooks, L., Hampton, T. H., & Madden, D. R. (2020). Specificity in PDZ-peptide interaction networks: Computational analysis and review. Journal of Structural Biology: X, 4, 100022. https://doi.org/10.1016/j.yjsbx.2020.100022

Amaya, J., Ryan, V. H., & Fawzi, N. L. (2018). The SH3 domain of Fyn kinase interacts with and induces liquid–liquid phase separation of the low-complexity domain of hnRNPA2. Journal of Biological Chemistry, 293(51), 19522–19531. https://doi.org/10.1074/jbc.RA118.005120

American Psychiatric Association & American Psychiatric Association (Eds.). (2013). Diagnostic and statistical manual of mental disorders: DSM-5 (5th ed). American Psychiatric Association.

Ango, F., Prézeau, L., Muller, T., Tu, J. C., Xiao, B., Worley, P. F., Pin, J. P., Bockaert, J., & Fagni, L. (2001). Agonist-independent activation of metabotropic glutamate receptors by the intracellular protein Homer. Nature, 411(6840), 962–965. https://doi.org/10.1038/35082096

Araki, Y., Rajkovich, K. E., Gerber, E. E., Gamache, T. R., Johnson, R. C., Tran, T. H. N., Liu, B., Zhu, Q., Hong, I., Kirkwood, A., & Huganir, R. (2024). SynGAP regulates synaptic plasticity and cognition independently of its catalytic activity. Science, 383(6686), eadk1291. https://doi.org/10.1126/science.adk1291

Arbesú, M., & Pons, M. (2019). Integrating disorder in globular multidomain proteins: Fuzzy sensors and the role of SH3 domains. Archives of Biochemistry and Biophysics, 677, 108161. https://doi.org/10.1016/j.abb.2019.108161

Aschrafi, A., Cunningham, B. A., Edelman, G. M., & Vanderklish, P. W. (2005). The fragile X mental retardation protein and group I metabotropic glutamate receptors regulate levels of mRNA granules in brain. Proceedings of the National Academy of Sciences, 102(6), 2180–2185. https://doi.org/10.1073/pnas.0409803102

Banani, S. F., Lee, H. O., Hyman, A. A., & Rosen, M. K. (2017). Biomolecular condensates: Organizers of cellular biochemistry. Nature Reviews Molecular Cell Biology, 18(5), Article 5. https://doi.org/10.1038/nrm.2017.7

Banjade, S., & Rosen, M. K. (2014). Phase transitions of multivalent proteins can promote clustering of membrane receptors. eLife, 3, e04123. https://doi.org/10.7554/eLife.04123

Barry, M. F., & Ziff, E. B. (2002). Receptor trafficking and the plasticity of excitatory synapses. Current Opinion in Neurobiology, 12(3), 279–286. https://doi.org/10.1016/s0959-4388(02)00329-x

Basak, S., Saikia, N., Kwun, D., Choi, U. B., Ding, F., & Bowen, M. E. (2023). Different Forms of Disorder in NMDA-Sensitive Glutamate Receptor Cytoplasmic Domains Are Associated with Differences in Condensate Formation. Biomolecules, 13(1), Article 1. https://doi.org/10.3390/biom13010004

Baude, A., Nusser, Z., Roberts, J. D. B., Mulvihill, E., Mcllhinney, R. A. J., & Somogyi, P. (1993). The metabotropic glutamate receptor (mGluRlα) is concentrated at perisynaptic membrane of neuronal subpopulations as detected by immunogold reaction. Neuron, 11(4), 771–787. https://doi.org/10.1016/0896-6273(93)90086-7

Bhattarai, A., & Emerson, I. A. (2020). Dynamic conformational flexibility and molecular interactions of intrinsically disordered proteins. Journal of Biosciences, 45(1), 29. https://doi.org/10.1007/s12038-020-0010-4

Boccuto, L., Lauri, M., Sarasua, S. M., Skinner, C. D., Buccella, D., Dwivedi, A., Orteschi, D., Collins, J. S., Zollino, M., Visconti, P., DuPont, B., Tiziano, D., Schroer, R. J., Neri, G., Stevenson, R. E., Gurrieri, F., & Schwartz, C. E. (2013). Prevalence of SHANK3 variants in patients with different subtypes of autism spectrum disorders. European Journal of Human Genetics, 21(3), 310–316. https://doi.org/10.1038/ejhg.2012.175

Borcherds, W., Bremer, A., Borgia, M. B., & Mittag, T. (2021). How do intrinsically disordered protein regions encode a driving force for liquid-liquid phase separation? Current Opinion in Structural Biology, 67, 41–50. https://doi.org/10.1016/j.sbi.2020.09.004

Brakeman, P. R., Lanahan, A. A., O'Brien, R., Roche, K., Barnes, C. A., Huganir, R. L., & Worley, P. F. (1997). Homer: A protein that selectively binds metabotropic glutamate receptors. Nature, 386(6622), 284–288. https://doi.org/10.1038/386284a0

Brangwynne, C. P., Eckmann, C. R., Courson, D. S., Rybarska, A., Hoege, C., Gharakhani, J., Jülicher, F., & Hyman, A. A. (2009). Germline P Granules Are Liquid Droplets That Localize by Controlled Dissolution/Condensation. Science, 324(5935), 1729–1732. https://doi.org/10.1126/science.1172046

Cai, L.-H., Panyukov, S., & Rubinstein, M. (2011). Mobility of Nonsticky Nanoparticles in Polymer Liquids. Macromolecules, 44(19), 7853–7863. https://doi.org/10.1021/ma201583q

Cai, Q., Chen, X., Zhu, S., Nicoll, R. A., & Zhang, M. (2023). Differential roles of CaMKII isoforms in phase separation with NMDA receptors and in synaptic plasticity. Cell Reports, 42(3), 112146. https://doi.org/10.1016/j.celrep.2023.112146

Chen, J., Alberts, I., & Li, X. (2014). Dysregulation of the IGF-I/PI3K/AKT/mTOR signaling pathway in autism spectrum disorders. International Journal of Developmental Neuroscience, 35, 35–41. https://doi.org/10.1016/j.ijdevneu.2014.03.006

Chen, X., Jia, B., Araki, Y., Liu, B., Ye, F., Huganir, R., & Zhang, M. (2022). Arc weakens synapses by dispersing AMPA receptors from postsynaptic density via modulating PSD phase separation. Cell Research, 32(10), 914–930. https://doi.org/10.1038/s41422-022-00697-9

Chen, X., Jia, B., Zhu, S., & Zhang, M. (2023). Phase separation-mediated actin bundling by the postsynaptic density condensates. eLife, 12, e84446. https://doi.org/10.7554/eLife.84446

Chen, X., Wu, X., Wu, H., & Zhang, M. (2020). Phase separation at the synapse. Nature Neuroscience, 23(3), 301–310. https://doi.org/10.1038/s41593-019-0579-9

Chokshi, V., Gao, M., Grier, B. D., Owens, A., Wang, H., Worley, P. F., & Lee, H.-K. (2019). Input-Specific Metaplasticity in the Visual Cortex Requires Homer1a-Mediated mGluR5 Signaling. Neuron, 104(4), 736-748.e6. https://doi.org/10.1016/j.neuron.2019.08.017

Chowdhury, S., Shepherd, J. D., Okuno, H., Lyford, G., Petralia, R. S., Plath, N., Kuhl, D., Huganir, R. L., & Worley, P. F. (2006). Arc Interacts with the Endocytic Machinery to Regulate AMPA Receptor Trafficking. Neuron, 52(3), 445–459. https://doi.org/10.1016/j.neuron.2006.08.033

Cirnigliaro, M., Chang, T. S., Arteaga, S. A., Pérez-Cano, L., Ruzzo, E. K., Gordon, A., Bicks, L. K., Jung, J.-Y., Lowe, J. K., Wall, D. P., & Geschwind, D. H. (2023). The contributions of rare inherited and polygenic risk to ASD in multiplex families. Proceedings of the National Academy of Sciences, 120(31), e2215632120. https://doi.org/10.1073/pnas.2215632120

Cohen, A. S., Coussens, C. M., Raymond, C. R., & Abraham, W. C. (1999). Long-Lasting Increase in Cellular Excitability Associated With the Priming of LTP Induction in Rat Hippocampus. Journal of Neurophysiology, 82(6), 3139–3148. https://doi.org/10.1152/jn.1999.82.6.3139

Cortese, M. S., Uversky, V. N., & Dunker, A. K. (2008). Intrinsic disorder in scaffold proteins: Getting more from less. Progress in Biophysics and Molecular Biology, 98(1), 85–106. https://doi.org/10.1016/j.pbiomolbio.2008.05.007

Cushing, P. R., Fellows, A., Villone, D., Boisguerin, P., & Madden, D. R. (2008). The Relative Binding Affinities of PDZ Partners for CFTR: A Biochemical Basis for Efficient Endocytic Recycling. Biochemistry, 47(38), 10084–10098. https://doi.org/10.1021/bi8003928

Das, R. K., Ruff, K. M., & Pappu, R. V. (2015). Relating sequence encoded information to form and function of intrinsically disordered proteins. Current Opinion in Structural Biology, 32, 102–112. https://doi.org/10.1016/j.sbi.2015.03.008

de Bartolomeis, A., Barone, A., Buonaguro, E. F., Tomasetti, C., Vellucci, L., & Iasevoli, F. (2022). The Homer1 family of proteins at the crossroad of dopamine-glutamate signaling: An emerging molecular "Lego" in the pathophysiology of psychiatric disorders. A systematic review and translational insight. Neuroscience & Biobehavioral Reviews, 136, 104596. https://doi.org/10.1016/j.neubiorev.2022.104596

Dean, C., Scholl, F. G., Choih, J., DeMaria, S., Berger, J., Isacoff, E., & Scheiffele, P. (2003). Neurexin mediates the assembly of presynaptic terminals. Nature Neuroscience, 6(7), 708–716. https://doi.org/10.1038/nn1074

Dine, E., Gil, A. A., Uribe, G., Brangwynne, C. P., & Toettcher, J. E. (2018). Protein Phase Separation Provides Long-Term Memory of Transient Spatial Stimuli. Cell Systems, 6(6), 655-663.e5. https://doi.org/10.1016/j.cels.2018.05.002

Durand, C. M., Betancur, C., Boeckers, T. M., Bockmann, J., Chaste, P., Fauchereau, F., Nygren, G., Rastam, M., Gillberg, I. C., Anckarsäter, H., Sponheim, E., Goubran-Botros, H., Delorme, R., Chabane, N., Mouren-Simeoni, M.-C., de Mas, P., Bieth, E., Rogé, B., Héron, D., … Bourgeron, T. (2007). Mutations in the gene encoding the synaptic scaffolding protein SHANK3 are associated with autism spectrum disorders. Nature Genetics, 39(1), 25–27. https://doi.org/10.1038/ng1933

Enz, R. (2012). Structure of metabotropic glutamate receptor C-terminal domains in contact with interacting proteins. Frontiers in Molecular Neuroscience, 5. https://doi.org/10.3389/fnmol.2012.00052

Erlendsson, S., & Teilum, K. (2021). Binding Revisited—Avidity in Cellular Function and Signaling. Frontiers in Molecular Biosciences, 7. https://doi.org/10.3389/fmolb.2020.615565

Fagni, L., Worley, P. F., & Ango, F. (2002). Homer as Both a Scaffold and Transduction Molecule. Science's STKE, 2002(137), re8–re8. https://doi.org/10.1126/stke.2002.137.re8

Farahani, M., Rezaei-Tavirani, M., Zali, A., & Zamanian-Azodi, M. (2022). Systematic Analysis of Protein–Protein and Gene–Environment Interactions to Decipher the Cognitive Mechanisms of Autism Spectrum Disorder. Cellular and Molecular Neurobiology, 42(4), 1091–1103. https://doi.org/10.1007/s10571-020-00998-w

Feng, Z., Jia, B., & Zhang, M. (2021). Liquid–Liquid Phase Separation in Biology: Specific Stoichiometric Molecular Interactions vs Promiscuous Interactions Mediated by Disordered Sequences. Biochemistry, 60(31), 2397–2406. https://doi.org/10.1021/acs.biochem.1c00376

Gamache, T. R., Araki, Y., & Huganir, R. L. (2020). Twenty Years of SynGAP Research: From Synapses to Cognition. The Journal of Neuroscience, 40(8), 1596–1605. https://doi.org/10.1523/JNEUROSCI.0420-19.2020

Gamba, A., de Candia, A., Di Talia, S., Coniglio, A., Bussolino, F., & Serini, G. (2005). Diffusion-limited phase separation in eukaryotic chemotaxis. Proceedings of the National Academy of Sciences, 102(47), 16927–16932. https://doi.org/10.1073/pnas.0503974102

Gauthier, J., Champagne, N., Lafrenière, R. G., Xiong, L., Spiegelman, D., Brustein, E., Lapointe, M., Peng, H., Côté, M., Noreau, A., Hamdan, F. F., Addington, A. M., Rapoport, J. L., DeLisi, L. E., Krebs, M.-O., Joober, R., Fathalli, F., Mouaffak, F., Haghighi, A. P., … Rouleau, G. A. (2010). De novo mutations in the gene encoding the synaptic scaffolding protein SHANK3 in patients ascertained for schizophrenia. Proceedings of the National Academy of Sciences of the United States of America, 107(17), 7863–7868. https://doi.org/10.1073/pnas.0906232107

Ghosh, A., Mazarakos, K., & Zhou, H.-X. (2019). Three archetypical classes of macromolecular regulators of protein liquid–liquid phase separation. Proceedings of the National Academy of Sciences, 116(39), 19474–19483. https://doi.org/10.1073/pnas.1907849116

Goncalves, J., Bartol, T. M., Camus, C., Levet, F., Menegolla, A. P., Sejnowski, T. J., Sibarita, J.-B., Vivaudou, M., Choquet, D., & Hosy, E. (2020). Nanoscale co-organization and coactivation of AMPAR, NMDAR, and mGluR at excitatory synapses. Proceedings of the National Academy of Sciences of the United States of America, 117(25), 14503–14511. https://doi.org/10.1073/pnas.1922563117

Guo, W., Molinaro, G., Collins, K. A., Hays, S. A., Paylor, R., Worley, P. F., Szumlinski, K. K., & Huber, K. M. (2016). Selective Disruption of Metabotropic Glutamate Receptor 5-Homer Interactions Mimics Phenotypes of Fragile X Syndrome in Mice. Journal of Neuroscience, 36(7), 2131–2147. https://doi.org/10.1523/JNEUROSCI.2921-15.2016

Harris, K. M., & Weinberg, R. J. (2012). Ultrastructure of Synapses in the Mammalian Brain. Cold Spring Harbor Perspectives in Biology, 4(5), a005587. https://doi.org/10.1101/cshperspect.a005587

Heavner, W. E., Lautz, J. D., Speed, H. E., Gniffke, E. P., Immendorf, K. B., Welsh, J. P., Baertsch, N. A., & Smith, S. E. P. (2021). Remodeling of the Homer-Shank interactome mediates homeostatic plasticity. Science Signaling, 14(681), Article 681. https://doi.org/10.1126/scisignal.abd7325

Heavner, W. E., & Smith, S. E. P. (2020). Resolving the Synaptic versus Developmental Dichotomy of Autism Risk Genes. Trends in Neurosciences, 43(4), 227–241. https://doi.org/10.1016/j.tins.2020.01.009

Henry, F. E., Wang, X., Serrano, D., Perez, A. S., Carruthers, C. J. L., Stuenkel, E. L., & Sutton, M. A. (2018). A Unique Homeostatic Signaling Pathway Links Synaptic Inactivity to Postsynaptic mTORC1. Journal of Neuroscience, 38(9), 2207–2225. https://doi.org/10.1523/JNEUROSCI.1843-17.2017

Hoeffer, C. A., & Klann, E. (2010). mTOR signaling: At the crossroads of plasticity, memory and disease. Trends in Neurosciences, 33(2), 67–75. https://doi.org/10.1016/j.tins.2009.11.003

Holder, J. L., Hamdan, F. F., & Michaud, J. L. (1993). SYNGAP1-Related Intellectual Disability. In M. P. Adam, J. Feldman, G. M. Mirzaa, R. A. Pagon, S. E. Wallace, L. J. Bean, K. W. Gripp, & A. Amemiya (Eds.), GeneReviews®. University of Washington, Seattle. http://www.ncbi.nlm.nih.gov/books/NBK537721/

Holehouse, A. S., & Kragelund, B. B. (2024). The molecular basis for cellular function of intrinsically disordered protein regions. Nature Reviews Molecular Cell Biology, 25(3), 187–211. https://doi.org/10.1038/s41580-023-00673-0

Hosokawa, T., Liu, P.-W., Cai, Q., Ferreira, J. S., Levet, F., Butler, C., Sibarita, J.-B., Choquet, D., Groc, L., Hosy, E., Zhang, M., & Hayashi, Y. (2021). CaMKII activation persistently segregates postsynaptic proteins via liquid phase separation. Nature Neuroscience, 24(6), Article 6. https://doi.org/10.1038/s41593-021-00843-3

Hou, L., & Klann, E. (2004). Activation of the phosphoinositide 3-kinase-Akt-mammalian target of rapamycin signaling pathway is required for metabotropic glutamate receptor-dependent long-term depression. The Journal of Neuroscience: The Official Journal of the Society for Neuroscience, 24(28), 6352–6361. https://doi.org/10.1523/JNEUROSCI.0995-04.2004

Hruska, M., Henderson, N., Le Marchand, S. J., Jafri, H., & Dalva, M. B. (2018). Synaptic nanomodules underlie the organization and plasticity of spine synapses. Nature Neuroscience, 21(5), 671–682. https://doi.org/10.1038/s41593-018-0138-9

Hu, C., Chen, W., Myers, S. J., Yuan, H., & Traynelis, S. F. (2016). Human GRIN2B variants in neurodevelopmental disorders. Journal of Pharmacological Sciences, 132(2), 115–121. https://doi.org/10.1016/j.jphs.2016.10.002

Hu, J.-H., Park, J. M., Park, S., Xiao, B., Dehoff, M. H., Kim, S., Hayashi, T., Schwarz, M. K., Huganir, R. L., Seeburg, P. H., Linden, D. J., & Worley, P. F. (2010). Homeostatic scaling requires group I mGluR activation mediated by Homer1a. Neuron, 68(6), 1128–1142. https://doi.org/10.1016/j.neuron.2010.11.008

Huber, K. M., Gallagher, S. M., Warren, S. T., & Bear, M. F. (2002). Altered synaptic plasticity in a mouse model of fragile X mental retardation. Proceedings of the National Academy of Sciences of the United States of America, 99(11), 7746–7750. https://doi.org/10.1073/pnas.122205699

Huber, K. M., Kayser, M. S., & Bear, M. F. (2000). Role for Rapid Dendritic Protein Synthesis in Hippocampal mGluR-Dependent Long-Term Depression. Science, 288(5469), 1254–1256. https://doi.org/10.1126/science.288.5469.1254

Hyman, A. A., Weber, C. A., & Jülicher, F. (2014). Liquid-Liquid Phase Separation in Biology. Annual Review of Cell and Developmental Biology, 30(Volume 30, 2014), 39–58. https://doi.org/10.1146/annurev-cellbio-100913-013325

Inoki, K., Li, Y., Xu, T., & Guan, K.-L. (2003). Rheb GTPase is a direct target of TSC2 GAP activity and regulates mTOR signaling. Genes & Development, 17(15), 1829–1834. https://doi.org/10.1101/gad.1110003

Ivashko-Pachima, Y., Ganaiem, M., Ben-Horin-Hazak, I., Lobyntseva, A., Bellaiche, N., Fischer, I., Levy, G., Sragovich, S., Karmon, G., Giladi, E., Shazman, S., Barak, B., & Gozes, I. (2022). SH3- and actin-binding domains connect ADNP and SHANK3, revealing a fundamental shared mechanism underlying autism. Molecular Psychiatry, 27(8), 3316–3327. https://doi.org/10.1038/s41380-022-01603-w

Jaubert, P. J., Golub, M. S., Lo, Y. Y., Germann, S. L., Dehoff, M. H., Worley, P. F., Kang, S. H., Schwarz, M. K., Seeburg, P. H., & Berman, R. F. (2007). Complex, multimodal behavioral profile of the Homer1 knockout mouse. Genes, Brain, and Behavior, 6(2), 141–154. https://doi.org/10.1111/j.1601-183X.2006.00240.x

Jimenez-Gomez, A., Nguyen, M. X., & Gill, J. S. (2024). Understanding the role of AMPA receptors in autism: Insights from circuit and synapse dysfunction. Frontiers in Psychiatry, 15. https://doi.org/10.3389/fpsyt.2024.1304300

Jurado, S., Benoist, M., Lario, A., Knafo, S., Petrok, C. N., & Esteban, J. A. (2010). PTEN is recruited to the postsynaptic terminal for NMDA receptor-dependent long-term depression. The EMBO Journal, 29(16), 2827–2840. https://doi.org/10.1038/emboj.2010.160

Kellermayer, B., Ferreira, J. S., Dupuis, J., Levet, F., Grillo-Bosch, D., Bard, L., Linarès-Loyez, J., Bouchet, D., Choquet, D., Rusakov, D. A., Bon, P., Sibarita, J.-B., Cognet, L., Sainlos, M., Carvalho, A. L., & Groc, L. (2018). Differential Nanoscale Topography and Functional Role of GluN2-NMDA Receptor Subtypes at Glutamatergic Synapses. Neuron, 100(1), 106-119.e7. https://doi.org/10.1016/j.neuron.2018.09.012

Kennedy, M. B. (1997). The postsynaptic density at glutamatergic synapses. Trends in Neurosciences, 20(6), 264–268. https://doi.org/10.1016/S0166-2236(96)01033-8

Kim, E., & Sheng, M. (2004). PDZ domain proteins of synapses. Nature Reviews Neuroscience, 5(10), 771–781. https://doi.org/10.1038/nrn1517

Kiraly, D. D., Lemtiri-Chlieh, F., Levine, E. S., Mains, R. E., & Eipper, B. A. (2011). Kalirin binds the NR2B subunit of the NMDA receptor, altering its synaptic localization and function. The Journal of Neuroscience: The Official Journal of the Society for Neuroscience, 31(35), 12554–12565. https://doi.org/10.1523/JNEUROSCI.3143-11.2011

Kitano, J., Kimura, K., Yamazaki, Y., Soda, T., Shigemoto, R., Nakajima, Y., & Nakanishi, S. (2002). Tamalin, a PDZ Domain-Containing Protein, Links a Protein Complex Formation of Group 1 Metabotropic Glutamate Receptors and the Guanine Nucleotide Exchange Factor Cytohesins. Journal of Neuroscience, 22(4), 1280–1289. https://doi.org/10.1523/JNEUROSCI.22-04-01280.2002

Kurochkina, N., & Guha, U. (2012). SH3 domains: Modules of protein–protein interactions. Biophysical Reviews, 5(1), 29–39. https://doi.org/10.1007/s12551-012-0081-z

Kursula, P. (2019). Shanks—Multidomain molecular scaffolds of the postsynaptic density. Current Opinion in Structural Biology, 54, 122–128. https://doi.org/10.1016/j.sbi.2019.01.007

Lau, Y., Oamen, H. P., & Caudron, F. (2020). Protein Phase Separation during Stress Adaptation and Cellular Memory. Cells, 9(5), Article 5. https://doi.org/10.3390/cells9051302

Lenoir, M., Kufareva, I., Abagyan, R., & Overduin, M. (2015). Membrane and Protein Interactions of the Pleckstrin Homology Domain Superfamily. Membranes, 5(4), 646–663. https://doi.org/10.3390/membranes5040646

Li, B., Wang, Y., Hou, D., Song, Z., Zhang, L., Li, N., Yang, R., & Sun, P. (2023). Identification and functional characterization of de novo variant in the SYNGAP1 gene causing intellectual disability. Frontiers in Genetics, 14. https://doi.org/10.3389/fgene.2023.1270175

Li, P., Banjade, S., Cheng, H.-C., Kim, S., Chen, B., Guo, L., Llaguno, M., Hollingsworth, J. V., King, D. S., Banani, S. F., Russo, P. S., Jiang, Q.-X., Nixon, B. T., & Rosen, M. K. (2012). Phase transitions in the assembly of multivalent signalling proteins. Nature, 483(7389), 336–340. https://doi.org/10.1038/nature10879

Lin, R., Learman, L. N., Bangash, M. A., Melnikova, T., Leyder, E., Reddy, S. C., Naidoo, N., Park, J. M., Savonenko, A., & Worley, P. F. (2021). Homer1a regulates Shank3 expression and underlies behavioral vulnerability to stress in a model of Phelan-McDermid syndrome. Cell Reports, 37(7), 110014. https://doi.org/10.1016/j.celrep.2021.110014

Lipton, J. O., & Sahin, M. (2014). The Neurology of mTOR. Neuron, 84(2), 275–291. https://doi.org/10.1016/j.neuron.2014.09.034

Liu, G. Y., & Sabatini, D. M. (2020). mTOR at the nexus of nutrition, growth, ageing and disease. Nature Reviews Molecular Cell Biology, 21(4), 183–203. https://doi.org/10.1038/s41580-019-0199-y

Liu, S., Zhou, L., Yuan, H., Vieira, M., Sanz-Clemente, A., Badger, J. D., Lu, W., Traynelis, S. F., & Roche, K. W. (2017). A Rare Variant Identified Within the

GluN2B C-Terminus in a Patient with Autism Affects NMDA Receptor Surface Expression and Spine Density. The Journal of Neuroscience: The Official Journal of the Society for Neuroscience, 37(15), 4093–4102. https://doi.org/10.1523/JNEUROSCI.0827-16.2017

Lombardo, S. D., Battaglia, G., Petralia, M. C., Mangano, K., Basile, M. S., Bruno, V., Fagone, P., Bella, R., Nicoletti, F., & Cavalli, E. (2020). Transcriptomic Analysis Reveals Abnormal Expression of Prion Disease Gene Pathway in Brains from Patients with Autism Spectrum Disorders. Brain Sciences, 10(4), Article 4. https://doi.org/10.3390/brainsci10040200

Luck, K., Charbonnier, S., & Travé, G. (2012). The emerging contribution of sequence context to the specificity of protein interactions mediated by PDZ domains. FEBS Letters, 586(17), 2648–2661. https://doi.org/10.1016/j.febslet.2012.03.056

MacGillavry, H. D., Song, Y., Raghavachari, S., & Blanpied, T. A. (2013). Nanoscale scaffolding domains within the postsynaptic density concentrate synaptic AMPA receptors. Neuron, 78(4), 615–622. https://doi.org/10.1016/j.neuron.2013.03.009

Magidovich, E., Fleishman, S. J., & Yifrach, O. (2006). Intrinsically disordered C-terminal segments of voltage-activated potassium channels: A possible fishing rod-like mechanism for channel binding to scaffold proteins. Bioinformatics, 22(13), 1546–1550. https://doi.org/10.1093/bioinformatics/btl137

Malaney, P., Pathak, R. R., Xue, B., Uversky, V. N., & Davé, V. (2013). Intrinsic disorder in PTEN and its interactome confers structural plasticity and functional versatility. Scientific Reports, 3, 2035. https://doi.org/10.1038/srep02035

Milles, S., Mercadante, D., Aramburu, I. V., Jensen, M. R., Banterle, N., Koehler, C., Tyagi, S., Clarke, J., Shammas, S. L., Blackledge, M., Gräter, F., & Lemke, E. A. (2015). Plasticity of an Ultrafast Interaction between Nucleoporins and Nuclear Transport Receptors. Cell, 163(3), 734–745. https://doi.org/10.1016/j.cell.2015.09.047

Mistry, J., Chuguransky, S., Williams, L., Qureshi, M., Salazar, G. A., Sonnhammer, E. L. L., Tosatto, S. C. E., Paladin, L., Raj, S., Richardson, L. J., Finn, R. D., & Bateman, A. (2021). Pfam: The protein families database in 2021. Nucleic Acids Research, 49(D1), D412–D419. https://doi.org/10.1093/nar/gkaa913

Moses, D., Guadalupe, K., Yu, F., Flores, E., Perez, A. R., McAnelly, R., Shamoon, N. M., Kaur, G., Cuevas-Zepeda, E., Merg, A. D., Martin, E. W., Holehouse, A. S., & Sukenik, S. (2024). Structural biases in disordered proteins are prevalent in the cell. Nature Structural & Molecular Biology, 31(2), 283–292. https://doi.org/10.1038/s41594-023-01148-8

Nair, D., Hosy, E., Petersen, J. D., Constals, A., Giannone, G., Choquet, D., & Sibarita, J.-B. (2013). Super-resolution imaging reveals that AMPA receptors inside synapses are dynamically organized in nanodomains regulated by PSD95. The Journal of Neuroscience: The Official Journal of the Society for Neuroscience, 33(32), 13204–13224. https://doi.org/10.1523/JNEUROSCI.2381-12.2013

Naisbitt, S., Kim, E., Tu, J. C., Xiao, B., Sala, C., Valtschanoff, J., Weinberg, R. J., Worley, P. F., & Sheng, M. (1999). Shank, a Novel Family of Postsynaptic Density Proteins that Binds to the NMDA Receptor/PSD-95/GKAP Complex and Cortactin. Neuron, 23(3), 569–582. https://doi.org/10.1016/S0896-6273(00)80809-0

Narayanan, U., Nalavadi, V., Nakamoto, M., Thomas, G., Ceman, S., Bassell, G. J., & Warren, S. T. (2008). S6K1 Phosphorylates and Regulates Fragile X Mental Retardation Protein (FMRP) with the Neuronal Protein Synthesis-dependent Mammalian Target of Rapamycin (mTOR) Signaling Cascade. Journal of Biological Chemistry, 283(27), 18478–18482. https://doi.org/10.1074/jbc.C800055200

Niswender, C. M., & Conn, P. J. (2010). Metabotropic Glutamate Receptors: Physiology, Pharmacology, and Disease. Annual Review of Pharmacology and Toxicology, 50(Volume 50, 2010), 295–322. https://doi.org/10.1146/annurev.pharmtox.011008.145533

Nott, T. J., Petsalaki, E., Farber, P., Jervis, D., Fussner, E., Plochowietz, A., Craggs, T. D., Bazett-Jones, D. P., Pawson, T., Forman-Kay, J. D., & Baldwin, A. J. (2015). Phase Transition of a Disordered Nuage Protein Generates Environmentally Responsive Membraneless Organelles. Molecular Cell, 57(5), 936–947. https://doi.org/10.1016/j.molcel.2015.01.013

Nusser, Z., Mulvihill, E., Streit, P., & Somogyi, P. (1994). Subsynaptic segregation of metabotropic and ionotropic glutamate receptors as revealed by immunogold localization. Neuroscience, 61(3), 421–427. https://doi.org/10.1016/0306-4522(94)90421-9

Parnell, E., Shapiro, L. P., Voorn, R. A., Forrest, M. P., Jalloul, H. A., Loizzo, D. D., & Penzes, P. (2021). KALRN: A central regulator of synaptic function and synaptopathies. Gene, 768, 145306. https://doi.org/10.1016/j.gene.2020.145306

Pascoe, H. G., Gutowski, S., Chen, H., Brautigam, C. A., Chen, Z., Sternweis, P. C., & Zhang, X. (2015). Secondary PDZ domain-binding site on class B plexins enhances the affinity for PDZ–RhoGEF. Proceedings of the National Academy of Sciences of the United States of America, 112(48), 14852–14857. https://doi.org/10.1073/pnas.1508931112

Paskus, J. D., Herring, B. E., & Roche, K. W. (2020). Kalirin and Trio: RhoGEFs in Synaptic Transmission, Plasticity, and Complex Brain Disorders. Trends in Neurosciences, 43(7), 505–518. https://doi.org/10.1016/j.tins.2020.05.002

Pawson, T. (1995). Protein modules and signalling networks. Nature, 373(6515), Article 6515. https://doi.org/10.1038/373573a0

Pawson, T., & Nash, P. (2000). Protein–protein interactions define specificity in signal transduction. Genes & Development, 14(9), 1027–1047. https://doi.org/10.1101/gad.14.9.1027

Pawson, T., & Nash, P. (2003). Assembly of cell regulatory systems through protein interaction domains. Science (New York, N.Y.), 300(5618), Article 5618. https://doi.org/10.1126/science.1083653

Peça, J., Feliciano, C., Ting, J. T., Wang, W., Wells, M. F., Venkatraman, T. N., Lascola, C. D., Fu, Z., & Feng, G. (2011). Shank3 mutant mice display autistic-like behaviours and striatal dysfunction. Nature, 472(7344), 437–442. https://doi.org/10.1038/nature09965

Phair, R. D., & Misteli, T. (2000). High mobility of proteins in the mammalian cell nucleus. Nature, 404(6778), 604–609. https://doi.org/10.1038/35007077

Pontius, B. W. (1993). Close encounters: Why unstructured, polymeric domains can increase rates of specific macromolecular association. Trends in Biochemical Sciences, 18(5), 181–186. https://doi.org/10.1016/0968-0004(93)90111-y

Powis, G., Meuillet, E. J., Indarte, M., Booher, G., & Kirkpatrick, L. (2023). Pleckstrin Homology [PH] domain, structure, mechanism, and contribution to human disease. Biomedicine & Pharmacotherapy, 165, 115024. https://doi.org/10.1016/j.biopha.2023.115024

Raymond, C. R., Thompson, V. L., Tate, W. P., & Abraham, W. C. (2000). Metabotropic glutamate receptors trigger homosynaptic protein synthesis to prolong long-term potentiation. The Journal of Neuroscience: The Official Journal of the Society for Neuroscience, 20(3), 969–976. https://doi.org/10.1523/JNEUROSCI.20-03-00969.2000

Ren, R., Mayer, B. J., Cicchetti, P., & Baltimore, D. (1993). Identification of a ten-amino acid proline-rich SH3 binding site. Science (New York, N.Y.), 259(5098), 1157–1161. https://doi.org/10.1126/science.8438166

Rickles, R. J., Botfield, M. C., Weng, Z., Taylor, J. A., Green, O. M., Brugge, J. S., & Zoller, M. J. (1994). Identification of Src, Fyn, Lyn, PI3K and Abl SH3 domain ligands using phage display libraries. The EMBO Journal, 13(23), 5598–5604. https://doi.org/10.1002/j.1460-2075.1994.tb06897.x

Ronesi, J. A., Collins, K. A., Hays, S. A., Tsai, N.-P., Guo, W., Birnbaum, S. G., Hu, J.-H., Worley, P. F., Gibson, J. R., & Huber, K. M. (2012). Disrupted Homer scaffolds mediate abnormal mGluR5 function in a mouse model of fragile X syndrome. Nature Neuroscience, 15(3), 431–440. https://doi.org/10.1038/nn.3033

Salpietro, V., Dixon, C. L., Guo, H., Bello, O. D., Vandrovcova, J., Efthymiou, S., Maroofian, R., Heimer, G., Burglen, L., Valence, S., Torti, E., Hacke, M., Rankin, J., Tariq, H., Colin, E., Procaccio, V., Striano, P., Mankad, K., Lieb, A., … Houlden, H. (2019). AMPA receptor GluA2 subunit defects are a cause of neurodevelopmental disorders. Nature Communications, 10(1), 3094. https://doi.org/10.1038/s41467-019-10910-w

Satterstrom, F. K., Kosmicki, J. A., Wang, J., Breen, M. S., De Rubeis, S., An, J.-Y., Peng, M., Collins, R., Grove, J., Klei, L., Stevens, C., Reichert, J., Mulhern, M. S., Artomov, M., Gerges, S., Sheppard, B., Xu, X., Bhaduri, A., Norman, U., … Buxbaum, J. D. (2020). Large-Scale Exome Sequencing Study Implicates Both Developmental and Functional Changes in the Neurobiology of Autism. Cell, 180(3), 568-584.e23. https://doi.org/10.1016/j.cell.2019.12.036

Scheefhals, N., & MacGillavry, H. D. (2018). Functional organization of postsynaptic glutamate receptors. Molecular and Cellular Neuroscience, 91, 82–94. https://doi.org/10.1016/j.mcn.2018.05.002

Scheefhals, N., Westra, M., & MacGillavry, H. D. (2023). mGluR5 is transiently confined in perisynaptic nanodomains to shape synaptic function. Nature Communications, 14(1), 244. https://doi.org/10.1038/s41467-022-35680-w

Schuler, B., Borgia, A., Borgia, M. B., Heidarsson, P. O., Holmstrom, E. D., Nettels, D., & Sottini, A. (2020). Binding without folding—The biomolecular function of disordered polyelectrolyte complexes. Current Opinion in Structural Biology, 60, 66–76. https://doi.org/10.1016/j.sbi.2019.12.006

Shao, L., Akkari, Y., Cooley, L. D., Miller, D. T., Seifert, B. A., Wolff, D. J., Mikhail, F. M., & ACMG Laboratory Quality Assurance Committee. (2021). Chromosomal microarray analysis, including constitutional and neoplastic disease applications, 2021 revision: A technical standard of the American College of Medical Genetics and Genomics (ACMG). Genetics in Medicine: Official Journal of the American College of Medical Genetics, 23(10), 1818–1829. https://doi.org/10.1038/s41436-021-01214-w

Sheng, M., & Kim, E. (2011). The Postsynaptic Organization of Synapses. Cold Spring Harbor Perspectives in Biology, 3(12), a005678. https://doi.org/10.1101/cshperspect.a005678

Shiraishi-Yamaguchi, Y., & Furuichi, T. (2007). The Homer family proteins. Genome Biology, 8(2), 206. https://doi.org/10.1186/gb-2007-8-2-206

Singh, N., Reyes-Ordoñez, A., Compagnone, M. A., Moreno, J. F., Leslie, B. J., Ha, T., & Chen, J. (2021). Redefining the specificity of phosphoinositide-binding by human PH domain-containing proteins. Nature Communications, 12(1), 4339. https://doi.org/10.1038/s41467-021-24639-y

Sinnen, B. L., Bowen, A. B., Forte, J. S., Hiester, B. G., Crosby, K. C., Gibson, E. S., Dell'Acqua, M. L., & Kennedy, M. J. (2017). Optogenetic control of synaptic composition and function. Neuron, 93(3), 646-660.e5. https://doi.org/10.1016/j.neuron.2016.12.037

Sipeki, S., Koprivanacz, K., Takács, T., Kurilla, A., László, L., Vas, V., & Buday, L. (2021). Novel Roles of SH2 and SH3 Domains in Lipid Binding. Cells, 10(5), Article 5. https://doi.org/10.3390/cells10051191

Soden, M. E., & Chen, L. (2010). Fragile X Protein FMRP Is Required for Homeostatic Plasticity and Regulation of Synaptic Strength by Retinoic Acid. The Journal of Neuroscience, 30(50), 16910–16921. https://doi.org/10.1523/JNEUROSCI.3660-10.2010

Songyang, Z., Fanning, A. S., Fu, C., Xu, J., Marfatia, S. M., Chishti, A. H., Crompton, A., Chan, A. C., Anderson, J. M., & Cantley, L. C. (1997). Recognition of Unique Carboxyl-Terminal Motifs by Distinct PDZ Domains. Science, 275(5296), 73–77. https://doi.org/10.1126/science.275.5296.73

Sotelo, N. S., Schepens, J. T. G., Valiente, M., Hendriks, W. J. A. J., & Pulido, R. (2015). PTEN–PDZ domain interactions: Binding of PTEN to PDZ domains of PTPN13. Methods, 77–78, 147–156. https://doi.org/10.1016/j.ymeth.2014.10.017

Srinivasan, B., Samaddar, S., Mylavarapu, S. V. S., Clement, J. P., & Banerjee, S. (2021). Homeostatic scaling is driven by a translation-dependent degradation axis that recruits miRISC remodeling. PLoS Biology, 19(11), e3001432. https://doi.org/10.1371/journal.pbio.3001432

Stamenkovic, V., Lautz, J. D., Harsh, F. M., & Smith, S. E. P. (2024). SRC family kinase inhibition rescues molecular and behavioral phenotypes, but not protein interaction network dynamics, in a mouse model of Fragile X syndrome. Molecular Psychiatry, 1–14. https://doi.org/10.1038/s41380-024-02418-7

Starke, E. L., Zius, K., & Barbee, S. A. (2022). FXS causing missense mutations disrupt FMRP granule formation, dynamics, and function. PLOS Genetics, 18(2), Article 2. https://doi.org/10.1371/journal.pgen.1010084

Stiffler, M. A., Chen, J. R., Grantcharova, V. P., Lei, Y., Fuchs, D., Allen, J. E., Zaslavskaia, L. A., & MacBeath, G. (2007). PDZ domain binding selectivity is optimized across the mouse proteome. Science (New York, N.Y.), 317(5836), 364–369. https://doi.org/10.1126/science.1144592

Stillman, M., Lautz, J. D., Johnson, R. S., MacCoss, M. J., & Smith, S. E. P. (2022). Activity dependent dissociation of the Homer1 interactome. Scientific Reports, 12(1), 3207. https://doi.org/10.1038/s41598-022-07179-3

Sturgill, J. F., Steiner, P., Czervionke, B. L., & Sabatini, B. L. (2009). Distinct Domains within PSD-95 Mediate Synaptic Incorporation, Stabilization, and Activity-Dependent Trafficking. Journal of Neuroscience, 29(41), 12845–12854. https://doi.org/10.1523/JNEUROSCI.1841-09.2009

Su, X., Ditlev, J. A., Hui, E., Xing, W., Banjade, S., Okrut, J., King, D. S., Taunton, J., Rosen, M. K., & Vale, R. D. (2016). Phase separation of signaling molecules promotes T cell receptor signal transduction. Science, 352(6285), 595–599. https://doi.org/10.1126/science.aad9964

Tan, H. L., Chiu, S.-L., Zhu, Q., & Huganir, R. L. (2020). GRIP1 regulates synaptic plasticity and learning and memory. Proceedings of the National Academy of Sciences of the United States of America, 117(40), 25085–25091. https://doi.org/10.1073/pnas.2014827117

Tatavarty, V., Pacheco, A. T., Kuhnle, C. G., Lin, H., Koundinya, P., Miska, N. J., Hengen, K. B., Wagner, F. F., Hooser, S. D. V., & Turrigiano, G. G. (2020). Autism-associated Shank3 is essential for homeostatic compensation in rodent V1. Neuron, 106(5), 769-777.e4. https://doi.org/10.1016/j.neuron.2020.02.033

Teyra, J., Huang, H., Jain, S., Guan, X., Dong, A., Liu, Y., Tempel, W., Min, J., Tong, Y., Kim, P. M., Bader, G. D., & Sidhu, S. S. (2017). Comprehensive Analysis of the Human SH3 Domain Family Reveals a Wide Variety of Non-canonical Specificities. Structure, 25(10), 1598-1610.e3. https://doi.org/10.1016/j.str.2017.07.017

Tompa, P., & Fuxreiter, M. (2008). Fuzzy complexes: Polymorphism and structural disorder in protein-protein interactions. Trends in Biochemical Sciences, 33(1), 2–8. https://doi.org/10.1016/j.tibs.2007.10.003

Tsang, B., Arsenault, J., Vernon, R. M., Lin, H., Sonenberg, N., Wang, L.-Y., Bah, A., & Forman-Kay, J. D. (2019). Phosphoregulated FMRP phase separation models activity-dependent translation through bidirectional control of mRNA granule formation. Proceedings of the National Academy of Sciences, 116(10), Article 10. https://doi.org/10.1073/pnas.1814385116

Tu, J. C., Xiao, B., Naisbitt, S., Yuan, J. P., Petralia, R. S., Brakeman, P., Doan, A., Aakalu, V. K., Lanahan, A. A., Sheng, M., & Worley, P. F. (1999). Coupling of mGluR/Homer and PSD-95 Complexes by the Shank Family of Postsynaptic Density Proteins. Neuron, 23(3), 583–592. https://doi.org/10.1016/S0896-6273(00)80810-7

Tullis, J. E., Larsen, M. E., Rumian, N. L., Freund, R. K., Boxer, E. E., Brown, C. N., Coultrap, S. J., Schulman, H., Aoto, J., Dell'Acqua, M. L., & Bayer, K. U. (2023). LTP induction by structural rather than enzymatic functions of CaMKII. Nature, 621(7977), 146–153. https://doi.org/10.1038/s41586-023-06465-y

Tümer, Z., Dye, T. J., Prada, C., White-Brown, A. M., MacKenzie, A., & Levy, A. M. (1993). DLG4-Related Synaptopathy. In M. P. Adam, J. Feldman, G. M. Mirzaa, R. A. Pagon, S. E. Wallace, L. J. Bean, K. W. Gripp, & A. Amemiya (Eds.), GeneReviews®. University of Washington, Seattle. http://www.ncbi.nlm.nih.gov/books/NBK592682/

Turrigiano, G. (2012). Homeostatic synaptic plasticity: Local and global mechanisms for stabilizing neuronal function. Cold Spring Harbor Perspectives in Biology, 4(1), a005736. https://doi.org/10.1101/cshperspect.a005736

van der Lee, R., Buljan, M., Lang, B., Weatheritt, R. J., Daughdrill, G. W., Dunker, A. K., Fuxreiter, M., Gough, J., Gsponer, J., Jones, D. T., Kim, P. M., Kriwacki, R. W., Oldfield, C. J., Pappu, R. V., Tompa, P., Uversky, V. N., Wright, P. E., & Babu, M. M. (2014). Classification of Intrinsically Disordered Regions and Proteins. Chemical Reviews, 114(13), Article 13. https://doi.org/10.1021/cr400525m

Vazquez, F., & Devreotes, P. (2006). Regulation of PTEN Function as a PIP3 Gatekeeper Through Membrane Interaction. Cell Cycle, 5(14), 1523–1527. https://doi.org/10.4161/cc.5.14.3005

Vistrup-Parry, M., Chen, X., Johansen, T. L., Bach, S., Buch-Larsen, S. C., Bartling, C. R. O., Ma, C., Clemmensen, L. S., Nielsen, M. L., Zhang, M., & Strømgaard, K. (2021). Site-specific phosphorylation of PSD-95 dynamically regulates the postsynaptic density as observed by phase separation. iScience, 24(11), 103268. https://doi.org/10.1016/j.isci.2021.103268

Waites, C. L., Specht, C. G., Härtel, K., Leal-Ortiz, S., Genoux, D., Li, D., Drisdel, R. C., Jeyifous, O., Cheyne, J. E., Green, W. N., Montgomery, J. M., & Garner, C. C. (2009). Synaptic SAP97 Isoforms Regulate AMPA Receptor Dynamics and Access to Presynaptic Glutamate. Journal of Neuroscience, 29(14), 4332–4345. https://doi.org/10.1523/JNEUROSCI.4431-08.2009

Wang, Y., Lin, J., Li, J., Yan, L., Li, W., He, X., & Ma, H. (2023). Chronic Neuronal Inactivity Utilizes the mTOR-TFEB Pathway to Drive Transcription-Dependent Autophagy for Homeostatic Up-Scaling. Journal of Neuroscience, 43(15), 2631–2652. https://doi.org/10.1523/JNEUROSCI.0146-23.2023

Warnet, X. L., Bakke Krog, H., Sevillano-Quispe, O. G., Poulsen, H., & Kjaergaard, M. (2021). The C-terminal domains of the NMDA receptor: How intrinsically disordered tails affect signalling, plasticity and disease. European Journal of Neuroscience, 54(8), 6713–6739. https://doi.org/10.1111/ejn.14842

Weako, J., Jang, H., Keskin, O., Nussinov, R., & Gursoy, A. (2021). The structural basis of Akt PH domain interaction with calmodulin. Biophysical Journal, 120(10), 1994–2008. https://doi.org/10.1016/j.bpj.2021.03.018

Wicky, B. I. M., Shammas, S. L., & Clarke, J. (2017). Affinity of IDPs to their targets is modulated by ion-specific changes in kinetics and residual structure. Proceedings of the National Academy of Sciences of the United States of America, 114(37), 9882–9887. https://doi.org/10.1073/pnas.1705105114

Winden, K. D., Ebrahimi-Fakhari, D., & Sahin, M. (2018). Abnormal mTOR Activation in Autism. Annual Review of Neuroscience, 41(Volume 41, 2018), 1–23. https://doi.org/10.1146/annurev-neuro-080317-061747

Wright, P. E., & Dyson, H. J. (2015). Intrinsically disordered proteins in cellular signalling and regulation. Nature Reviews Molecular Cell Biology, 16(1), 18–29. https://doi.org/10.1038/nrm3920

Wu, S., Wang, D., Liu, J., Feng, Y., Weng, J., Li, Y., Gao, X., Liu, J., & Wang, W. (2017). The Dynamic Multisite Interactions between Two Intrinsically Disordered Proteins. Angewandte Chemie International Edition, 56(26), 7515–7519. https://doi.org/10.1002/anie.201701883

Wunderlich, L. (1999). Requirement of multiple SH3 domains of Nck for ligand binding. Cellular Signalling, 11(4), 253–262. https://doi.org/10.1016/S0898-6568(98)00054-0

Yang, L., Wei, M., Wang, Y., Zhang, J., Liu, S., Liu, M., Wang, S., Li, K., Dong, Z., & Zhang, C. (2023). Rabphilin-3A undergoes phase separation to regulate GluN2A mobility and surface clustering. Nature Communications, 14(1), 379. https://doi.org/10.1038/s41467-023-36046-6

Yang, M., Bozdagi, O., Scattoni, M. L., Wöhr, M., Roullet, F. I., Katz, A. M., Abrams, D. N., Kalikhman, D., Simon, H., Woldeyohannes, L., Zhang, J. Y., Harris, M. J., Saxena, R., Silverman, J. L., Buxbaum, J. D., & Crawley, J. N. (2012). Reduced Excitatory Neurotransmission and Mild Autism-Relevant Phenotypes in Adolescent Shank3 Null Mutant Mice. Journal of Neuroscience, 32(19), 6525–6541. https://doi.org/10.1523/JNEUROSCI.6107-11.2012

Yu, H., Chen, J. K., Feng, S., Dalgarno, D. C., Brauer, A. W., & Schrelber, S. L. (1994). Structural basis for the binding of proline-rich peptides to SH3 domains. Cell, 76(5), 933–945. https://doi.org/10.1016/0092-8674(94)90367-0

Zarrinpar, A., Bhattacharyya, R. P., & Lim, W. A. (2003). The structure and function of proline recognition domains. Science's STKE: Signal Transduction Knowledge Environment, 2003(179), RE8. https://doi.org/10.1126/stke.2003.179.re8

Zeng, M., Bai, G., & Zhang, M. (2017). Anchoring high concentrations of SynGAP at postsynaptic densities via liquid-liquid phase separation. Small GTPases, 10(4), 296–304. https://doi.org/10.1080/21541248.2017.1320350

Zeng, M., Díaz-Alonso, J., Ye, F., Chen, X., Xu, J., Ji, Z., Nicoll, R. A., & Zhang, M. (2019). Phase Separation-Mediated TARP/MAGUK Complex Condensation and AMPA Receptor Synaptic Transmission. Neuron, 104(3), 529-543.e6. https://doi.org/10.1016/j.neuron.2019.08.001

Zeng, M., Shang, Y., Araki, Y., Guo, T., Huganir, R. L., & Zhang, M. (2016). Phase Transition in Postsynaptic Densities Underlies Formation of Synaptic Complexes and Synaptic Plasticity. Cell, 166(5), 1163-1175.e12. https://doi.org/10.1016/j.cell.2016.07.008

Zhang, G., Wang, Z., Du, Z., & Zhang, H. (2018). mTOR Regulates Phase Separation of PGL Granules to Modulate Their Autophagic Degradation. Cell, 174(6), 1492-1506.e22. https://doi.org/10.1016/j.cell.2018.08.006

Zhang, J., & Diamond, J. S. (2006). Distinct perisynaptic and synaptic localization of NMDA and AMPA receptors on ganglion cells in rat retina. The Journal of Comparative Neurology, 498(6), 810–820. https://doi.org/10.1002/cne.21089

Zhou, Z., Liu, A., Xia, S., Leung, C., Qi, J., Meng, Y., Xie, W., Park, P., Collingridge, G. L., & Jia, Z. (2018). The C-terminal tails of endogenous GluA1 and GluA2

differentially contribute to hippocampal synaptic plasticity and learning. Nature Neuroscience, 21(1), 50–62. https://doi.org/10.1038/s41593-017-0030-z

Zhu, F., Shi, Q., Jiang, Y., Zhang, Y. Q., & Zhao, H. (2024). Impaired synaptic function and hyperexcitability of the pyramidal neurons in the prefrontal cortex of autism-associated Shank3 mutant dogs. Molecular Autism, 15(1), 9. https://doi.org/10.1186/s13229-024-00587-4

Zhu, P. J., Chen, C.-J., Mays, J., Stoica, L., & Costa-Mattioli, M. (2018). mTORC2, but not mTORC1, is required for hippocampal mGluR-LTD and associated behaviors. Nature Neuroscience, 21(6), 799–802. https://doi.org/10.1038/s41593-018-0156-7

Chapter 2:

Protein interaction network analysis of mTOR signaling reveals modular organization

Abstract

The mammalian target of rapamycin (mTOR) is a serine-threonine kinase that acts as a central mediator of translation, and plays important roles in cell growth, synaptic plasticity, cancer, and a wide range of developmental disorders. The signaling cascade linking lipid kinases (PI3Ks), protein kinases (AKT) and translation initiation complexes (EIFs) to mTOR has been extensively modeled, but does not fully describe mTOR system behavior. Here, we use quantitative multiplex co-immunoprecipitation to monitor a protein interaction network (PIN) composed of 300+ binary interactions among mTOR-related proteins. Using a simple model system of serum-deprived or fresh-media-fed mouse 3T3 fibroblasts, we observed extensive PIN remodeling involving 27+ individual protein interactions after one hour, despite phosphorylation changes observed after only five minutes. Using small molecule inhibitors of PI3K, AKT, mTOR, MEK and ERK, we define subsets of the PIN, termed ‘modules’, that respond differently to each inhibitor. Using primary fibroblasts from individuals with overgrowth disorders caused by pathogenic *PIK3CA* or *MTOR* variants, we find that hyperactivation of mTOR pathway components is reflected in a hyperactive PIN. Our data define a “modular” organization of the mTOR PIN in which coordinated groups of interactions respond to activation or inhibition of distinct nodes, and demonstrate that kinase inhibitors affect the modular network architecture in a complex manner, inconsistent with simple linear models of signal transduction.

Introduction:

Signal transduction networks have traditionally been modeled as linear cascades, where one protein acts upon the next in an orderly series of molecular events. Decades of research on mTOR signaling have demonstrated that signal-induced translocation of phosphoinositide 3-kinase (PI3K) phosphorylates membrane inositol PIP2 to PIP3, leading to AKT phosphorylation by the kinase PDK1 and the mTOR-containing protein complex mTORC2 (reviewed in Liu and Sabatini, 2020). Activated AKT phosphorylates TSC2, leading to TSC2 degradation and the release and disinhibition of the small GTPase Rheb. Rheb then activates mTORC1 by binding distally from the kinase site and causing a conformational change that accelerates catalysis and functionally activates mTOR kinase activity (Yang et al., 2017). Activated mTORC1 promotes initiation of cap-dependent translation and protein synthesis through the phosphorylation/activation of two related proteins, S6K1 and EIF4E binding protein (4EBP), which promotes the formation of the ribosomal complexes that initiate translation (Brunn et al., 1997; Burnett et al., 1998). In this manner, mTOR regulates the translation of hundreds of mRNA targets with a wide array of cellular functions (Masvidal et al., 2017), making mTOR a critical regulator of the life cycle of eukaryotic cells (Figure S1A).

While linear depictions of signaling networks can be conceptually useful by illustrating a hierarchy of kinase signaling, they do not accurately reflect the underlying molecular interactions of the protein interaction network (PIN); biology is not linear (Figure S1.1B, C). Rather, the protein components of signaling networks interact to form a complex network topology that includes feed-back or feed-forward loops, or cross-talk

between seemingly unrelated pathways (Mendoza et al., 2011). For example, PI3K-dependent membrane phosphorylation potentially recruits 247 human proteins that contain a plextrin homology (PH) domain (Rusten and Stenmark, 2006) (although only perhaps 10% of PH-domain containing proteins bind phosphoinositide (Lemmon, 2007)). AKT affects the phosphorylation of 100s of targets (Manning and Cantley, 2007; Wiechmann et al., 2021), including GSK3B and mSin1, an obligate component of mTORC2 (Humphrey et al., 2013). Moreover, proteins that are primarily thought of as acting at the “top” of the signaling cascade physically interact with proteins at the ‘bottom’ of the pathway, e.g. PDK1 phosphorylates p70S6 kinase directly (Pullen et al., 1998). Thus, conceptualizing mTOR signaling as a sequence of phosphorylation events may give an incomplete view of how the signal transduction network functions.

An alternative conceptual framework for modeling signal transduction relies on protein interaction networks, whose network topography is acutely post-translationally modified during signaling events. In response to environmental stimuli, coordinated groups of protein-protein interactions change their co-associations in unison, modifying the structure and function of the cellular interactome (Heavner et al., 2021; Lautz et al., 2021, 2018; Lundby et al., 2019; Smith et al., 2016). The dynamic composition of these protein complexes (Pawson and Nash, 2003), and the magnitude of their activation (Neier et al., 2019), is thought to instruct specific cellular responses. Different stimuli may engage different groups of coordinated interactions, termed “modules” (Coba et al., 2009; Lautz et al., 2018; Pawson and Nash, 2003), or engage identical modules of interactions with different intensities or kinetics (Neier et al., 2019), allowing the cell to disambiguate multiple environmental cues by activating signal transduction networks in

subtly different ways. Here, for the first time, we characterize a dynamic protein interaction network composed of mTOR-related signaling proteins by activating or inhibiting different nodes of the mTOR pathway and measuring the PIN response using quantitative multiplex co-immunoprecipitation (QMI). Our data reveal a complex network structure with extensive interactions among ‘upstream’ and ‘downstream’ components and demonstrate an unexpected modular organization in which PI3K and mTOR inhibition act on distinct groups of binary interactions spanning all levels of the linear mTOR hierarchy.

RESULTS

mTOR target selection and assay development:

QMI is an antibody-based approach that measures dynamic changes in protein interaction networks by simultaneous immunoprecipitation of multiple protein targets onto flow cytometry beads, followed by simultaneous detection using a set of fluorescently labeled “probe” antibodies that bind to different epitopes (Figure 1.1A). The median fluorescent intensity (MFI) of each IP_Probe pair is used as a proxy for the magnitude of the interaction between the IP antibody target and the probe antibody target. Experiments are run on carefully matched pairs of samples that are identical except for a recent experimental manipulation; any differences between the IP-probe data matrices are assumed to be due to acute changes in protein complexes caused by the manipulation. Extensive internal controls account for background fluorescence and differences in bead distributions between replicates, and correct for batch-to-batch variability (Brown et al., 2019; Smith et al., 2016). Critically, because multiple binary interactions are measured simultaneously, we can use network approaches such as

weighted correlation network analysis (Langfelder and Horvath, 2008) to model the behavior of multiple interactions changing in unison, which may reduce biological noise associated with single-protein measurements and reveal modules of interactions that encode features of the experimental manipulation (Brown et al., 2019; Lautz et al., 2018; Smith et al., 2016).

Targets for the mTOR antibody panel were selected based on four criteria: known relevance to mTOR signaling (Figure S1.1A), known co-associations in at least one protein complex, as listed in BioGrid, IntACT or specific literature searches (Figure S1.1B); known association with autism spectrum disorder using the SFARI Gene database (queried in 2018); and the existence of suitable, commercially available antibodies. We screened 3-5 antibodies for each target to identify two different antibodies that could simultaneously bind in the native state, and validated antibody specificity in immunoprecipitation-flow cytometry using knockout or overexpression strategies (detailed in Figure S1.2, S1.3 and Table S1.1) to identify antibody pairs that specifically recognized 17 members of the mTOR PIN in mouse and human. Since lysis buffer detergent has a strong effect on which interactions are detected (Lautz et al., 2019), we optimized detergent conditions and determined 1% Digitonin identified the largest number of interactions (Figure S1.4).

mTOR PIN kinetics following starvation/refeeding

To establish a basic framework for QMI measurement of mTOR PIN dynamics, we serum-starved NIH 3T3 cells for 12 hours to dampen constitutively active mTOR signaling, then stimulated by re-feeding with fresh media for 5, 15 or 60 minutes before lysis; controls included cells that were never starved (baseline) or starved cells that

were never re-fed (Figure 1.1A-B). Western blots showed the expected pattern of AKT phosphorylation peaking at 5 minutes and gradually diminishing over the subsequent timepoints, while phospho-S6 increased at 15 min and remained elevated at 60 min (Figure 1C-E). QMI was performed on cell lysates, resulting in a data matrix consisting of ~50-150 individual flow cytometry bead reads for each of 384 binary interactions measured, in duplicate, for each of 28 experimental total measurements, for over 2.1 x 10^6 total bead reads. The bead distributions were collapsed into a single median fluorescent intensity value (MFI) for each IP_Probe, and principal component analysis (PCA) was used to visualize the overall data structure. Starved cells clustered separately from baseline (Figure 1F), but, contrary to western blot data, after 5 or 15 minutes of re-feeding samples still overlapped with the starved condition, only resembling the baseline condition after 60 min. Correlation network analysis (Langfelder et al., 2008) of the same MFI dataset identified a single module of interactions whose behavior correlated with other interactions in the module across the 28 experimental replicates, as visualized by a topological overlap matrix (TOM) plot (Figure 1G). The eigenvector defining the overall behavior of this module, arbitrarily color-coded “red” by the analysis program, showed that its behavior was best correlated with a binary-coded hypothesis of “time since refeeding” (correlation coefficient = 0.83, $p = 4 \times 10^{-8}$) (Figure 1H), indicating a slow increase in the median scaled value of the module. No other module correlated with any experimental variables, causing us to focus on this “red” module.

To ensure reporting of only robust, high-confidence interactions, we performed a second adaptive, non-parametric statistical test corrected for multiple comparisons

(ANC, see methods). ANC does not collapse bead distributions, but instead incorporates features of the distributions and the consistency of replicates to establish interactions that change in >70% of pair-wise comparisons at a multiple-comparison-corrected P<0.05 for each interaction across the entire experiment (Brown et al., 2019; Smith et al., 2016). ANC-significant interactions that were also significantly correlated with the “red” module were considered high-confidence interactions identified by both independent tests. Twenty-seven such interactions were visualized as a row-normalized heatmap, with rows sorted by the time at which the Interaction first became significant and columns arranged by re-feeding time (Figure 1I). At five minutes, two interactions slightly increased in abundance- EIF4G_EIF4E (Figure 1J) and PIKE_TSC1 (log_2 Fold Change (log_2FC) = 0.24 and 0.19, respectively) and were significant by ANC and CNA analysis. Additionally, the apparent abundance of three targets was reduced: AKT_AKT, p70S6_ p70S6 and RICTOR_ RICTOR. Changes in apparent abundance may reflect rapid proteasomal degradation, or a change in binding partners or a post-translational modification that occludes IP or probe antibody binding. Regardless, it was striking that, despite AKT phosphorylation clearly peaking at 5 minutes (Figure 1D), the overall network at 5 minutes was essentially unchanged. By 15 minutes, the two aforementioned interactions continued to increase (log_2FC = 0.11 and 0.44, respectively), and 7 other interactions including EIF4G_RICTOR (Figure 1K), EIF4E_RICTOR and PIKE_FMRP began to increase (log_2FC = 0.28, 0.25 and 0.31, respectively). By 60 min, these interactions further increased, and 9 additional interactions reached significance, including EIF4G_AKT (Figure 1L), RICTOR_mTOR (Figure 1M) and RAPTOR_EIF4E (log_2FC = 0.39, 0.37 and 0.38, respectively). These

data represent a core network of dynamic protein interactions that acutely change following mTOR activation.

Inhibition of the mTOR pathway

To explore the relationship between a traditional linear model of mTOR signal transduction and our QMI approach, we starved cells and re-fed for 60 minutes while including one of three inhibitors of the mTOR pathway that act at different levels of the linear signaling model (Figure 1.2A). BKM120, which inhibits all four catalytic isoforms of class I PI3K in an ATP-competitive manner but does not inhibit mTOR (Maira et al., 2012), prevented the phosphorylation of both AKT and S6 by western blot, as expected (Figure 1.2B-C). RAD001 (Everolimus), which inhibits mTORC1 by forming a complex with FKBP-12 and partially occluding substrate entry into the mTORC1 active site (Yang et al., 2013), prevented S6 phosphorylation but not AKT phosphorylation, as expected. AZD5363, an ATP-competitive pan-AKT inhibitor (which also inhibits PKA and P70S6K) (Davies et al., 2012), caused an apparent increase in AKT phosphorylation and inhibited S6.

Following QMI, we independently re-calculated modules based on the new dataset using correlation network analysis. The inclusion of inhibitors in the experiment caused the “red” module identified in Figure 1.1 to fracture into three modules that correlated with different binary-coded hypotheses (Figure 1.2D). First, a module color-coded “turquoise” most strongly correlated with the hypothesis of activation across all re-fed conditions, regardless of drug (correlation coefficient = 0.55; p = 0.0002). Next, a module coded “yellow” most significantly correlated with activation during refeeding and inhibition by *all* drugs (correlation coefficient = 0.51; p = 0.0007). Finally, a module

coded “blue” most strongly correlated with activation by refeeding and inhibition by RAD only (correlation coefficient = 0.42; p = 0.007). Again, interactions correlated with each module were merged with interactions identified by the ANC statistical test, and twenty-nine significant interactions were visualized as a row-normalized heatmap, with rows ordered by module membership and columns by treatment. The “turquoise” module was activated by refeeding and partially (although not completely) inhibited by all three drugs (Figure 1.2E, top), as demonstrated by the behavior of the protein interaction most highly correlated to module behavior, PIKE_EIF4E (Figure 1.2F), and by the mean scaled value of all interactions in the module (Figure 1.2G). The yellow module, exemplified by EIF4E_TSC1 (Figure 1.2H), was increased by re-feeding, and inhibited by all drugs, most strongly BKM (Figure 1.2I). Finally, a blue module, exemplified by mTOR_Rictor (Figure 1.2J) was significantly inhibited by RAD and AZD, but surprisingly not by BKM (Figure 1.2K).

To visualize the entire network, we represented all significant interactions in a node-edge diagram, where the thickness/color of the edges indicates the magnitude/direction of the change in each binary measurement (Figure 1.2L), as well as the subset of interactions that comprise each module (Figure 1.2M-O). The poorly inhibited “turquoise” module included proteins involved at all levels of mTOR signaling, including GSK3B, PIKE, PICTOR, p70S6 and EIF4E. Partial activation of this module in the presence of all inhibitor drugs may reflect crosstalk with other signaling pathways that respond to refeeding, including GSK3B or ERK activity, which were not manipulated in this experiment. The “blue” (RAD-responsive) module contained interactions including mTOR, RAPTOR, and RICTOR that one might have expected to

be strongly inhibited by RAD, including mTOR_RAPTOR. This module was inhibited by AZD and RAD, but surprisingly, not by BKM, suggesting other parallel inputs may affect this module and can compensate for the loss of PI3K signaling. The “yellow” (inhibited) module contained the most downstream interactions, including EIF4E, EIF4G, p70S6 and FMRP. These interactions were significantly inhibited by all inhibitors, but the magnitude of inhibition was largest for BKM>RAD>AZD. In fact, AZD still permitted significant module activation. It is somewhat surprising that ‘upstream’ PI3K inhibition was so effective at targeting these ‘downstream’ interactions, despite BKM’s inability to inhibit the blue RAD-dependent module. Overall, these data demonstrate an unexpectedly complex modular organization of the mTOR PIN.

The reduction in both mTOR_Rictor and mTOR_Raptor by RAD was unexpected, since short-term treatment with RAD is thought to affect only mTORC1, and phospho-western blots showed the expected lack of effect of RAD on AKT phosphorylation (Figure 1.2C). We therefore performed co-immunoprecipitation-western blot assays on 3T3 fibroblasts treated with RAD, and confirmed a reduction of both IP:mTOR western blot:Raptor and IP:mTOR western blot:Rictor following RAD treatment (Figure S1.5). These data are consistent with previous reports showing disruption of both mTORC1 and mTORC2 protein complexes, although not necessarily AKT phosphorylation, by Rapamycin (Rosner and Hengstschläger, 2008; Sarbassov et al., 2006).

The contribution of the ERK Pathway

The failure of BKM to prevent changes in the RAD-responsive “blue” module suggested non-canonical routes of activation, i.e., crosstalk from other signal

transduction pathways. The ERK/MAPK pathway can affect mTOR signaling via inhibition of the TSC complex, as well as multi-level feedback inhibition (Mendoza et al., 2011). To observe the contribution of Erk signaling to stimulus-dependent changes in the mTOR PIN, we performed a starve-refeed experiment in the presence of three different ERK pathway inhibitors (Figure 1.3A) and confirmed their efficacy by western blot (Figure 1.3 B-E). FR180204, a selective ERK1/2 inhibitor that binds to the ATP binding pocket of ERK (Ohori et al., 2007), increased ERK phosphorylation and eliminated S6 phosphorylation while having no effect on AKT phosphorylation. Both U0126, a selective inhibitor of MEK1 and MEK2 (Favata et al., 1998), and PD98059, which binds to the inactive form of MEK and prevents its phosphorylation by RAF-1 and downstream activity (Dudley et al., 1995), inhibited ERK phosphorylation, increased AKT phosphorylation, and partially inhibited p-S6 (although U0126 was less effective than PD98059). RAD was included to delineate mTOR-dependent interactions, and inhibited S6 phosphorylation as expected while having no effect on ERK.

Following QMI, we again independently re-calculated CNA modules and identified two that correlated with experimental variables (Figure 1.3F). A “blue” RAD-responsive module (which was calculated independently from the blue module in Figure 1.2 but contained similar interactions) was increased by re-feeding and strongly inhibited by both RAD and FR180 (Figure 1.3G). The MEK inhibitors U0126 and PD98059 had an intermediate effect, as demonstrated by both the interaction most strongly correlated to the blue module, AKT_AKT (Figure 1.3G) and by the average scaled value of the module (Figure 1.3H). MEK inhibition significantly inhibited interactions compared to the re-fed/no drug condition, but not as strongly compared with

ERK or mTOR inhibition (although the difference between the starve/no drug and re-fed+drug conditions were not significant for any drug, Figure 1.3H). Of note, six interactions from the “blue” module that was independently identified in Figure 1.2, including mTOR_Raptor, were also included in this module. Overall, these data show strong inhibition of the blue module by both RAD and ERK inhibitors.

A second, yellow module (again derived independently from, but containing similar interaction to, the yellow module in Figure 1.2), contained a set of interactions that were inhibited in unexpectedly different ways by our drug panel. Exemplified by EIF4G_Raptor (Figure 1.3I), this module showed strong inhibition by FR180, which reduced activity significantly lower than the starved condition (Figure 1.3J). RAD and PD98059 significantly inhibited the activation of the yellow module compared to re-feeding alone, although RAD was still significantly increased over the starved state. Surprisingly, MEK inhibition with U0126 had no effect on yellow module activation. The yellow module contained many interactions related to the EIF4 translation initiation complex and included 6 (out of 8 total) of the BKM-sensitive yellow module interactions derived independently in Figure 1.2. Thus, direct ERK inhibition was similar to PI3K inhibition, while MEK inhibition produced strikingly different results: U0126 was ineffective, while PD98059 was as effective as RAD.

Next Generation mTOR Inhibitors

Multiple generations of mTOR inhibitors have been created since the discovery of rapamycin. TORIN1 (TRN) and Sapanisertib (SAP, also referred to as INK128) are both second-generation ATP competitive small molecule inhibitors that target mTOR in both mTORC1 and mTORC2 (Gökmen-Polar et al., 2012; Liu et al., 2010). Rapalink-1 (RLK)

is a third generation mTOR inhibitor formed by physically linking rapamycin and SAP with an inert chemical linker that simultaneously forms an inhibitory complex with FKBP-12 and blocks the mTOR ATP binding site (Rodrik-Outmezguine et al., 2016). We repeated the starve/refeed paradigm in the presence of each inhibitor to directly compare their effects on the mTOR PIN.

We first determined equivalent doses of the four drugs, which we defined as the lowest concentration that inhibited phosphorylation of AKT (where applicable), RPS6, p70S6K, and 4EBP1 in a titration experiment using increasing concentrations of drug, starting at each drug's cell-free IC-50 (Figure Figure S1.6A-D). Phospho-westerns showed that the selected doses of TRN and SAP inhibited AKT phosphorylation, indicating mTORC2 inhibition, while RAD and RLK did not (Figure 1.4A-B). As expected, both RPS6 and p70S6K1 were inhibited by all drugs (Figure 1.4C-D). However, only TRN and SAP affected 4EBP1 phosphorylation, consistent with previous studies (Liu et al., 2010; Rodrik-Outmezguine et al., 2016) (Figure 1.4E). QMI identified two modules that correlated with experimental variables: a yellow module that was most significantly correlated with activation during re-feeding and inhibition by all drugs (correlation coefficient 0.56; $p = 0.0004$) and a blue module that most significantly correlated with activation during re-feeding but inhibition by SAP (correlation coefficient -0.43; $p = 0.003$) or RLK treatment (correlation coefficient 0.41; $p = 0.04$) (Figure 1.4F). The thirty-two significant interactions identified by ANC and CNA were visualized as a row normalized heatmap (Figure 1.4G). The yellow module was composed of primarily EIF4E/EIF4G/p70S6 interactions, indicating changes in translation-related protein complexes downstream of mTOR. These interactions were increased by re-feeding,

inhibited by RAD, and strongly inhibited by next generation mTOR inhibitors such that the averaged scaled value of the module was lower than in the starved condition (Figure 1.4H,I). These data demonstrate that next generation mTOR inhibitors are significantly more efficient at mTOR inhibition compared to either RAD or overnight serum starvation.

The blue module was composed of mTOR complex interactions similar to those observed in the blue module in Figure 1.2 (which responded to RAD but not to BKM), including mTOR_Raptor and mTOR_Rictor. These interactions were strongly suppressed by both RAD and RLK, weakly suppressed by TRN, and not altered by SAP (Figure 1.4J,K). These data reflect a key difference in the mechanism of action between RAD-derived and ATP-competitive inhibitors: the former bind to FKBP12 and physically disrupt mTOR substrate accessibility (Yang et al., 2013), while latter bind the ATP binding site and inhibit mTOR in the absence of protein complex disruption.

Hyperactivating mutations drive mTOR PIN activation

As a central regulator of cellular growth, the mTOR pathway is implicated in several human overgrowth disorders, including Tuberous Sclerosis, *PTEN* hamartoma tumor syndrome, Megalencephaly-capillary malformation syndrome, Focal Cortical Dysplasia, and hemimegaencephaly. Among the common pathogenic variants associated with these neurodevelopmental disorders, sometimes referred to as ‘mTORopathies” (reviewed in Karalis and Bateup, 2021), are mutations of *PIK3CA* or *MTOR*. The *PIK3CA* p.H1047R variant is the most common hyperactivating mutation in the catalytic p110 subunit of the PI3K holoenzyme that renders it resistant to inhibition by the p85 regulatory subunit, increasing basal PI3K activity (D’Gama et al., 2015; Gymnopoulos et

al., 2007). The *MTOR* p.T1977I variant is a highly recurrent hyperactivating mutation in the FAT domain of mTOR, adjacent to the kinase domain, which may promote accessibility of substrates to the kinase domain (G. M. Mirzaa et al., 2016). We obtained fibroblasts from two individuals with overgrowth who had mutations in *PIK3CA*^{H1047R} (1y/o male) and *MTOR*^{T1977I} (13y/o female), as well as two unrelated healthy controls (4 y/o male and 9y/o female). While the cells were taken from genetically mosaic individuals, the mutant cells have an increased growth rate compared to wildtype cells (Mirzaa et al., 2016; Samuels et al., 2005), so the variable (mutant) allele frequency, measured by digital droplet PCR, was 49.9% for the PIKC3A mutant and 39.7% for the *MTOR* mutant, indicating 100% and 80% heterozygous mutant cells, respectively (Figure S1.7). Cells were serum starved for twelve hours and lysed immediately or stimulated with fresh serum-containing media for one hour before lysis. Western blot showed that the PIK3CA mutant fibroblasts displayed hyperphosphorylation of AKT and S6 during starvation (Figure 1.5A-C), while the mTOR mutant fibroblasts did not display any significant deficits in phosphorylation, consistent with previous reports (Di Donato et al., 2016; Grabiner et al., 2014).

Following QMI, we used ANC and CNA to independently identify two modules that correlated with refeeding (Figure 1.5D). A brown module, exemplified by mTOR_Rictor, was significantly elevated in re-fed control and *MTOR*^{T1977I} cells (compared to same-genotype starved cells), and trended towards significance in *PIK3CA*^{H1047R} cells (Figure 1.5E). There were no differences between genotypes in the starved or refed conditions. In contrast, a pink module, exemplified by EIF4G_EIF4E, was elevated in all comparisons tested (Figure 1.5F); not only did re-feeding increase

module intensity compared to unstarved cells within-genotype, but comparisons of starved or re-fed mutant cells to starved or refed control cells were significantly elevated. PIK3CA^{H1047R} fibroblasts showed greater elevation than did MTOR^{T1977I} fibroblasts. These data are consistent with clinical data suggesting that strongly activating variants in PIK3CA are associated with more severe overgrowth than MTOR (Pirozzi et al., 2022). Specifically, the PIK3CA H1047R variant has been associated with severe somatic or brain overgrowth phenotypes including focal cortical dysplasia with severe epilepsy (G. Mirzaa et al., 2016), whereas the MTOR T1977I variant is associated with megalencephaly and polymicrogyria and overall less severe epilepsy (G. M. Mirzaa et al., 2016). Notably, our analysis did not identify additional interaction modules that were associated with hyperactivating mutations independently of re-feeding, indicating that nutrient status and hyperactivating mutations affected a similar set of protein complexes.

Drug treatment of mutant fibroblasts

Most therapeutic approaches utilized for the ‘mTORopathies” focus on Rapamycin and its analogues, regardless of the location of the variant in the linear mTOR cascade (Karalis and Bateup, 2021; Nguyen and Bordey, 2021). However, given our results demonstrating differential regulation of the mTOR PIN by drugs targeting mTOR vs PI3K, we reasoned that a more targeted approach may improve network-scale rescue. We treated control, PIK3CA^{H1047R} and mTOR^{T1977I} fibroblasts with BKM or RAD to inhibit PI3K or mTORC1, respectively. Western blots from the starved samples for pAKT revealed control and mTOR^{T1977I} fibroblasts had low levels of p-AKT, while PIK3CA^{H1047R} had elevated basal p-AKT. BKM normalized pAKT in PIK3CA^{H1047R} fibroblasts, while

RAD did not affect pAKT levels (Figure 1.5G-H). PIK3CA^{H1047R} and mTOR^{T1977I} fibroblasts showed elevated S6 phosphorylation, which was reduced following BKM and RAD treatment (Figure 1.5I). QMI, performed with a smaller antibody panel due to technical limitations, identified a turquoise module, exemplified by EIF4G_EIF4E, which was significantly elevated in both starved and re-fed PIK3CA^{H1047R} fibroblasts (Figure S1.8A,B). We graphed the average scaled value of the turquoise module for starved (Figure 1.5J) or re-fed cells (Figure 1.5K). For starved cells, we observed a significant increase in module activation in mTOR^{T1977I} and PIK3CA^{H1047R} fibroblasts compared to controls (Figure 1.5J). This increase was normalized by both BKM and RAD treatment in *mTOR*^{T1977I} fibroblasts, and by BKM treatment in *PIK3CA*^{H1047R} fibroblasts; note, however, that RAD did not rescue hyperactivation in starved *PIK3CA*^{H1047R} fibroblasts (Figure 1.5J). For the re-fed condition, all mutant lines were hyperactive compared to control, and both mTOR-modifying drugs were ineffective, except for *mTOR*^{T1977I} fibroblasts treated with BKM (Figure 1.5K). These data suggest that drugs targeted to specific mutations may be more effective than generic treatment with rapamycin.

Discussion:

We developed a QMI panel targeted to key protein nodes in the mTOR pathway that allows direct measurement of mTOR PIN dynamics during signaling events, and we defined a PIN that is acutely modified by mTOR signaling. Following re-feeding with serum-derived growth factors, we observed a single module of coordinated protein-protein interactions that gradually increased over the course of an hour. Drugs targeting different nodes of the mTOR network, or drugs targeting mTOR using different mechanisms, altered complex sets of interactions (i.e. modules) that were not predicted

by a linear pathway model. QMI offers an alternative way to characterize the mTOR signal transduction network, traditionally observed via changes in phosphorylation events, and allows access to a new level of biological complexity in the dynamic protein interactome.

Kinetics of the mTOR PIN

In previous studies using QMI to monitor the T cell receptor signalosome and the glutamatergic synapse interactome (Lautz et al., 2021; Smith et al., 2016), peak signalosome activation occurred ~5 minutes after stimulus presentation. Similarly, data presented here (Figure 1.1B-D) and in the literature (Rahman and Haugh, 2017) suggest phosphorylation of AKT peaks ~5 minutes after stimulus presentation, and downstream activation of S6 peaks ~15 minutes. However, QMI observed virtually no PIN response at 5 minutes, and only a small, partial response at 15 minutes, with peak response not occurring for at least an hour. Additionally, the mTOR network still did not recover to its pre-starvation state even after an hour-long response. These data imply that changes in phosphorylation status are slow to translate into changes in protein complexes, which is unexpected because changes in the phosphorylation status of interacting proteins are thought to be directly responsible for changes in protein-protein interactions. For downstream interactions such as EIF4E_EIF4G, which represent the final transcriptional output of the mTOR system, this delay could be explained by a slow rate of signal progression through a linear cascade. However, for more upstream interactions such as RICTOR_mTOR (representing MTORC2) or PIKE_TSC1, the reason for the slow kinetics is unclear. Future work to reconcile the slow rate of network modification with the much faster rate of phosphorylation is warranted.

Linear vs. Network models of drug specificity

By adding different small molecule inhibitors of mTOR pathway nodes, we were able to fracture the single module of co-regulated interactions that responded to refeeding into two main modules of interactions, blue and yellow, that responded differently to each type of inhibition. We summarize the modules that we identified throughout this study in Figure 1.6. We expected that the modular organization of the network would follow the traditional linear model, with BKM inhibiting all modules, RAD inhibiting the fewest number of modules, and AZD being intermediate. Moreover, we expected Rapalogs and next-generation mTOR inhibitors to produce qualitatively similar changes to interaction modules, even if the magnitude of inhibition was different. Surprisingly, the modules did not follow this pattern.

The yellow “downstream" module was inhibited by all drugs except U01, and most strongly by BKM and the next generation mTOR inhibitors. It is somewhat counterintuitive that BKM produced stronger inhibition than RAD in head-to-head studies, since the yellow module contains interactions among the most downstream proteins (EIF4E and G, p70S6, and FMRP). Given that phosphorylation of p70S6 is mediated by both mTOR and PDK1 (Pullen et al., 1998), it is possible that BKM, by inhibiting PDK1 downstream of PI3K, provides double-inhibition not seen in AZD and RAD. It is also possible that ATP-competitive inhibitors like BKM, SAP and TOR provide more complete kinase inhibition compared to RAD. Indeed, next-generation inhibitors are known to more completely inhibit mTORC1 and mTORC2 compared to rapamycin derivatives (as evidenced by 4EBP1 and AKT phosphorylation), and are more effective at inhibiting the growth of cancer cells *in vitro* and in mouse models (Gökmen-Polar et

al., 2012; Liu et al., 2010; Rodrik-Outmezguine et al., 2016). Moreover, it has been suggested some mTOR signaling is RAD-resistant, but may be inhibited amino acid starvation (Peng et al., 2002), perhaps leading to a network state that resembles our next-generation mTOR inhibitor data. Future work comparing amino acid starvation to next-generation mTOR signaling may be warranted. Overall, these data suggest that the yellow module is a core mTOR-dependent readout, that is more effectively inhibited by ATP-competitive kinase inhibition of PI3K or mTOR than by Rapalogs.

The blue module is more difficult to interpret. This module was inhibited by RAD, AZD and ERK inhibition, and weakly inhibited by MEK inhibition, which suggests that mTOR signaling downstream of both AKT and ERK may mediate module behavior. However, PI3K inhibition and mTOR kinase inhibition by SAP were completely ineffective at preventing blue module activation, and mTOR kinase inhibition by TRN was weak, especially compared to the magnitude of TRN yellow module inhibition. Moreover, the ratio of inhibition of the blue module compared to the yellow module was different for each drug; for example ERK inhibition with FR1 produced equal inhibition of each module, AKT inhibition with AZD produced stronger inhibition of the blue module, and mTOR inhibition with TRN produced stronger inhibition of the yellow module.

Perhaps these differences reflect uncharacterized off-target effects on other relevant kinases, or are due to uncharacterized feedback loops or other non-linear relationships among the mTOR network. For example, inhibiting MEK with U01 vs PD9 produced strikingly different patterns of PIN inhibition. PD9 was less effective at inhibiting ERK phosphorylation by western blot compared to U01, but was much more effective at inhibiting “yellow” module interactions containing EIF4E/G and FMRP.

Despite sharing a mutually exclusive binding site on MEK, and despite U0126 binding with a 100-fold higher affinity to MEK (Favata et al., 1998), U0126 failed to inhibit the yellow module. While both PD98059 and U0126 have known off-target (i.e. non-MEK-mediated) effects, for example, activating AMP-activated protein kinase (Dokladda et al., 2005) or Kinase Suppressor of RAS (KSR-1) (Wang and Studzinski, 2001), these off-target effects are thought to be similar for both drugs. Similarly, the next-generation mTOR inhibitor experiments identified clear differences in “blue” module inhibition between TRN and SAP, which also function through similar ATP-competitive mechanisms. These data are reminiscent of a recent phospho-mass spectrometry study comparing 5 different AKT inhibitors, which showed only limited overlap: of 1700 altered phospho-peptides, only 276 were perturbed by all 5 compounds (Wiechmann 2021). The strikingly different effects of the inhibitor drugs on the mTOR PIN highlights the emerging concept that “specific” inhibitor drugs are often not very specific at all. A potential advantage of QMI-based network measurements is that they can highlight differences between inhibitor drugs better than traditional phospho-western readouts.

Correcting pathogenic network hyperactivity

The human patient fibroblast model gives us the ability to observe how a chronically overactive member of the mTOR cascade contributes to the response of the PIN. Hyperactivity at the top of the mTOR pathway, at PI3K, produced more robust differences than further downstream at mTOR, consistent with BKM vs. RAD inhibitor data, as well as with clinical data showing more severe phenotypes in patients with PI3K vs mTOR mutations (G. Mirzaa et al., 2016). PI3K and mTOR mutations did not produce novel PIN states; rather, they increased the fluorescent intensity of the

interactions that composed the stimulation-responsive module in both the starved and re-fed states compared to wildtype. Importantly, we did not identify modules that correlated with the presence of a mutation, independent of starvation/refeeding, which would have indicated changes to the mTOR network independent of nutrient sensing. These data imply that simple inhibition of signaling may normalize the dynamic range of the system. Indeed, BKM was able to normalize PI3K hyperactivation, and RAD and BKM were both able to normalize mTOR hyperactivity. However, RAD was not able to normalize the hyperactive network state produced by PI3K mutation, likely because PI3K has direct links to downstream signaling nodes that bypass mTOR, as demonstrated also by the BKM inhibition data. Future experiments should focus on how mTOR inhibitors might affect mTOR network hyperactivation at more physiologically relevant states, outside of the context of serum-starvation, since the effect of hyperactivation in non-physiological starvation conditions that may not be fully applicable to an untreated condition.

This result, while somewhat intuitive, speaks directly to clinical trials occurring in overgrowth disorders, cancer, or ASD-related mTOR-opathies. Ongoing translational research is attempting to correct upstream mutations in PI3K (Byeon et al., 2020; Parker et al., 2019), PTEN (Schmid et al., 2014), or TSC (Krueger et al., 2017; Overwater et al., 2019) with rapamycin or its analogs, with mixed outcomes. Perhaps this treatment strategy, based on linear models implying upstream effects filter through mTORC1, ignores the complexity of the pathway. Our data, as well as recent work correcting PI3K-dependent (Roy et al., 2021) or TSC2-dependent (Nguyen et al., 2022)

epilepsies with more targeted drugs, imply that direct correction of a hyperactive node may be more effective than the simple use of rapalogs for all mTOR pathway disorders.

Limitations

A general limitation of QMI is that it measures the epitope-specific binding of commercially available antibodies, so differences in fluorescent signal may be due to differences in the targeted protein-protein interaction, or due occlusion of an antibody binding site by an unknown protein joining a complex. While we validated some interactions by IP-western blotting, the sensitivity of QMI exceeds that of IP-westerns (Smith et al., 2012). Thus, while the overall behavior of modules observed by QMI is robust, the behavior of any specific interaction may require further validation.

A second limitation of this study is that the inhibitors used to block specific kinases may have affected other kinases whose inhibition may have contributed to the observed changes in the mTOR PIN. With the exception of the next-generation mTOR inhibitor experiments, we used single concentrations of drugs based on previously published reports, so we cannot rule out off-target effects. Future work using genetic knockouts or knockdown of mTOR components could address these limitations, but also presents further difficulties due to the requirement of mTOR signaling for growth and cell cycle, as well as due to extensive feedback loops within the mTOR network.

Finally, we focused on a single starve-refeed paradigm, while other avenues exist to either activate (i.e. growth factor stimulation) or inhibit (i.e. amino acid starvation) the network. Future experiments using QMI to more fully characterize the mTOR signal transduction network could further disentangle the complex relationships

between experimental manipulations and the response of the mTOR signal transduction network.

Experimental Procedures:

Cell Culture – NIH 3T3 mouse fibroblasts were acquired from the American Type Culture Collection. The cells were cultured at 37° C at 5% CO2 in Dulbecco's modified Eagle's medium supplemented with 10% fetal bovine serum, 1 % non-essential amino acids [Gibco-11140],1% GlutaMax [Gibco-35050], and 1 % penicillin and streptomycin.

Patient derived fibroblast were obtained from punch biopsies of affected children enrolled in the IRB-approved developmental brain disorders research program at Seattle Childrens' Research Institute. Fibroblasts were cultured at 37° C at 5% CO2 in Dulbecco's modified Eagle's medium with nutrient mixture F-12 (Gibco-11330) and supplemented with 15% fetal bovine serum, 1 % non-essential amino acids [Gibco-11140],1% GlutaMax [Gibco-35050], and 1 % penicillin and streptomycin. ddPCR was performed on validated probes using a QX200 ddPCR system following the manufacturer's instructions, as detailed in (Pirozzi et al., 2022).

Antibodies and Other Reagents – The following antibodies for the purpose of western blotting were acquired from Cell Signaling Technologies: pAKT S473 (Catalog number 4060), PAN-AKT (#2920), Phospho-p44/42 MAPK (#4370), p44/42 MAPK (#4695), S6 Ribosomal Protein (#2317), Phospho-S6 Ribosomal Protein (#4858), Phospho-p70S6 Kinase Thr389 (#97596), p70S6 Kinase (#9202), Phospho-4EBP1 Thr37/46 (#2855), 4EBP1 (#9452). Antibodies against Beta-Actin were purchased from GeneTex (catalog number 109639). MAPK inhibitors were purchased from Tocris: FR180204 (catalog number 3706), U0126 (catalog number 1144), PD980595 (catalog number 1213). Sapanisertib (Cat# HY-13328) and Rapalink-1 (Cat# HY-111373) were purchased from MedChem Express. Torin-1 (Cat #4247) was purchased from Tocris. PI3K/AKT/mTOR

inhibitors BKM120 (Buparlisib; Novartis, Switzerland), AZD5363 (Capivasertib; Selleckchem, USA), and RAD001 (Everolimus, Chem Express Cat# 159351-69-6) were generously provided by Dr. Kathleen Millen.

Serum Starvation, Stimulation, Drug Treatment, and Lysate Preparation - Fibroblast cultures were grown to ~70-80% confluence in 10-cm dishes or 6-well plates and were serum starved for 12 hours. During pharmacological inhibition experiments, inhibitors were added at the eleventh hour of starvation. After starvation, cells were re-fed with fresh media. Inhibitors were present during re-feeding in the respective experiments. Inhibitors were used at the following concentrations: BKM120 (2 uM), AZD5363 (1 uM), RAD001 (40 nM), FR180204 (100 uM), U0126 (25 uM), PD980595 (50 uM), TORIN1 (40 nM), Sapanisertib (125 nM), and Rapalink-1 (10 nM). Media was removed, and cells were washed in PBS and scraped on ice with ice cold lysis buffer [1% Digitonin, 150 mM NaCl, 50 mM Tris (pH 7.4), 10 mM NaF, 2 mM sodium orthovanadate, protease inhibitor cocktail (Sigma-Aldrich), and phosphatase inhibitor cocktail (Sigma-Aldrich)] and transferred to a centrifuge tube. After fifteen minutes of incubation on ice, samples were centrifuged at high speed for fifteen minutes to remove nuclei and debris. The protein concentration of the lysate was determined with a Bradford assay (Pierce).

Quantitative Multiplex Immunoprecipitation - QMI was performed as described previously (Brown et al., 2019). A master mix containing each antibody-coupled Luminex bead was prepared and distributed to lysates normalized for protein concentration. Samples were incubated overnight at 4°C on a rotator. The following day, samples were washed in cold FlyP buffer [50 mM tris (pH7.4), 100 mM NaCl, 1% bovine serum albumin, and 0.02% sodium azide] and distributed into twice as many wells of a

96-well plate as there were probe antibodies for technical replicates. Biotinylated probe antibodies were added and the plate was incubated at 4°C with gentle agitation for one hour. The resulting complexes were washed three times with FlyP buffer on an automatic plate washer. The samples were then incubated for thirty minutes with streptavidin-phycoerythrin at 4°C with gentle agitation. Samples were washed three times again and resuspended in 120 ul of cold FlyP buffer and processed with a customized refrigerated Bio-Plex 200.

Adaptive nonparametric analysis with an empirical alpha cutoff (ANC) - Statistically significant differences in bead distributions between conditions for each of ~400 individual interactions, after correcting for multiple comparisons, were identified using ANC as described in previous work (Brown et al., 2019; Smith et al., 2016). Any Interaction that was found to be significant by an ANC comparison was considered a "hit."

Correlation Network Analysis (CNA) - Modules of Interactions that covaried with experimental conditions were identified using weighted correlation network analysis (Langfelder and Horvath, 2008) as described in previous work (Brown et al., 2019; Smith et al., 2016). Bead distributions used in ANC were collapsed and the median fluorescent intensity (MFI) value was averaged across technical replicates for input into the WGCNA package for R. Interactions with an MFI less than 100 were removed as noise, and batch effects were corrected using COMBAT (Leek et al., 2012). Power values giving the approximation of scale-free topology were determined using soft thresholding with a power adjacency function, and modules were determined by the TOM matrix function in WGCNA. Modules whose eigenvectors were correlated with an

experimental trait ($P < 0.05$) were of interest. Interactions whose probability of membership in a module of interest was ($P < 0.05$) were considered “hits”. Interaction that were “hits” by both ANC and CNA for a given experimental condition were considered high confidence interactions affected in that condition.

Hierarchical Clustering and PCA - Post-COMBAT, $\log_2$ transformed MFI values were clustered using the hclust function in R with a correlation distance matrix and average clustering method. Approximately unbiased (AU) P values were determined using the pvclust package in R. PCA was performed using the prcomp function in R.

Statistical Analysis. For western blot quantification, intensity was quantified in ImageJ (NIH) and values were input into Prism (Graphpad). Student’s T tests were used for comparisons between two groups, and one-way ANOVA followed by multiple-comparison-corrected pairwise comparisons using the Sidak method was used for comparisons between multiple groups.

Acknowledgements:

We thank the people who generously donated knockout cell lines or lysates for use as negative antibody controls: Drs. Andrew Hsieh, David Sabatini, David Kwiatkowski, Paul Titchenell and Paul Monga. We would also like to thank Dr. Kathleen Millen for providing reagents and insight, including editing the manuscript; Dr. Filomena Pirozzi for sharing insights regarding experimental design, protocols and troubleshooting of patient-derived fibroblast experiments, and Dr. Smita Yadav for thoughtful discussions. This work was supported by grants MH113545 and MH121487 (SEPS), Jordan’s Guardian Angels (G.M.M), the Sunderland Foundation (G.M.M) and the Brotman Baty

Institute (G.M.M. and D.T.W). Special gratitude to Barbara and Eric Mann for their support of our research (G.M.M.), as well as well as all donors to Seattle Children's Research Institute who invest in breakthrough discoveries that help prevent, treat, and eliminate childhood disease. The authors declare no conflicts of interest.

Publication Citation: Wehle, D. T., Bass, C. S., Sulc, J., Mirzaa, G., & Smith, S. E. P. (2023). Protein interaction network analysis of mTOR signaling reveals modular organization. *Journal of Biological Chemistry*, *299*(11), 105271. https://doi.org/10.1016/j.jbc.2023.105271

Author Contributions: Devin T Wehle (DTW) DTW and Stephen EP Smith (SEPS) designed the study. DTW and Carter S Bass (CSB) performed all experiments. Josef Sulc (JS) characterized the patient-derived mutant fibroblasts. Ghayda M Mirzaa (GMM) obtained the fibroblasts and assisted with the design and analysis of all experiments performed on patient-derived cell lines. DTW, JS, GMM and SEPS analyzed data. DTW and SEPS wrote the manuscript. All authors read and approved the manuscript.

Data Availability Statement: All data necessary to evaluate the conclusions presented in the manuscript are contained within the manuscript and the supplementary data files. Original raw QMI data files are available upon request from Dr. Smith (seps@uw.edu).

References:

Brown EA, Neier SC, Neuhauser C, Schrum AG, Smith SEP. 2019. Quantification of Protein Interaction Network Dynamics using Multiplexed Co-Immunoprecipitation. *JoVE (Journal of Visualized Experiments)* e60029. doi:10.3791/60029

Brunn GJ, Hudson CC, Sekulić A, Williams JM, Hosoi H, Houghton PJ, Lawrence JC, Abraham RT. 1997. Phosphorylation of the translational repressor PHAS-I by the mammalian target of rapamycin. *Science* **277**:99–101. doi:10.1126/science.277.5322.99

Burnett PE, Barrow RK, Cohen NA, Snyder SH, Sabatini DM. 1998. RAFT1 phosphorylation of the translational regulators p70 S6 kinase and 4E-BP1. *Proceedings of the National Academy of Sciences* **95**:1432–1437. doi:10.1073/pnas.95.4.1432

Byeon S, Kang MJ, Choi YJ, Kim YJ, Kim M, Yun J, Yi SY, Kim JY, Kim ST, Lee J. 2020. Antitumor activity and safety of sirolimus for solid tumors with PIK3CA mutations: A multicenter, open-label, prospective single-arm study (KM 02-01, KCSG UN17-16). *Transl Cancer Res* **9**:3222–3230. doi:10.21037/tcr.2020.04.07

Coba MP, Pocklington AJ, Collins MO, Kopanitsa MV, Uren RT, Swamy S, Croning MDR, Choudhary JS, Grant SGN. 2009. Neurotransmitters Drive Combinatorial Multistate Postsynaptic Density Networks. *Sci Signal* **2**:ra19. doi:10.1126/scisignal.2000102

Davies BR, Greenwood H, Dudley P, Crafter C, Yu D-H, Zhang J, Li J, Gao B, Ji Q, Maynard J, Ricketts S-A, Cross D, Cosulich S, Chresta CC, Page K, Yates J, Lane C, Watson R, Luke R, Ogilvie D, Pass M. 2012. Preclinical pharmacology of AZD5363, an inhibitor of AKT: pharmacodynamics, antitumor activity, and correlation of monotherapy activity with genetic background. *Mol Cancer Ther* **11**:873–887. doi:10.1158/1535-7163.MCT-11-0824-T

D'Gama AM, Geng Y, Couto JA, Martin B, Boyle EA, LaCoursiere CM, Hossain A, Hatem NE, Barry BJ, Kwiatkowski DJ, Vinters HV, Barkovich AJ, Shendure J, Mathern GW, Walsh CA, Poduri A. 2015. Mammalian target of rapamycin pathway mutations cause hemimegalencephaly and focal cortical dysplasia. *Ann Neurol* **77**:720–725. doi:10.1002/ana.24357

Di Donato N, Rump A, Mirzaa GM, Alcantara D, Oliver A, Schrock E, Dobyns WB, O'Driscoll M. 2016. Identification and Characterization of a Novel Constitutional PIK3CA Mutation in a Child Lacking the Typical Segmental Overgrowth of "PIK3CA-Related Overgrowth Spectrum." *Hum Mutat* **37**:242–245. doi:10.1002/humu.22933

Dokladda K, Green KA, Pan DA, Hardie DG. 2005. PD98059 and U0126 activate AMP-activated protein kinase by increasing the cellular AMP:ATP ratio and not via inhibition of the MAP kinase pathway. *FEBS Lett* **579**:236–240. doi:10.1016/j.febslet.2004.11.084

Dudley DT, Pang L, Decker SJ, Bridges AJ, Saltiel AR. 1995. A synthetic inhibitor of the mitogen-activated protein kinase cascade. *Proceedings of the National Academy of Sciences* **92**:7686–7689. doi:10.1073/pnas.92.17.7686

Favata MF, Horiuchi KY, Manos EJ, Daulerio AJ, Stradley DA, Feeser WS, Van Dyk DE, Pitts WJ, Earl RA, Hobbs F, Copeland RA, Magolda RL, Scherle PA,

Trzaskos JM. 1998. Identification of a novel inhibitor of mitogen-activated protein kinase kinase. *J Biol Chem* **273**:18623–18632. doi:10.1074/jbc.273.29.18623
Gökmen-Polar Y, Liu Y, Toroni RA, Sanders KL, Mehta R, Badve S, Rommel C, Sledge GW. 2012. Investigational drug MLN0128, a novel TORC1/2 inhibitor, demonstrates potent oral antitumor activity in human breast cancer xenograft models. *Breast Cancer Res Treat* **136**:673–682. doi:10.1007/s10549-012-2298-8
Grabiner BC, Nardi V, Birsoy K, Possemato R, Shen K, Sinha S, Jordan A, Beck AH, Sabatini DM. 2014. A Diverse Array of Cancer-Associated MTOR Mutations Are Hyperactivating and Can Predict Rapamycin Sensitivity. *Cancer Discovery* **4**:554–563. doi:10.1158/2159-8290.CD-13-0929
Gymnopoulos M, Elsliger M-A, Vogt PK. 2007. Rare cancer-specific mutations in PIK3CA show gain of function. *Proc Natl Acad Sci U S A* **104**:5569–5574. doi:10.1073/pnas.0701005104
Heavner WE, Lautz JD, Speed HE, Gniffke EP, Immendorf KB, Welsh JP, Baertsch NA, Smith SEP. 2021. Remodeling of the Homer-Shank interactome mediates homeostatic plasticity. *Sci Signal* **14**:eabd7325. doi:10.1126/scisignal.abd7325
Humphrey SJ, Yang G, Yang P, Fazakerley DJ, Stöckli J, Yang JY, James DE. 2013. Dynamic Adipocyte Phosphoproteome Reveals that Akt Directly Regulates mTORC2. *Cell Metabolism* **17**:1009–1020. doi:10.1016/j.cmet.2013.04.010
Karalis V, Bateup HS. 2021. Current Approaches and Future Directions for the Treatment of mTORopathies. *Dev Neurosci* **43**:143–158. doi:10.1159/000515672
Krueger DA, Sadhwani A, Byars AW, de Vries PJ, Franz DN, Whittemore VH, Filip-Dhima R, Murray D, Kapur K, Sahin M. 2017. Everolimus for treatment of tuberous sclerosis complex-associated neuropsychiatric disorders. *Ann Clin Transl Neurol* **4**:877–887. doi:10.1002/acn3.494
Langfelder P, Horvath S. 2008. WGCNA: an R package for weighted correlation network analysis. *BMC Bioinformatics* **9**:559. doi:10.1186/1471-2105-9-559
Lautz JD, Brown EA, Williams VanSchoiack AA, Smith SEP. 2018. Synaptic activity induces input-specific rearrangements in a targeted synaptic protein interaction network. *Journal of Neurochemistry* **146**:540–559. doi:10.1111/jnc.14466
Lautz JD, Gniffke EP, Brown EA, Immendorf KB, Mendel RD, Smith SEP. 2019. Activity-dependent changes in synaptic protein complex composition are consistent in different detergents despite differential solubility. *Sci Rep* **9**:10890. doi:10.1038/s41598-019-46690-y
Lautz JD, Tsegay KB, Zhu Z, Gniffke EP, Welsh JP, Smith SEP. 2021. Synaptic protein interaction networks encode experience by assuming stimulus-specific and brain-region-specific states. *Cell Rep* **37**:110076. doi:10.1016/j.celrep.2021.110076
Leek JT, Johnson WE, Parker HS, Jaffe AE, Storey JD. 2012. The sva package for removing batch effects and other unwanted variation in high-throughput experiments. *Bioinformatics* **28**:882–883. doi:10.1093/bioinformatics/bts034
Lemmon MA. 2007. Pleckstrin homology (PH) domains and phosphoinositides. *Biochem Soc Symp* 81–93. doi:10.1042/BSS0740081
Liu GY, Sabatini DM. 2020. mTOR at the nexus of nutrition, growth, ageing and disease. *Nat Rev Mol Cell Biol* **21**:183–203. doi:10.1038/s41580-019-0199-y
Liu Q, Chang JW, Wang J, Kang SA, Thoreen CC, Markhard A, Hur W, Zhang J, Sim T, Sabatini DM, Gray NS. 2010. Discovery of 1-(4-(4-Propionylpiperazin-1-yl)-3-

(trifluoromethyl)phenyl)-9-(quinolin-3-yl)benzo[h][1,6]naphthyridin-2(1H)-one as a Highly Potent, Selective Mammalian Target of Rapamycin (mTOR) Inhibitor for the Treatment of Cancer. *J Med Chem* **53**:7146–7155. doi:10.1021/jm101144f

Lundby A, Franciosa G, Emdal KB, Refsgaard JC, Gnosa SP, Bekker-Jensen DB, Secher A, Maurya SR, Paul I, Mendez BL, Kelstrup CD, Francavilla C, Kveiborg M, Montoya G, Jensen LJ, Olsen JV. 2019. Oncogenic Mutations Rewire Signaling Pathways by Switching Protein Recruitment to Phosphotyrosine Sites. *Cell* **179**:543-560.e26. doi:10.1016/j.cell.2019.09.008

Maira S-M, Pecchi S, Huang A, Burger M, Knapp M, Sterker D, Schnell C, Guthy D, Nagel T, Wiesmann M, Brachmann S, Fritsch C, Dorsch M, Chène P, Shoemaker K, De Pover A, Menezes D, Martiny-Baron G, Fabbro D, Wilson CJ, Schlegel R, Hofmann F, García-Echeverría C, Sellers WR, Voliva CF. 2012. Identification and characterization of NVP-BKM120, an orally available pan-class I PI3-kinase inhibitor. *Mol Cancer Ther* **11**:317–328. doi:10.1158/1535-7163.MCT-11-0474

Manning BD, Cantley LC. 2007. AKT/PKB Signaling: Navigating Downstream. *Cell* **129**:1261–1274. doi:10.1016/j.cell.2007.06.009

Masvidal L, Hulea L, Furic L, Topisirovic I, Larsson O. 2017. mTOR-sensitive translation: Cleared fog reveals more trees. *RNA Biol* **14**:1299–1305. doi:10.1080/15476286.2017.1290041

Mendoza MC, Er EE, Blenis J. 2011. The Ras-ERK and PI3K-mTOR pathways: cross-talk and compensation. *Trends in Biochemical Sciences* **36**:320–328. doi:10.1016/j.tibs.2011.03.006

Mirzaa G, Timms AE, Conti V, Boyle EA, Girisha KM, Martin B, Kircher M, Olds C, Juusola J, Collins S, Park K, Carter M, Glass I, Krägeloh-Mann I, Chitayat D, Parikh AS, Bradshaw R, Torti E, Braddock S, Burke L, Ghedia S, Stephan M, Stewart F, Prasad C, Napier M, Saitta S, Straussberg R, Gabbett M, O'Connor BC, Keegan CE, Yin LJ, Lai AHM, Martin N, McKinnon M, Addor M-C, Boccuto L, Schwartz CE, Lanoel A, Conway RL, Devriendt K, Tatton-Brown K, Pierpont ME, Painter M, Worgan L, Reggin J, Hennekam R, Tsuchiya K, Pritchard CC, Aracena M, Gripp KW, Cordisco M, Van Esch H, Garavelli L, Curry C, Goriely A, Kayserilli H, Shendure J, Graham J, Guerrini R, Dobyns WB. 2016. PIK3CA-associated developmental disorders exhibit distinct classes of mutations with variable expression and tissue distribution. *JCI Insight* **1**:87623. doi:10.1172/jci.insight.87623

Mirzaa GM, Campbell CD, Solovieff N, Goold C, Jansen LA, Menon S, Timms AE, Conti V, Biag JD, Adams C, Boyle EA, Collins S, Ishak G, Poliachik S, Girisha KM, Yeung KS, Chung BHY, Rahikkala E, Gunter SA, McDaniel SS, Macmurdo CF, Bernstein JA, Martin B, Leary R, Mahan S, Liu S, Weaver M, Doerschner M, Jhangiani S, Muzny DM, Boerwinkle E, Gibbs RA, Lupski JR, Shendure J, Saneto RP, Novotny EJ, Wilson CJ, Sellers WR, Morrissey M, Hevner RF, Ojemann JG, Guerrini R, Murphy LO, Winckler W, Dobyns WB. 2016. Association of MTOR Mutations With Developmental Brain Disorders, Including Megalencephaly, Focal Cortical Dysplasia, and Pigmentary Mosaicism. *JAMA Neurol* **73**:836–845. doi:10.1001/jamaneurol.2016.0363

Neier SC, Ferrer A, Wilton KM, Smith SEP, Kelcher AMH, Pavelko KD, Canfield JM, Davis TR, Stiles RJ, Chen Z, McCluskey J, Burrows SR, Rossjohn J, Hebrink DM, Carmona EM, Limper AH, Kappes DJ, Wettstein PJ, Johnson AJ, Pease LR, Daniels MA, Neuhauser C, Gil D, Schrum AG. 2019. The early proximal αβ TCR signalosome specifies thymic selection outcome through a quantitative protein interaction network. *Sci Immunol* **4**:eaal2201. doi:10.1126/sciimmunol.aal2201

Nguyen LH, Bordey A. 2021. Convergent and Divergent Mechanisms of Epileptogenesis in mTORopathies. *Front Neuroanat* **15**:664695. doi:10.3389/fnana.2021.664695

Nguyen LH, Leiser SC, Song D, Brunner D, Roberds SL, Wong M, Bordey A. 2022. Inhibition of MEK-ERK signaling reduces seizures in two mouse models of tuberous sclerosis complex. *Epilepsy Res* **181**:106890. doi:10.1016/j.eplepsyres.2022.106890

Ohori M, Takeuchi M, Maruki R, Nakajima H, Miyake H. 2007. FR180204, a novel and selective inhibitor of extracellular signal-regulated kinase, ameliorates collagen-induced arthritis in mice. *Naunyn Schmiedebergs Arch Pharmacol* **374**:311–316. doi:10.1007/s00210-006-0117-7

Overwater IE, Rietman AB, Mous SE, Bindels-de Heus K, Rizopoulos D, Ten Hoopen LW, van der Vaart T, Jansen FE, Elgersma Y, Moll HA, de Wit M-CY, ENCORE Expertise Centre for Neurodevelopmental Disorders. 2019. A randomized controlled trial with everolimus for IQ and autism in tuberous sclerosis complex. *Neurology* **93**:e200–e209. doi:10.1212/WNL.0000000000007749

Parker VER, Keppler-Noreuil KM, Faivre L, Luu M, Oden NL, De Silva L, Sapp JC, Andrews K, Bardou M, Chen KY, Darling TN, Gautier E, Goldspiel BR, Hadj-Rabia S, Harris J, Kounidas G, Kumar P, Lindhurst MJ, Loffroy R, Martin L, Phan A, Rother KI, Widemann BC, Wolters PL, Coubes C, Pinson L, Willems M, Vincent-Delorme C, PROMISE Working Group, Vabres P, Semple RK, Biesecker LG. 2019. Safety and efficacy of low-dose sirolimus in the PIK3CA-related overgrowth spectrum. *Genet Med* **21**:1189–1198. doi:10.1038/s41436-018-0297-9

Pawson T, Nash P. 2003. Assembly of cell regulatory systems through protein interaction domains. *Science* **300**:445–452. doi:10.1126/science.1083653

Pirozzi F, Berkseth M, Shear R, Gonzalez L, Timms AE, Sulc J, Pao E, Oyama N, Forzano F, Conti V, Guerrini R, Doherty ES, Saitta SC, Lockwood CM, Pritchard CC, Dobyns WB, Novotny E, Wright JNN, Saneto RP, Friedman S, Hauptman J, Ojemann J, Kapur RP, Mirzaa GM. 2022. Profiling PI3K-AKT-MTOR variants in focal brain malformations reveals new insights for diagnostic care. *Brain* **145**:925–938. doi:10.1093/brain/awab376

Pullen N, Dennis PB, Andjelkovic M, Dufner A, Kozma SC, Hemmings BA, Thomas G. 1998. Phosphorylation and activation of p70s6k by PDK1. *Science* **279**:707–710. doi:10.1126/science.279.5351.707

Rahman A, Haugh JM. 2017. Kinetic Modeling and Analysis of the Akt/Mechanistic Target of Rapamycin Complex 1 (mTORC1) Signaling Axis Reveals Cooperative, Feedforward Regulation *. *Journal of Biological Chemistry* **292**:2866–2872. doi:10.1074/jbc.M116.761205

Rodrik-Outmezguine VS, Okaniwa M, Yao Z, Novotny CJ, McWhirter C, Banaji A, Won H, Wong W, Berger M, de Stanchina E, Barratt DG, Cosulich S, Klinowska T, Rosen N, Shokat KM. 2016. Overcoming mTOR resistance mutations with a new-generation mTOR inhibitor. *Nature* **534**:272–276. doi:10.1038/nature17963

Rosner M, Hengstschläger M. 2008. Cytoplasmic and nuclear distribution of the protein complexes mTORC1 and mTORC2: rapamycin triggers dephosphorylation and delocalization of the mTORC2 components rictor and sin1. *Hum Mol Genet* **17**:2934–2948. doi:10.1093/hmg/ddn192

Roy A, Han VZ, Bard AM, Wehle DT, Smith SEP, Ramirez J-M, Kalume F, Millen KJ. 2021. Suppression of PIK3CA-driven epileptiform activity by acute pathway control. *bioRxiv* 2021.03.03.433821. doi:10.1101/2021.03.03.433821

Rusten TE, Stenmark H. 2006. Analyzing phosphoinositides and their interacting proteins. *Nat Methods* **3**:251–258. doi:10.1038/nmeth867

Sarbassov DD, Ali SM, Sengupta S, Sheen J-H, Hsu PP, Bagley AF, Markhard AL, Sabatini DM. 2006. Prolonged rapamycin treatment inhibits mTORC2 assembly and Akt/PKB. *Mol Cell* **22**:159–168. doi:10.1016/j.molcel.2006.03.029

Schmid GL, Kässner F, Uhlig HH, Körner A, Kratzsch J, Händel N, Zepp F-P, Kowalzik F, Laner A, Starke S, Wilhelm FK, Schuster S, Viehweger A, Hirsch W, Kiess W, Garten A. 2014. Sirolimus treatment of severe PTEN hamartoma tumor syndrome: case report and in vitro studies. *Pediatr Res* **75**:527–534. doi:10.1038/pr.2013.246

Smith SEP, Bida AT, Davis TR, Sicotte H, Patterson SE, Gil D, Schrum AG. 2012. IP-FCM Measures Physiologic Protein-Protein Interactions Modulated by Signal Transduction and Small-Molecule Drug Inhibition. *PLOS ONE* **7**:e45722. doi:10.1371/journal.pone.0045722

Smith SEP, Neier SC, Reed BK, Davis TR, Sinnwell JP, Eckel-Passow JE, Sciallis GF, Wieland CN, Torgerson RR, Gil D, Neuhauser C, Schrum AG. 2016. Multiplex matrix network analysis of protein complexes in the human TCR signalosome. *Science Signaling* **9**:rs7–rs7. doi:10.1126/scisignal.aad7279

Wang X, Studzinski GP. 2001. Phosphorylation of raf-1 by kinase suppressor of ras is inhibited by “MEK-specific” inhibitors PD 098059 and U0126 in differentiating HL60 cells. *Exp Cell Res* **268**:294–300. doi:10.1006/excr.2001.5292

Wiechmann S, Ruprecht B, Siekmann T, Zheng R, Frejno M, Kunold E, Bajaj T, Zolg DP, Sieber SA, Gassen NC, Kuster B. 2021. Chemical Phosphoproteomics Sheds New Light on the Targets and Modes of Action of AKT Inhibitors. *ACS Chem Biol* **16**:631–641. doi:10.1021/acschembio.0c00872

Yang H, Jiang X, Li B, Yang HJ, Miller M, Yang A, Dhar A, Pavletich NP. 2017. Mechanisms of mTORC1 activation by RHEB and inhibition by PRAS40. *Nature* **552**:368–373. doi:10.1038/nature25023

Yang H, Rudge DG, Koos JD, Vaidialingam B, Yang HJ, Pavletich NP. 2013. mTOR kinase structure, mechanism and regulation. *Nature* **497**:217–223. doi:10.1038/nature12122

Figures:

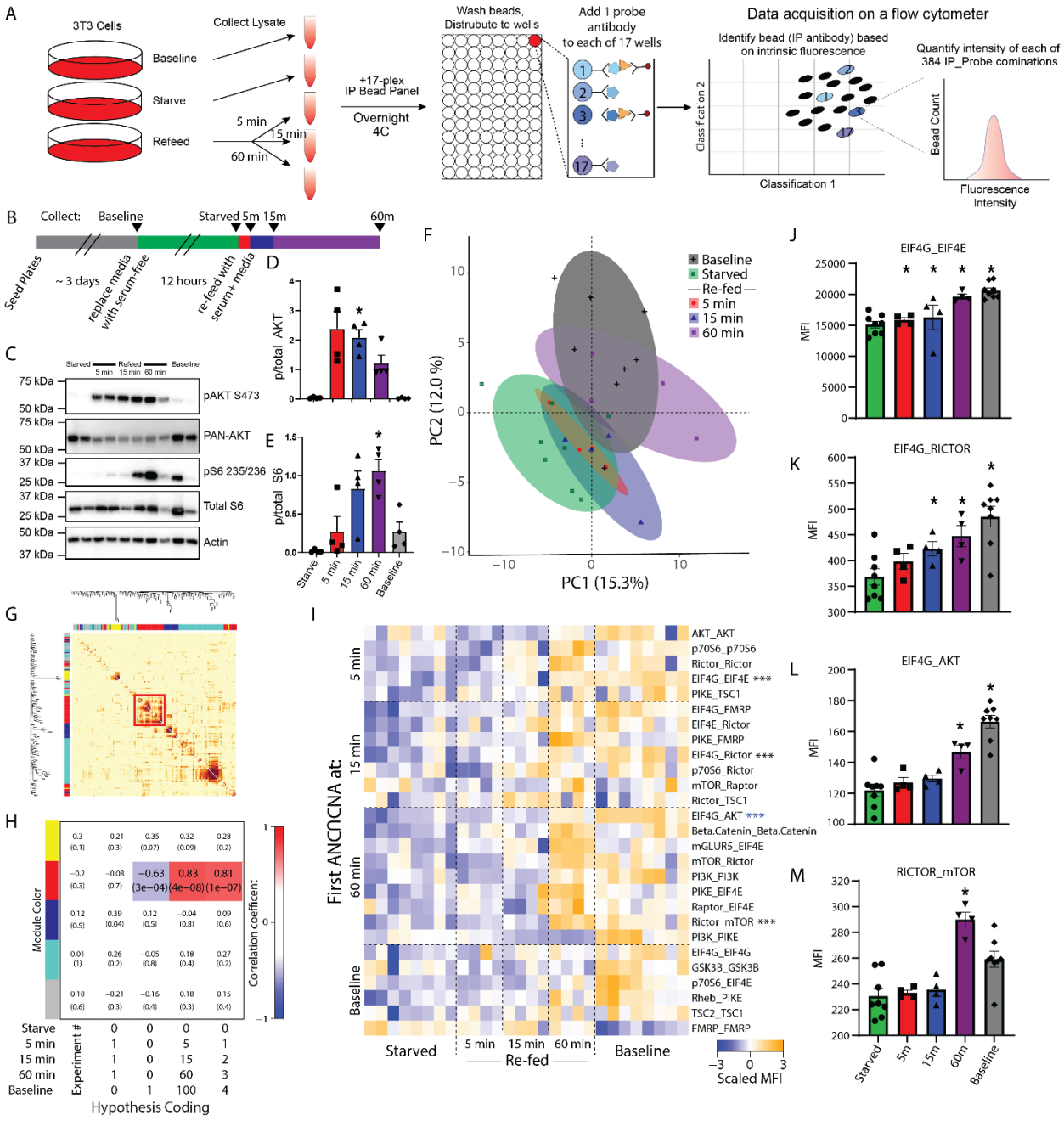

Figure 1.1: Kinetics of mTOR protein network dynamics. A) Quantitative multiplex co-immunoprecipitation (QMI) procedure. See methods for details. B) Experimental design. C) Representative western blots showing phospho- and total AKT and S6, with actin for a loading control. C-E) Quantification of blots shown in B. * indicates

significantly different from starved by ANOVA followed by Bonferroni-correction post-hoc testing, $p<0.05$. N = 4. F) Principal component graph of QMI data, N=4-8. G) Topological overlap matrix (TOM) clusters interactions into modules as indicated by the colored rectangles at top and left. Each pixel indicates the level of overlap between the interactions in the corresponding row and column, red color indicates high overlap. The significant “red” module is bounded by a red box. H) Module-trait table showing the correlation coefficient (top number) and p-value (bottom number) between the eigenvector of each color-coded module (colored rectangles at left) and binary-coded trait labels (“hypotheses”) shown in the table below. I) Heatmap of the median scaled values of all significantly altered interactions. Each box represents a single interaction measurement from a single biological replicate; columns correspond to a biological replicate while rows correspond to an interaction (IP_Probe), ordered by the timepoint that the interaction first reached significance. N = 4-8. Statistical significance calculated by ANC and CNA statistics as detailed in methods, only interactions significant by both tests are listed. *** indicates an interaction that is being represented by subsequent bar graphs. J-L) Bar graphs showing the median fluorescent intensity (MFI) of representative interactions, indicated with asterisks in H. * indicates significantly different from starved by ANC, a paired statistical test designed for QMI data.

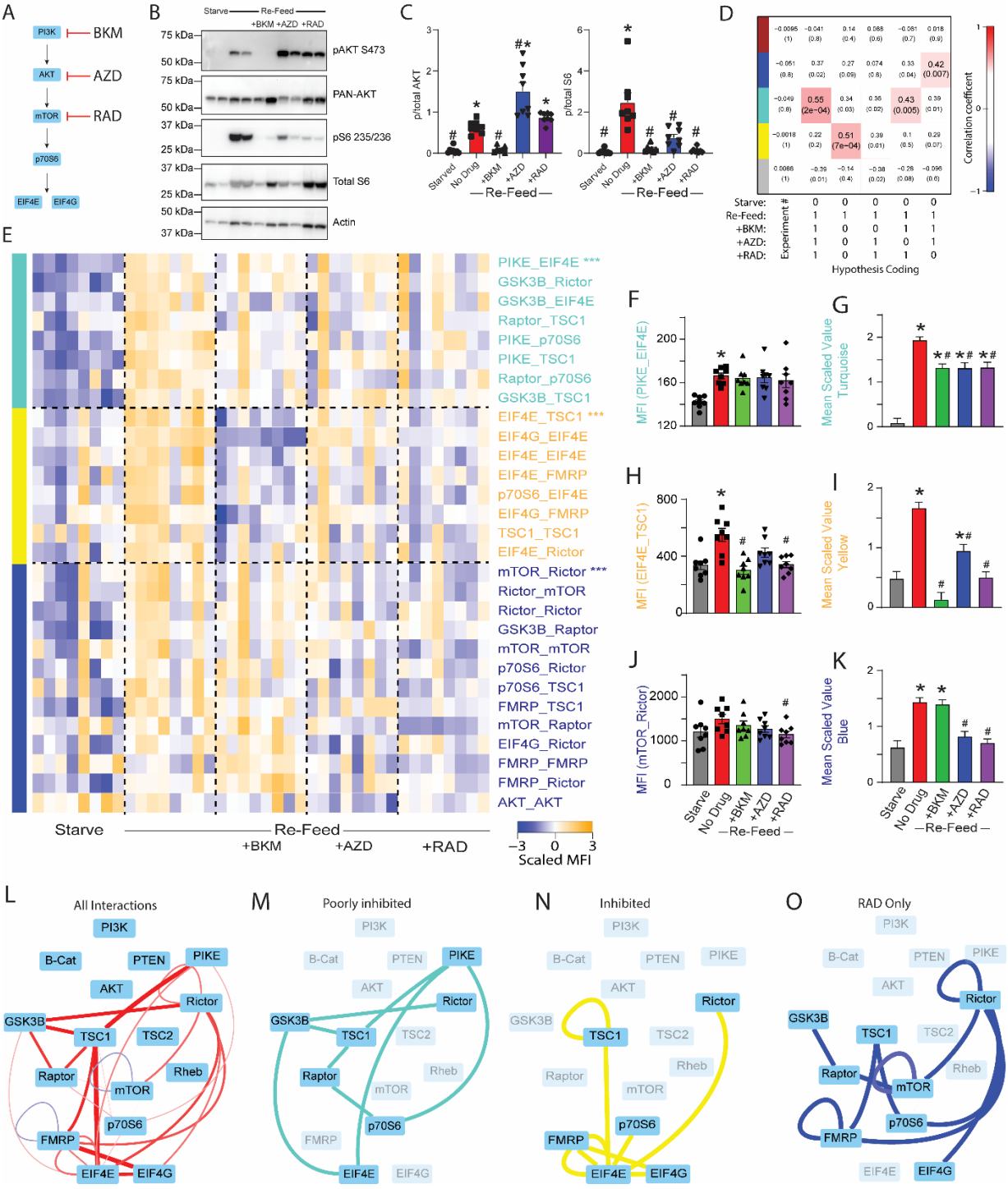

Figure 1.2: Inhibitors of PI3K/AKT/mTOR reveal modular pathway organization A) Small molecule inhibitors of PI3K/AKT/mTOR were applied during a starve-refeed experiment. B) Western blots of phospho- and total AKT and S6, and actin for loading

control, in 3T3 fibroblasts that were starved and re-fed in the presence of mTOR drugs. C) Quantification of blots in B. * indicates significantly different from starved, # indicates significantly different from re-fed by ANOVA followed by Bonferroni-corrected post-hoc testing, $p<0.05$. N=4. D) Module-trait table showing the correlation (top number) and the p-value (bottom number) between the eigenvector of each color-coded module (colored rectangles at left) and binary-coded trait labels (“hypotheses”) shown in the table below. E) Heatmap of the median scaled values of all significant interactions. Each box represents a single interaction measurement from a single biological replicate; columns correspond to a biological replicate while rows correspond to an interaction. Interactions are listed in descending order by module membership, color-coded by rectangles at left and by text color. N = 4-8. F) Median fluorescent intensity (MFI) of the interaction between PIKE_EIF4E, the interaction most correlated to turquoise module behavior. G) Mean scaled value of all interactions in the turquoise module, which corresponds to overall module behavior. H-K) Similar to F-G, but for yellow and blue modules. For F-K, * indicates significantly different from starved, # significantly different from re-fed, by ANOVA followed by Bonferroni-corrected post-hoc testing, $p<0.05$. L) Dynamic interactions that showed significant changes with re-feeding are represented by lines connecting protein nodes. Red indicates that the interaction was increased following re-feeding, blue indicates decreased; the thickness of the line indicates relative magnitude of the change. M) Interactions in the turquoise module that was partially inhibited by all drugs. N) Interactions in the yellow module that was inhibited by all drugs, most strongly by BKM. O) Interactions in the blue module that was inhibited by RAD and AZD, but not by BKM.

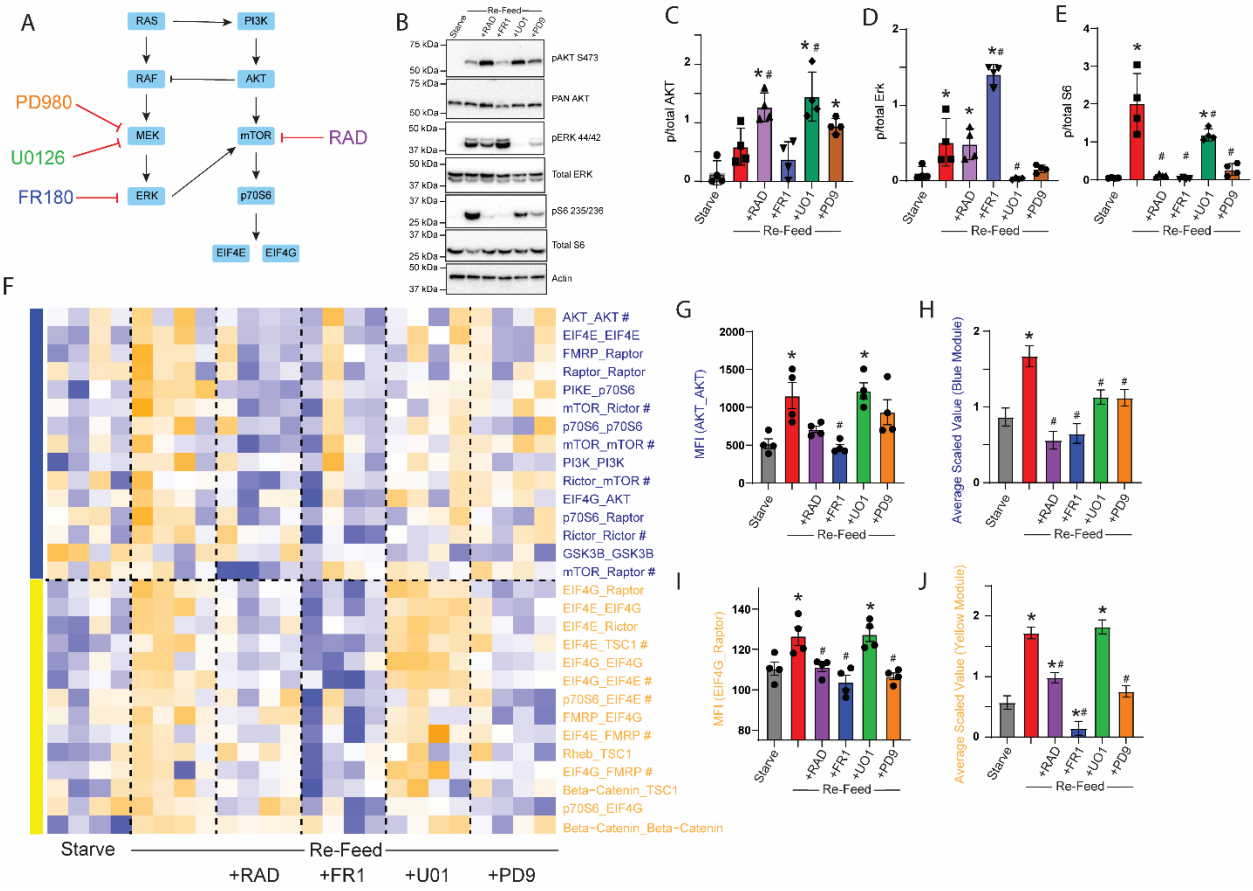

Figure 1.3: MEK and ERK inhibitors differentially affect mTOR modules A) Small molecule inhibitors of MEK, ERK or mTOR were applied during a starve-refeed experiment. B) Western blots of phospho- and total AKT, ERK and S6, and actin for loading control, in 3T3 fibroblasts that were starved and re-fed in the presence of drugs. C-E) Quantification of blots in B. * indicates significantly different from starved, # indicates significantly different from re-fed by ANOVA followed by Bonferroni-corrected post-hoc testing, $p<0.05$. N=4. F) Heatmap of the median scaled values of all significant interactions changed with re-feeding. Each box represents a single interaction measurement from a single experiment; columns correspond to an experiment while rows correspond to an interaction. N = 4. Interactions are ordered by module membership, represented by colored bars on the left, and coloring of Interaction. G)

Median fluorescent intensity (MFI) of AKT_AKT, the interaction most correlated with the blue module. H) Mean scaled value of all interactions in the blue (RAD-responsive) module, which corresponds to overall module behavior. I-J) Similar to G-H, but for the yellow module. For G-J, * indicates significantly different from starved, # significantly different from re-fed, by ANOVA followed by Bonferroni-corrected post-hoc testing, $p<0.05$.

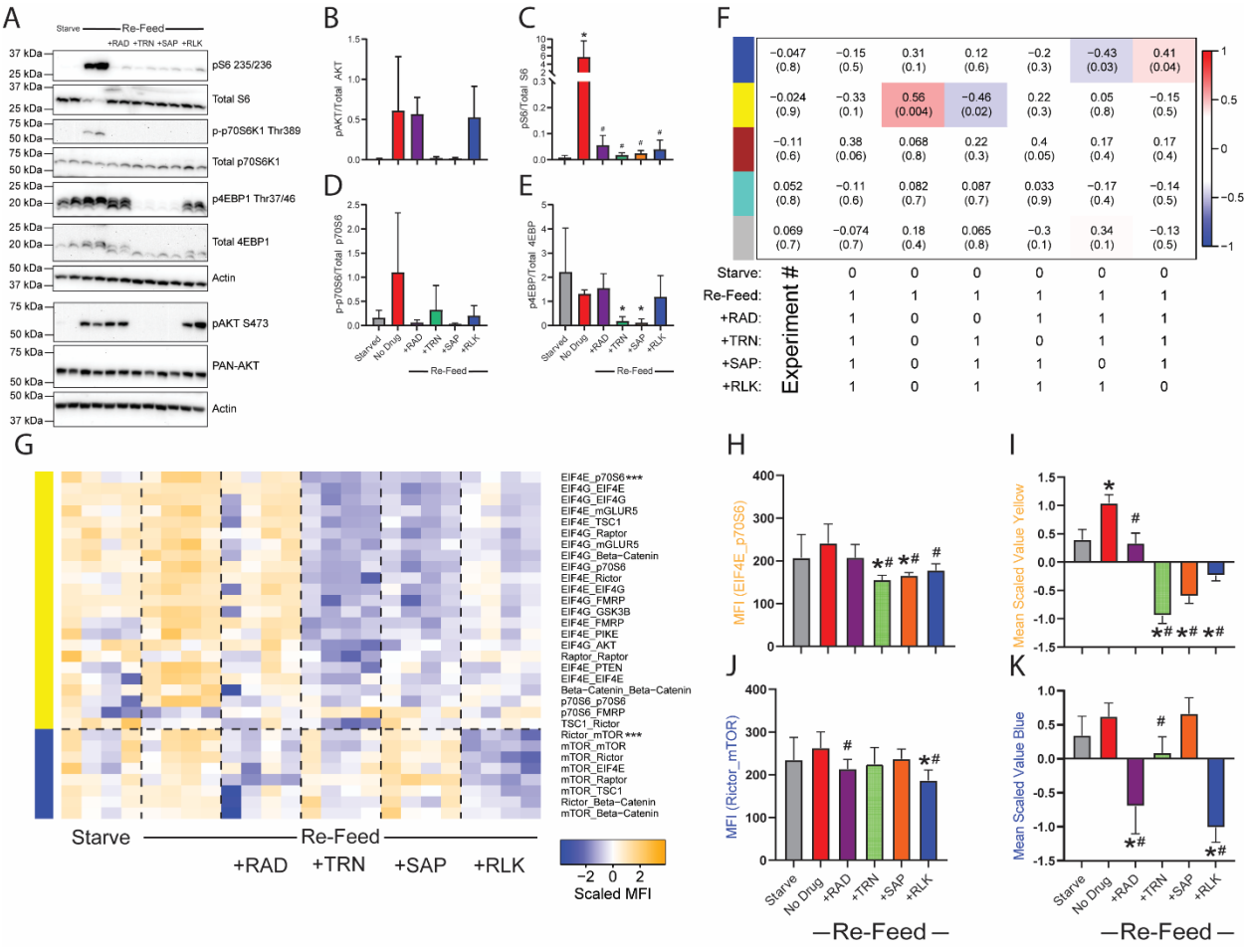

Figure 1.4: Different generations of mTOR Inhibitors differentially affect mTOR modules. A) Western blots of phospho- and total AKT, S6, p70S6K, 4EBP1 and actin for loading control, in 3T3 fibroblasts that were starved and re-fed in the presence of drugs. B-E) Quantification of blots in A. * indicates significantly different from starved, #

indicates significantly different from re-fed by ANOVA followed by Bonferroni-corrected post-hoc testing, $p<0.05$. N=4. F) Module-trait table showing the correlation (top number) and the p-value (bottom number) between the eigenvector of each color-coded module (colored rectangles at left) and binary-coded trait labels (“hypotheses”) shown in the table below. G) Heatmap of the median scaled values of all significant interactions. Each box represents a single interaction measurement from a single biological replicate; columns correspond to a biological replicate while rows correspond to an interaction. Interactions are listed in descending order by module membership, color-coded by rectangles at left and by text color. N = 4. H) Median fluorescent intensity (MFI) of the interaction between EIF4E_p70S6, the interaction most correlated to yellow module behavior. I) Mean scaled value of all interactions in the yellow module, which corresponds to overall module behavior. J-K) Similar to H-I, but the blue modules. For H-K, * indicates significantly different from starved, # significantly different from re-fed, by ANOVA followed by Bonferroni-corrected post-hoc testing, $p<0.05$.

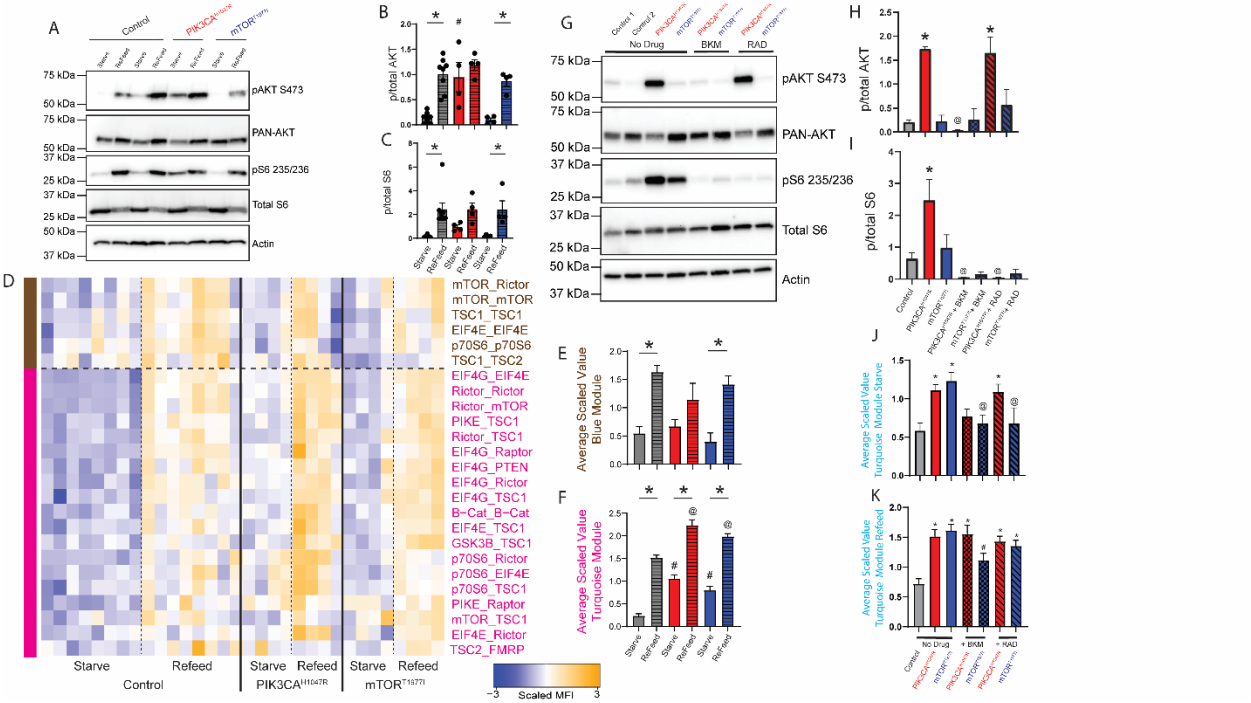

Figure 1.5: Activating mutations rescued by targeted drugs. Patient derived human fibroblasts with *PIK3CA*^{H1047R} and *mTOR*^{T1977I} gain of function mutations underwent a starve-refeed treatment. A) Representative western blots of phospho- and total AKT and S6, and actin for loading control. B-C) Quantification of blots in B. * indicates significantly different from starved within-genotype, # indicates significantly different from control-starved, by ANOVA followed by Bonferroni-corrected post-hoc testing, $p<0.05$. D) Heatmap of the median scaled values of all significant interactions. Each box represents a single interaction measurement from a single experiment; columns correspond to an experiment while rows correspond to an interaction. N = 4-8. Interactions are ordered by module, represented by colored bars on the left, and coloring of text. E) Mean scaled value of all interactions in the brown module. F) Mean scaled value of all interactions in the pink module. For E-F, * indicates significantly different from starved within-genotype, # significantly different from control-starved, and

@ significantly different from control-refed, by ANOVA followed by Bonferroni-corrected post-hoc testing, $p<0.05$. G) Following starvation, patient-derived fibroblasts were treated with BKM120 or RAD001 during the re-feed period. Representative western blots of starved samples phospho- and total AKT and S6, and actin for loading control. H-I) Quantification of blots in B. * indicates significantly different from control, @ indicates significantly different from no-drug condition within-genotype, by ANOVA followed by Bonferroni-corrected post-hoc testing, $p<0.05$. J) Mean scaled value of all interactions in the turquoise module for starved, drug-treated patient fibroblasts. * indicates significantly different from control, @ indicates significantly different from no-drug condition within-genotype, by ANOVA followed by Bonferroni-corrected post-hoc testing, $p<0.05$. K) Mean scaled value of all interactions in the turquoise module for re-fed, drug-treated patient fibroblasts, similar to Figure 1.6J. * indicates significantly different from control, # indicates significantly different from no-drug condition within-genotype, by ANOVA followed by Bonferroni-corrected post-hoc testing, $p<0.05$. N=4-8.

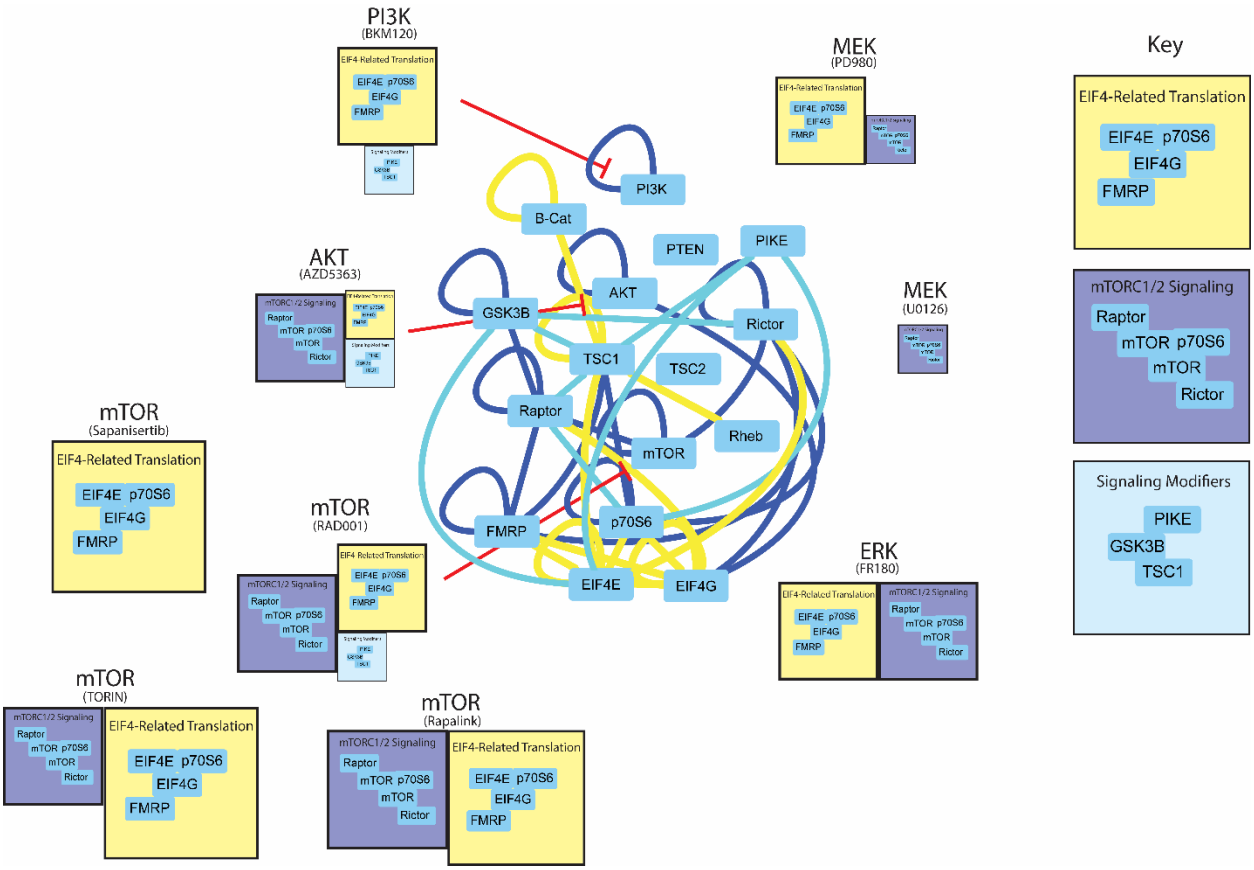

Figure 1.6: Modular organization of the mTOR PIN. Node-edge diagram represents all significant interactions that changed with re-feeding during the mTOR and ERK inhibitor experiments (Figure 1.2, 3, and 4). Edge color indicates the assigned module of each interaction. The boxes below each drug target indicate the modules that were inhibited by the drug; the size of the box corresponds to the intensity of inhibition, and the content of all similarly-colored boxes is consistent throughout.

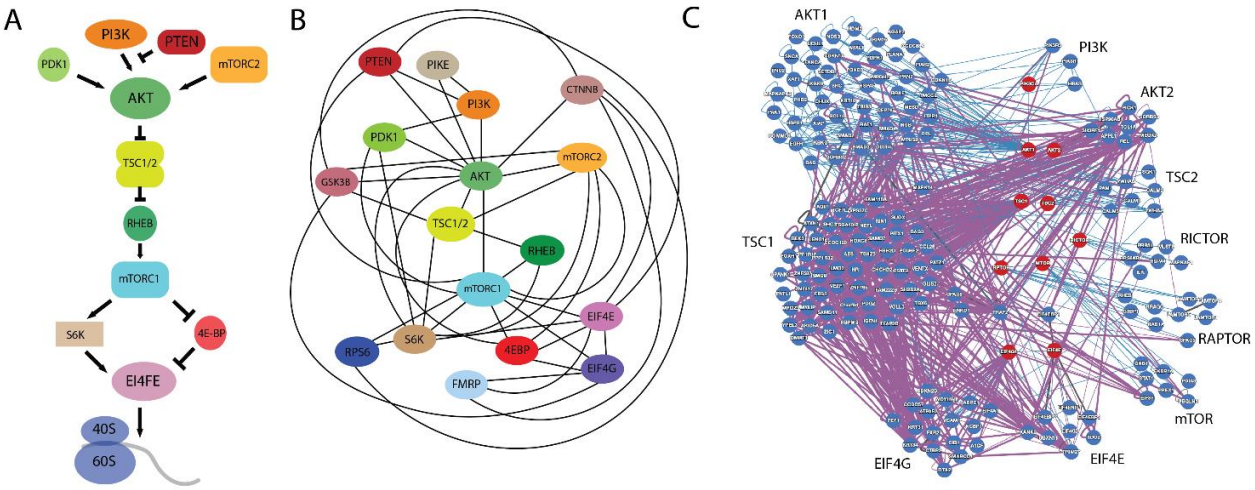

Figure S1.1: Linear vs. Network modeling of mTOR signal transduction. A) A linear model highlights how each node of the mTOR network affects the next in a simple, organized “cascade”. Arrows indicate activation, lines indicate inhibition. B) Known protein-protein interactions in human or mouse cell lines among members of the mTOR signal transduction network, as listed in BioGrid and String databases. The nodes shown are the proteins selected for inclusion in the mTOR QMI panel, lines indicate a documented physical interaction. C) Protein-protein interactions in the Human Reference Interactome database (Luck et al., 2020), based on yeast 2-hybrid screening in immortalized human cells. Red nodes are queried members of the mTOR linear pathway, blue nodes are first-degree interactors, and edges indicate all documented binary interactions between the protein nodes shown. Red nodes are arranged by pathway hierarchy, blue nodes are clustered by interaction partner as labeled.

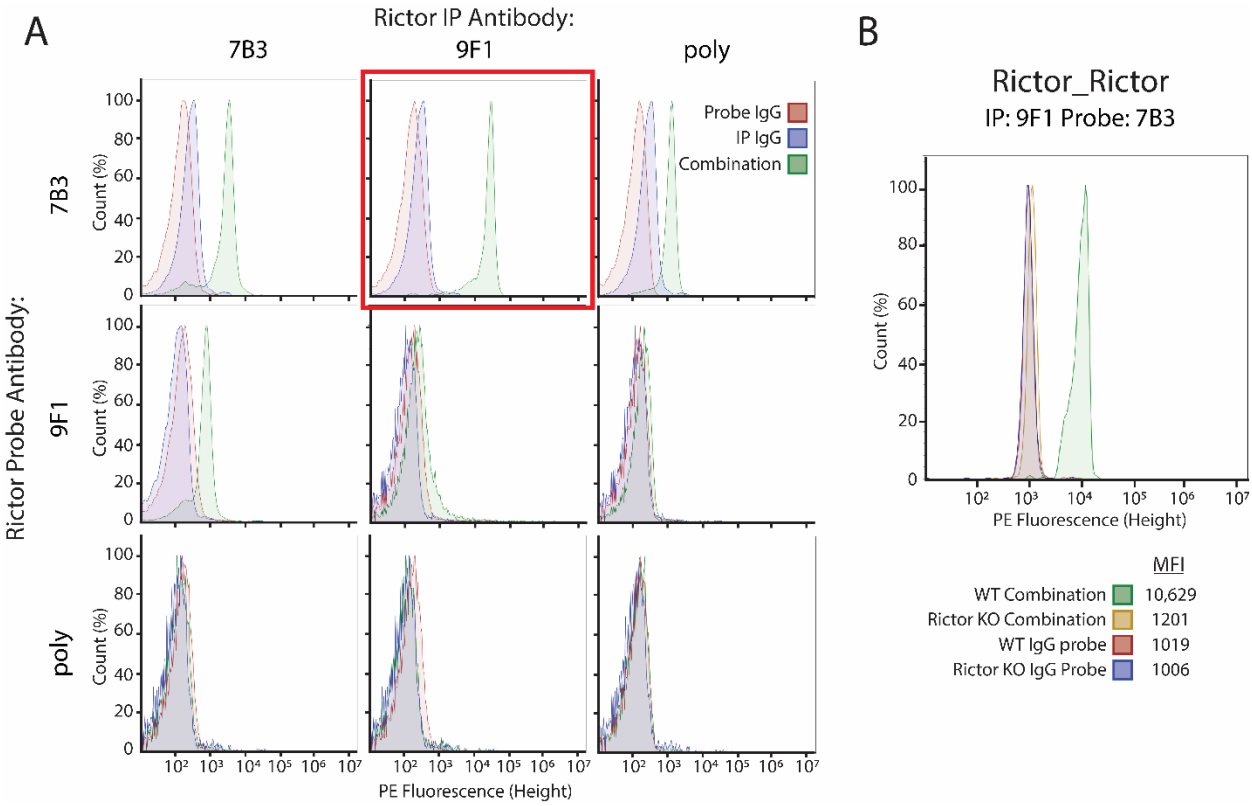

Figure S1.2. Specificity validation of QMI antibody pairs in mouse. A) Several candidate antibodies were bead-coupled (columns) and biotinylated (rows), and all IP-probe combinations were tested. Histograms for each IP_probe pair (green) were compared to IgG_probe (red) and IP_IgG (blue) controls, and the pair that produced the strongest signal over background was selected (7B3_9F1). B) Specificity was confirmed by comparing wildtype brain lysate to brain lysate from a KO mouse (yellow), which overlapped with IgG controls (red, blue).

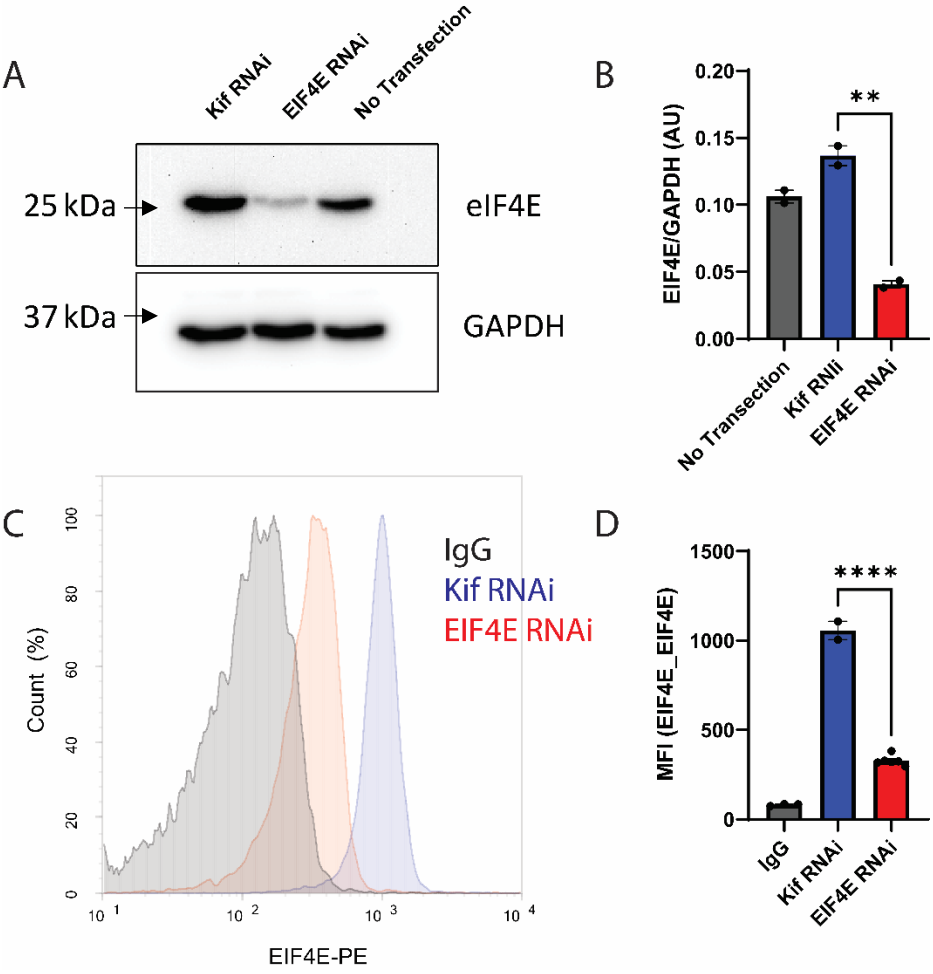

Figure S1.3: Specificity validation of QMI antibody pairs in human (A) Western blots from HEK 293 cells treated with RNAi to knockdown EIF4E. (B) Quantification of A, normalized to GAPDH levels. N=2 independent experiments, analyzed in duplicate. ** indicates significantly different from the KIF positive control by ANOVA followed by Bonferroni-corrected post-hoc testing, $p<0.05$. (C) Human specificity was confirmed by comparing KIF treated 293 cells (blue) to EIF4E RNAi treated 293 cells (red) and IGG precipitated samples (grey). (D) Quantification of the median fluorescent values from C. N=2 independent experiments, analyzed in duplicate. ** indicates significantly different from the KIF positive control by ANOVA followed by Bonferroni-corrected post-hoc testing, $p<0.05$.

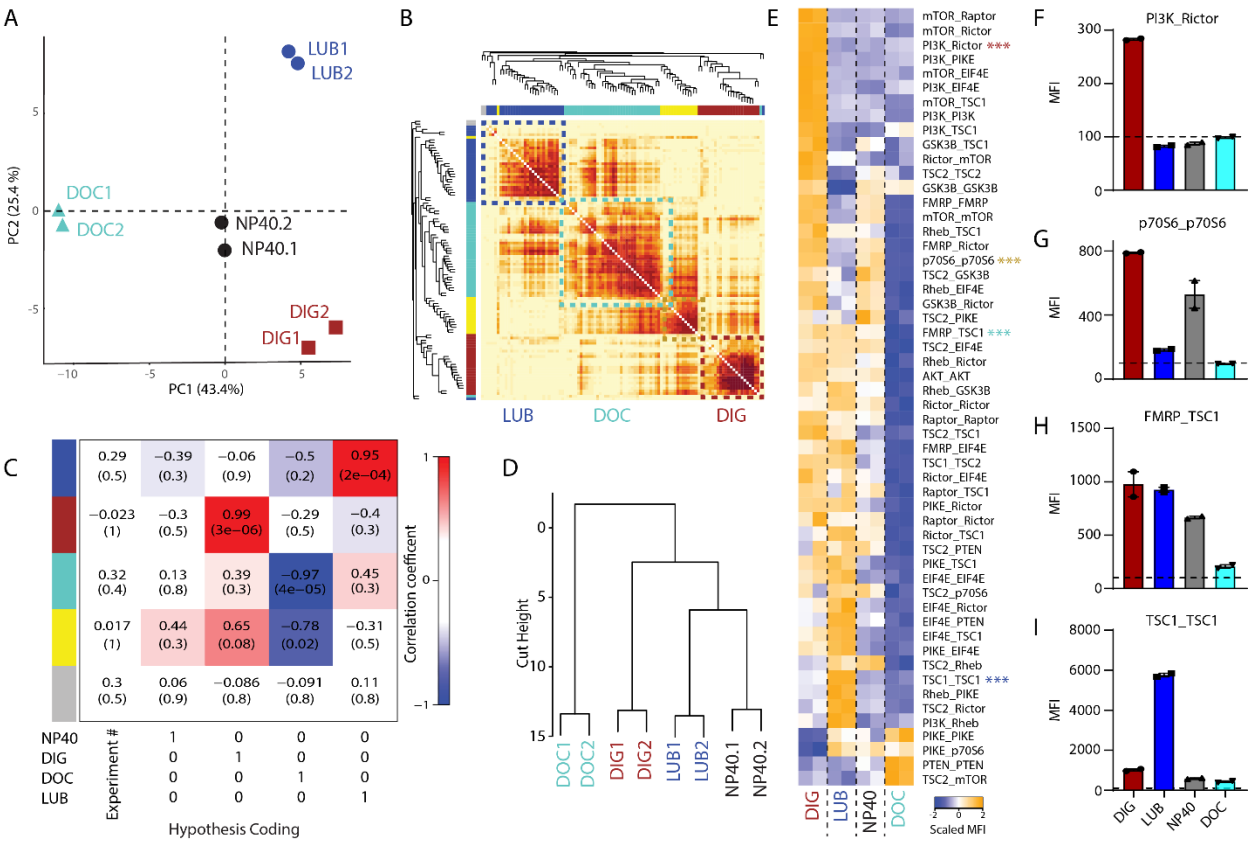

Figure S1.4: Detergent affects protein complexes detected by QMI (A) Principal component analysis (PCA) of P0 mouse cortical lysates lysed in four different detergents: Deoxycholate (DOC-turquoise), NP-40 (black), Lubrol (LUB-blue), and Digitonin (DIG-red) N=2 per condition. (B). A topological overlap matrix (TOM) reveals four modules of correlated PiSCES; dashed boxes outline each arbitrariliy-colored module. (C). Module-trait table showing the correlation (top number) and the p-value (bottom number) calculated by CNA for each trait. Hypothesis coding table below indicates the binary coding of detergent “traits”. (D). Hierarchical clustering of QMI data showing strong correlation between detergent repliates, and seperation of data by detergent (E). Heatmap of the median scaled values of all dynamic interactions that showed significant changes between deteregent conditions. Each box represents a single interaction measurement from a single experimental replicate; columns correspond to a replicate while rows correspond to an interaction. N=2. (F-I). Bar graphs of the median fluorescent intensity (MFI) from a representative interaction in each module across samples.

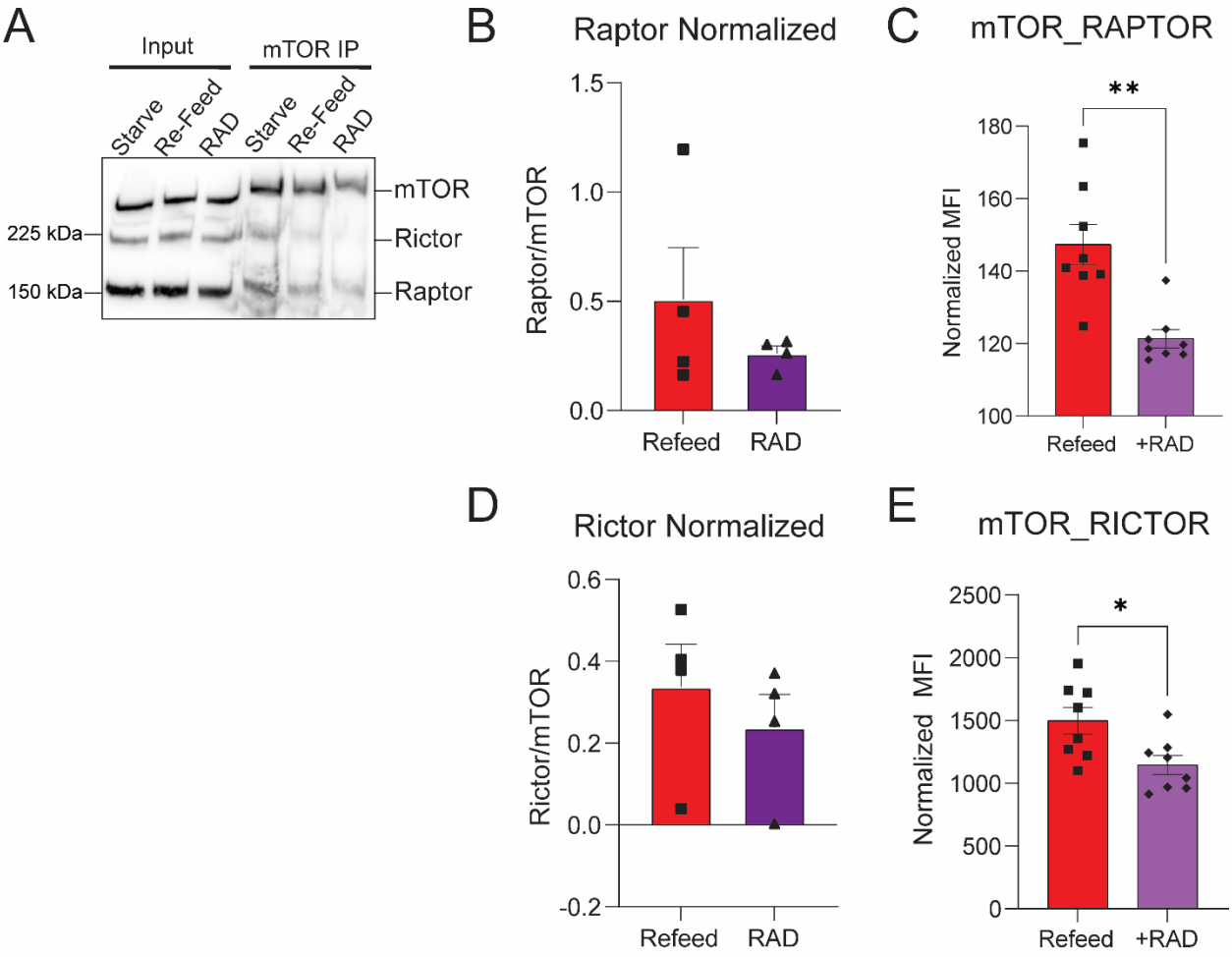

Figure S1.5: Co-immunoprecipitation of mTOR following serum starvation and RAD001 treatment (A) IP-western blots from 3T3 fibroblasts underwent serum starvation and refeeding protocol with or without 40 nM RAD001 and lysed in 0.3% Chaps buffer. (B) Quantification of Raptor probe from Refed and RAD treated samples normalized to mTOR (N=4). (C) The normalized median fluorescent values of the mTOR_RAPTOR interaction from Figure 1.2. ** indicates $p<0.01$ by t-test. (D) Quantification of Rictor probe from Refed and RAD treated samples normalized to mTOR (N=4). (C) The normalized median fluorescent values of the mTOR_RICTOR interaction from Figure 1.2. * indicates $p<0.05$ by t-test.

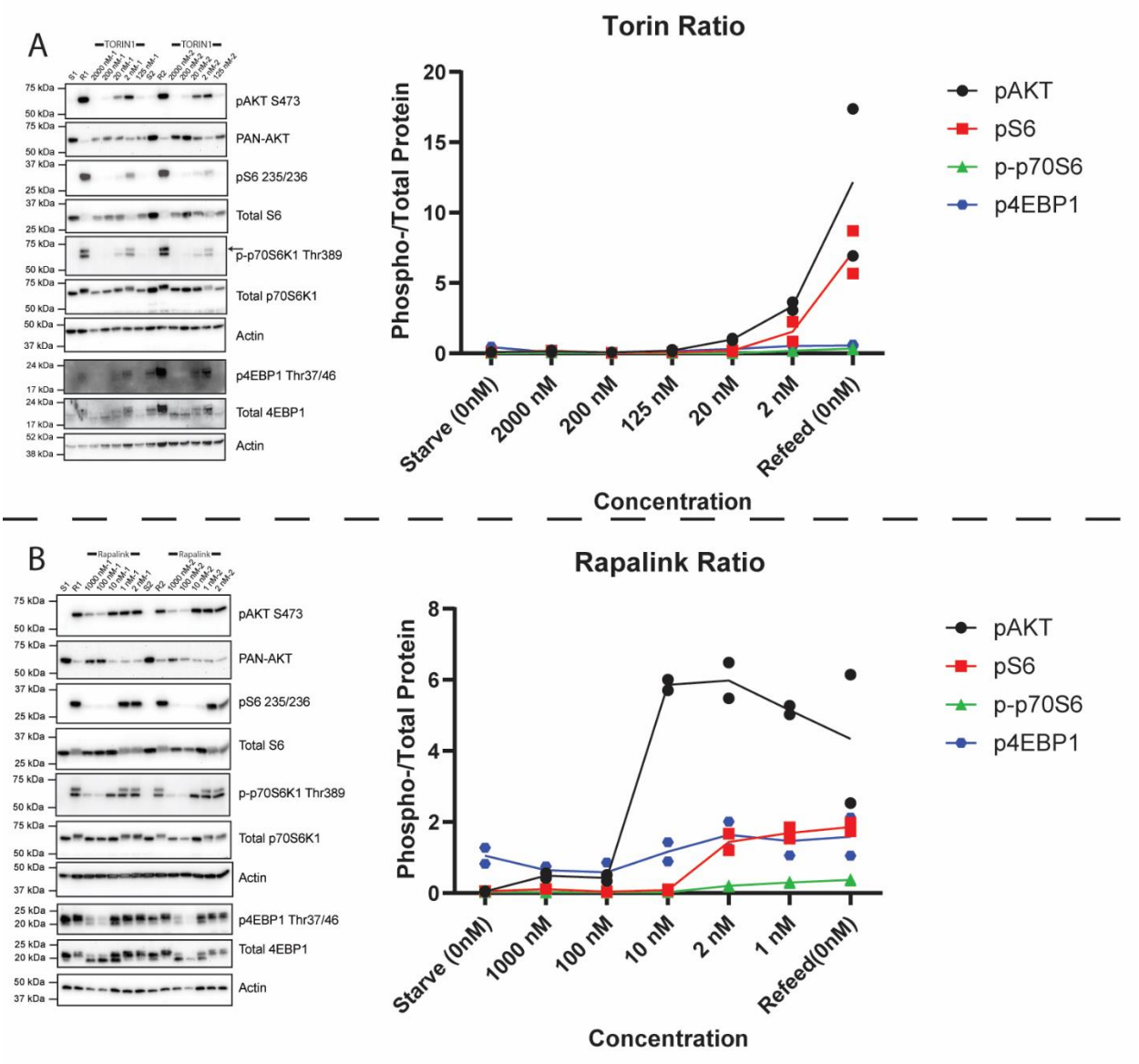

Figure S1.6: (continued on next page)

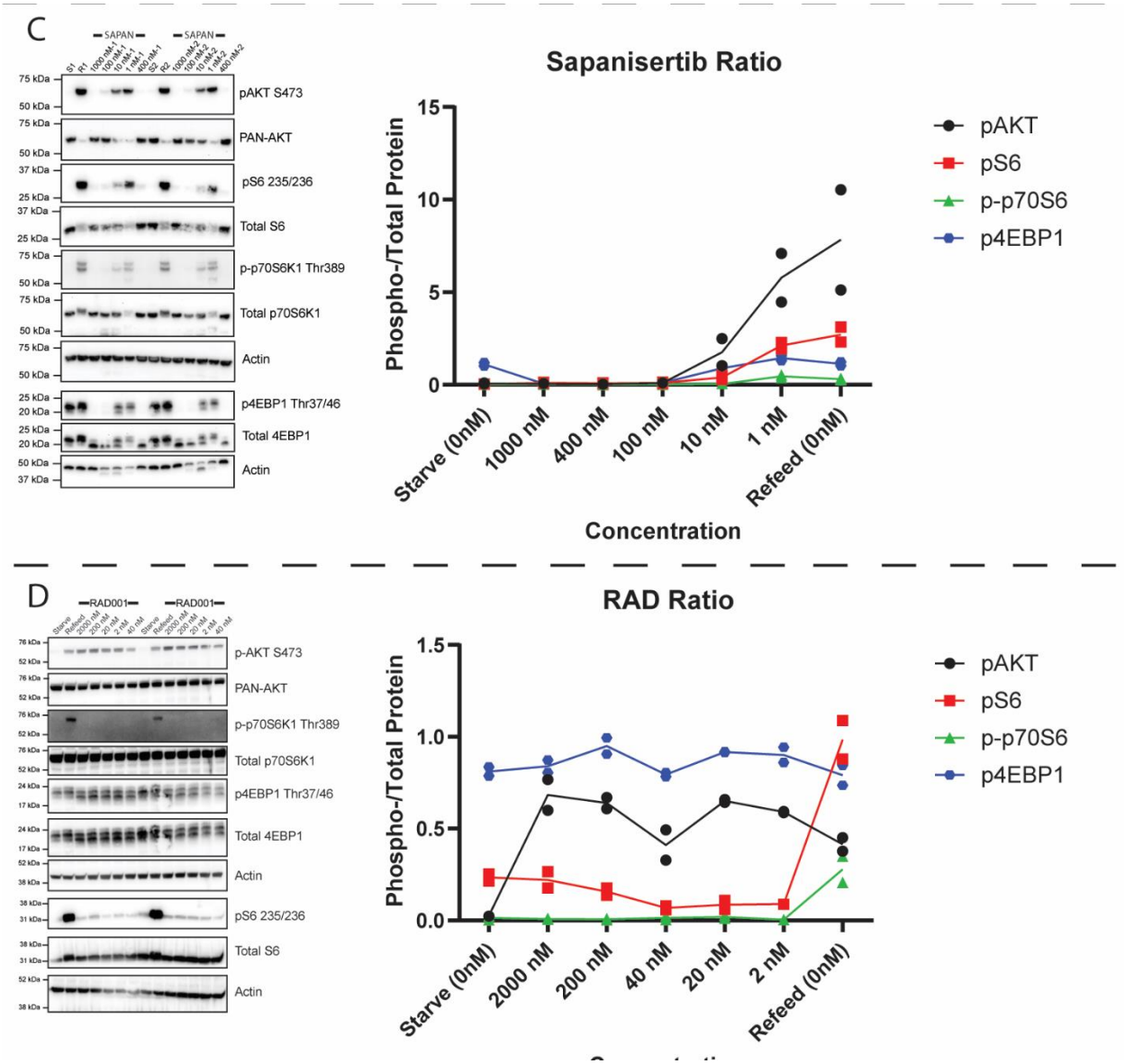

Figure S1.6: Phosphorylation level curves related to Figure 1.4. A) Phospho-western blots for AKT (black), S6 (red), p70S6 (green), and 4EBP1 (blue) from a serum-starvation experiment in the presence of various concentrations of TORIN1 along with a graph representing quantification at different concentrations using the ratio of phosphorylated to total protein (N=2). B-D) Similar figures as S4A but for Rapalink, Sapanisertib, and RAD001 respectively.

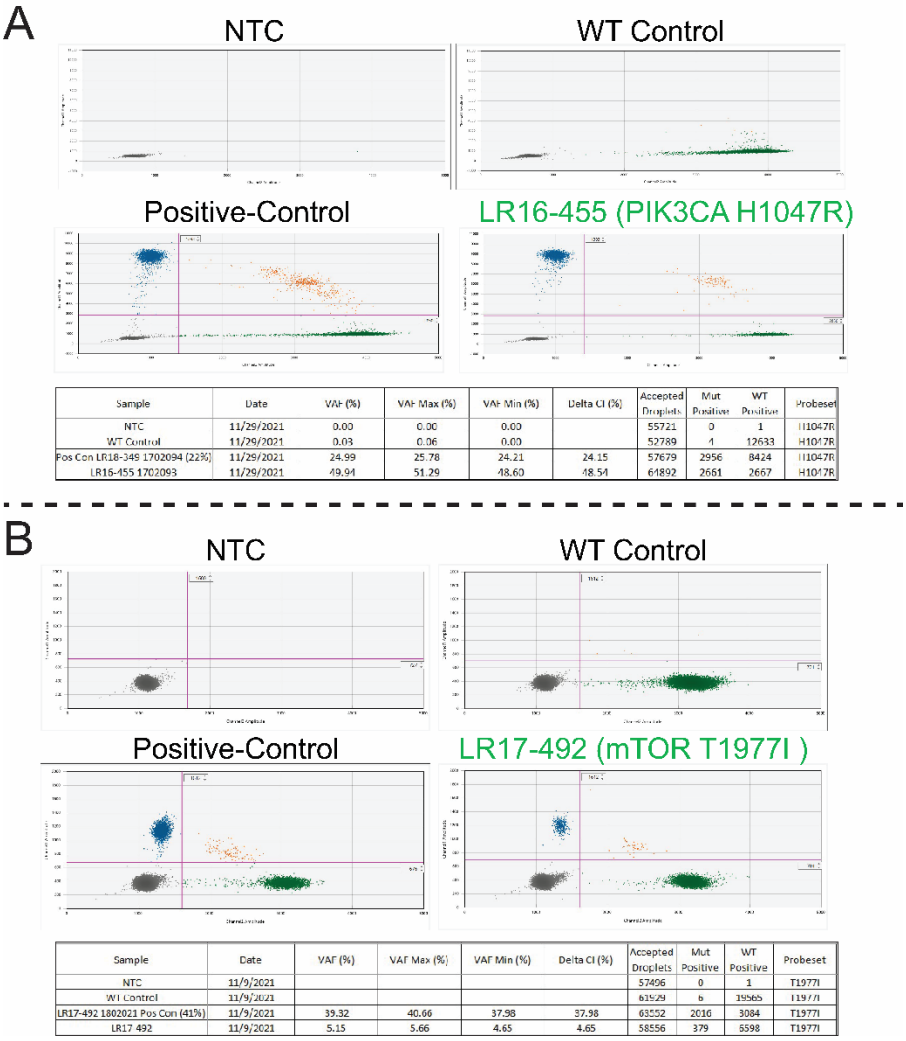

Sample	Date	VAF (%)	VAF Max (%)	VAF Min (%)	Delta CI (%)	Accepted Droplets	Mut Positive	WT Positive	Probeset
NTC	11/29/2021	0.00	0.00	0.00		55721	0	1	H1047R
WT Control	11/29/2021	0.03	0.06	0.00		52789	4	12633	H1047R
Pos Con LR18-349 1702094 (22%)	11/29/2021	24.99	25.78	24.21	24.15	57679	2956	8424	H1047R
LR16-455 1702093	11/29/2021	49.94	51.29	48.60	48.54	61892	2661	2667	H1047R

Sample	Date	VAF (%)	VAF Max (%)	VAF Min (%)	Delta CI (%)	Accepted Droplets	Mut Positive	WT Positive	Probeset
NTC	11/9/2021					57496	0	1	T1977I
WT Control	11/9/2021					61529	6	19565	T1977I
LR17-492 1802021 Pos Con (41%)	11/9/2021	39.32	40.66	37.98	37.98	63552	2010	3084	T1977I
LR17 492	11/9/2021	5.15	5.66	4.65	4.65	58556	379	5598	T1977I

Figure S1.7: Droplet digital PCR of patient derived mutant mTOR PIK3CA and mTOR (A) Droplet digital PCR results for the PIK3CA H1047R line, summarized in a table. (B) Droplet digital PCR results for the mTOR T1977I line, summarized in a table.

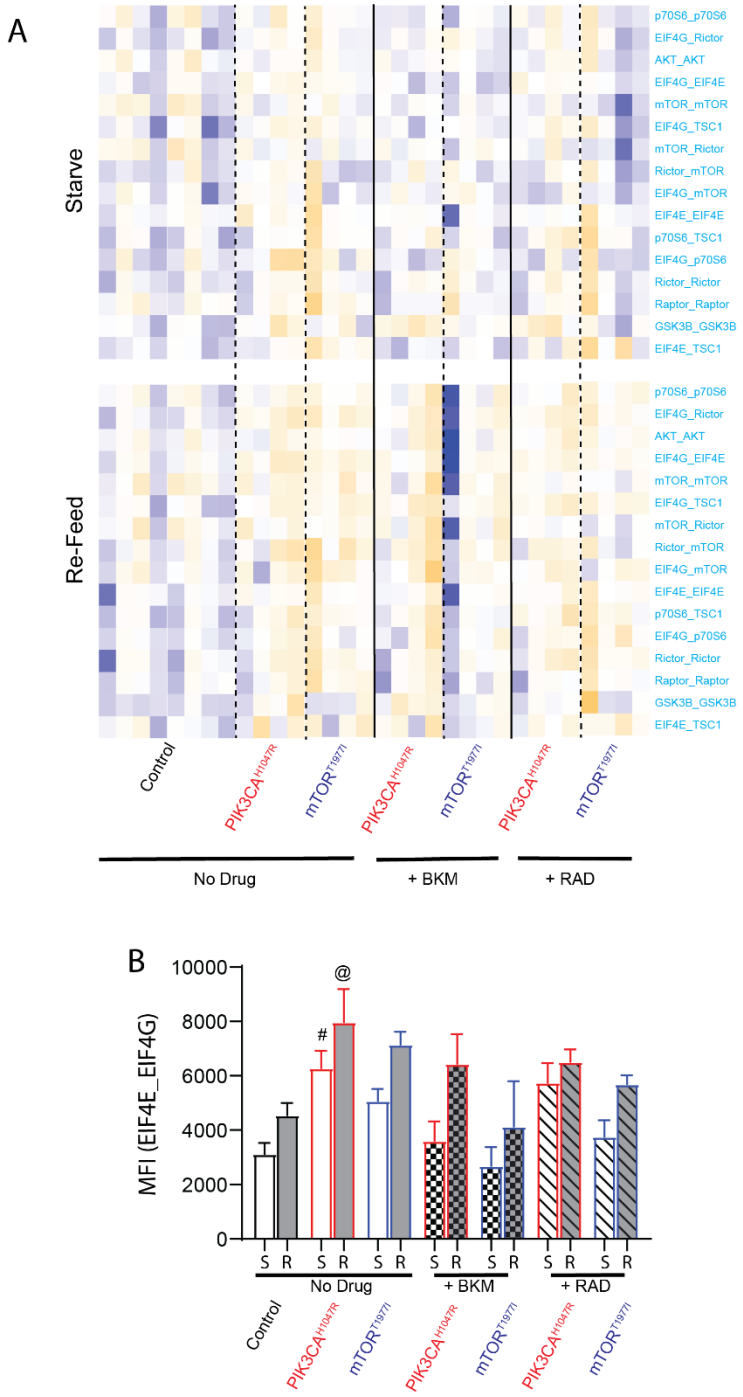

Figure S1.8: Mutant fibroblast drug inhibition experiment, related to Figure 1.5. A) Heatmap of the median scaled values of all dynamic PiSCES that showed ANC∩CNA-significant changes. Each box represents a single interaction measurement from a single experimental replicate; columns correspond to an experimental replicate while

rows correspond to an interaction. N = 4-8. B) Median fluorescent intensity (MFI) of EIF4E_EIF4G, the interaction most correlated with the turquoise module, shown for all conditions. * indicates significantly different from starved within-genotype, # significantly different from control-starved, and @ signficantly different from control-re-fed, by ANOVA followed by Bonferroni-corrected post-hoc testing, p<0.05. N=4-8

Target	Uniprot identifier	Uniprot #	IP antibody clone	IP antibody Catalog number	Probe antibody clone	Probe antibody Catalog number	QMI-specific Validation	Human siRNA
AKT1	AKT1_MOUSE	P31750	SKB1	05-591	B1	sc-5298	siRNA	Yes
Beta-Catenin	CTNB1_MOUSE	Q02248	196624	MAB13292	OTI2H7	NBP2-03615	Mouse KO liver lysate (B6.129-Ctnnb1tm2Kem/KnwJ)	Yes
eIF4E	IF4E_MOUSE	P63073	299910	MAB3228	Poluclonal	A301-153A	siRNA	Yes
EIF4G	IF4G1_MOUSE	Q6NZJ6	G6899	MA5-14971	3A10	SAB1403762	siRNA	
FMRP	FMR1_MOUSE	P35922	Polyclonal	F4055	5C2	MM5-5232	Mouse KO brain lystate (B6.129P2-Fmr1tm1Cgr/J)	Yes
GSK3B	GSK3B_MOUSE	Q9WV60	3D6B4	NBP2-52478	3D10	NBP1-47470	Mouse Embryonic fibroblast lysate (GSK3β(-/-); GSK3α(flox/-) (3/4KO)	Yes
mGluR5	GRM5_MOUSE	Q3UVX5	5675	AB5675	N75/3	75-115	Plasmid overexpression (Lautz et al 2018)	
mTOR	MTOR_MOUSE	Q9JLN9	2ID8.2	05-1592	30	sc-517464	siRNA	Yes
p70S6K	KS6A1_MOUSE	P18653	215247	MAB8962	Polyclonal	AF8962	Mouse KO liver lysate (C.129(B6)-Rps6kb1tm1Gtho/NsoJ)	Yes
PI3K	P85A_MOUSE	P26450	U5	MA1-74183	AB6	05-212	Plasmid overexpression (Lautz et al 2018)	
PIKE	AGAP2_MOUSE	Q3UHD9	263A	A304-263A	DN8	200-401-DN8	X63 Myeloma (Smith et al, 2016)	
PTEN	PTEN_MOUSE	O08586	217702	MAB847	6H2.1	04-035	Plasmid overexpression	
RAPTOR	RPTOR_MOUSE	Q8K4Q0	Polyclonal	42-4000	514208	MAB5957	siRNA in progress	Yes
Rheb	RHEB_MOUSE	Q921J2	344912	MAB3426	JG37-12	NBP2-75646	Plasmid overexpression	Yes
RICTOR	RICTR_mouse	Q6QJ06	7B3	Millipore 05-1471	9F1.2	Novus NBP1-51645	mouse KO ESC lysate	
TSC1	TSC1_MOUSE	Q9EP53	5C8A12	37-0400	Polyclonal	NB100-2315	Mouse Embryonic fibroblast lysate (TSC1(-/-);)	Yes
TSC2	TSC2_MOUSE	Q61037	614204	MAB40401	SC05-59	NBP2-67552	Plasmid overexpression	Yes

Table S1.1: Documentation of protein targets and IP-Probe antibody pairs.

Chapter 3:

Shank3-deficient mice display exaggerated signaling through the mTOR protein interaction network during homeostatic scaling

Abstract:

Homeostatic scaling is an important non-Hebbian form of synaptic plasticity that allows neurons to maintain a normalized level of activity and prevents saturation of the synapse. Synaptic scaling has been shown to be disrupted in various forms of autism spectrum disorder, including in the Shank3 knockout model. Shank3 deficiency also induces abnormal signaling through the mammalian target of rapamycin (mTOR) cascade. Here, we use the quantitative multiplex co-immunoprecipitation method to model how the mTOR interaction network responds during homeostatic scaling. Using TTX and BIC to induce homeostatic scaling in cultured cortical mouse neurons, we observe that synaptic scaling activates distinct combinations of mTOR interaction modules. One module is shared by both up- and down-scaling while two are unique to down-scaling. Additionally, the mTOR PIN of Shank3-deficient neurons exhibit 'pre-scaled' behavior and exhibits a warped response range. Finally, we treated wildtype and Shank3 mutant neurons with NV5138 and Rapalink-1. Treatment with the mTOR inhibitor Rapalink also produces an exaggerated response in the mTOR interaction network of Shank3 deficient neurons. Overall, we show that the loss of Shank3 warps the response range of the mTOR protein interaction networks. These deficits in mTOR signaling may contribute to dysregulation of homeostatic scaling and synaptic marker expression observed in Shank3 deficient mice.

Introduction:

Homeostatic scaling is a form of non-Hebbian plasticity that adjusts the strength of neuronal connections to maintain network stability and prevent runaway excitation (Turrigiano and Nelson 2004; Turrigiano 2012). At the synaptic level, the strength of individual synapses will adjust to maintain a neurons individual baseline rate of activity. There are many molecular mechanisms involved in the regulation of homeostatic scaling in synapases. Homeostatic scaling bidirectionally modifies surface level AMPAR expression through PKA-mediated phosphorylation of AMPARs at the S845 residue (Diering et al., 2014). Homeostatic up- and down-scaling is also translation dependent and causes opposing changes in protein expression, including in AMPA receptor subunit expression (Schanzenbacher et al., 2016; Dorrbaum et al., 2020). Scaling renormalizes global synaptic strength and is crucial for establishing memory specificity (Wu et al., 2021).

Several neurological disorders like autism spectrum disorder exhibit disruptions in synaptic scaling (Bulow et al., 2019). A variety of mouse models insufficient for autism risk genes – such as FMR1, Homer1a, and Shank3 - display deficits in homeostatic scaling (Hu et al., 2010; Soden and Chen 2010; Tatavarty et al., 2020). Shank3 is a multidomain synaptic scaffold protein, a prominent autism risk gene, and the genetic driver of Phelan-McDermid syndrome (Betancur and Buxbaum, 2013). The loss of Shank3 abolishes synaptic and intrinsic homeostatic scaling (Tatavarty et al., 2020; Heavner et al., 2021). This is due to Shank3's contributions to the integrity of the post-synaptic receptor signaling complex. The loss of Shank3 disrupts mGLUR5 and Homer

interactions and prevents activation of downstream signaling pathways such as Erk and mTOR (Moutin et al 2021).

Mammalian target of rapamycin (mTOR) is a serine-threonine kinase that acts as a central regulator of translation and is involved in many physiological processes like cell growth/survival, autophagy, and plasticity (Hoeffer and Klann 2010). The mTOR signaling pathway has also been shown to be a nexus for autism risk genes (Chen et al., 2014). The insufficiency of several components of the mTOR pathway are related to the syndromic form of autism (Hoeffer and Klann, 2010; Winden et al., 2018). The loss of Shank reduces the activity of the AKT/mTOR signaling pathway (Mossa et al., 2021; Moutin et al., 2021).

The mTOR cascade is also a key regulator of synaptic plasticity. mTORC1 activates in response to late-phase long term potentiation (LTP) as well as DHPG induced long term depression (Cammalleri et al., 2003; Antion et al., 2008). mTORC2 has also been demonstrated to be a major regulator of metabotropic glutamate receptor-mediated long-term depression (mGluR-LTD) and rapamycin blocks mGluR-LTD (Zhu et al., 2018). mTORC1 activity regulates the translation of the E3 ligase Trim32 that ubiquitinates components of the miRNA-induced silencing complex (miRISC), whose subsequent degradation induces downscaling (Srinivasan et al., 2021). During up-scaling, mTOR is dephosphorylated, leading to TFEB-signaling activation and autophagy mediated regulation of CaMKII and PSD95 (Wang et al., 2023). The roles that mTOR signaling have in the regulation of neuronal plasticity are multifaceted and indispensable. Understanding how the mTOR cascade fulfills these roles will provide key mechanistic insights into information processing in neurons.

Signal transduction cascades like the mTOR pathway are typically studied as a linear and sequential series of molecular events. However, these events are the result of dynamic and nonlinear physical interactions between the members of the signaling cascade that form protein complexes. Networks of protein-protein interactions may respond to stimuli with different intensities to achieve signal specificity. Unique signals could be differentiated through engaging different protein networks, engaging the same network with different intensities, or some combination of those mechanisms. Dysregulating a protein network's response during signaling may contribute to adverse physiological outcomes. Elucidating the mechanics of signaling through protein interaction networks is a crucial part for understanding the underlying mechanics of neuronal signaling and neurological disorders.

Previous work has demonstrated that the synaptic protein interaction network has a bi-directional response during homeostatic scaling that is disrupted by Shank3 mutant mice (Heavner et al., 2021). However, the behavior of the mTOR interaction network during homeostatic scaling remains opaque. Here, we characterize how the mTOR protein interaction network (PIN) responds to homeostatic scaling events and how that response is disrupted by the loss of Shank3. We find that synaptic scaling activates three mTOR modules: a translation-associated module and two signaling-associated modules. The translation-associated module is similarly active during both up and down-scaling, while the signaling-associated modules are unique to down-scaling. We also observe that untreated Shank3-deficient neurons exhibit protein module patterns that resemble the wildtype modules undergoing scaling. The translation-associated module in Shank3-deficient neurons is also overactive during scaling. Shank3-deficient

neurons also display an enhanced response during treatment with the mTOR inhibitor Rapalink-1. These results indicate that the loss of Shank3 warps the response range of the signaling through the mTOR protein interaction network.

RESULTS

Up- and downscaling act on different combinations of mTOR interaction modules

We treated primary neuron cultures from wildtype mice with TTX (2 µM) to induce upscaling, BIC (40 µM) to induce downscaling, or DMSO as a control for either twelve or forty-eight hours. Phospho-western blots were performed against a variety of mTOR pathway targets to observe the effect of scaling on the phosphorylation state of the signaling cascade (Figure 2.1A). AKT phosphorylation was reduced by TTX treatment and unaffected by BIC treatment after twelve hours. However, after forty-eight hours, BIC-treated neurons displayed an increase in AKT phosphorylation while TTX treated neurons were not significantly different from DMSO treated neurons. RPS6 phosphorylation was increased by treatment with BIC and decreased with TTX treatment after either twelve or forty-eight hours of treatment. P70S6K1 phosphorylation was only significantly affected by BIC treatment after forty-eight hours. mTOR phosphorylation was reduced by TTX treatment after either twelve or forty-eight hours. 4EBP1 was not affected by either TTX or BIC treatment.

We used Quantitative Multiplex Immunoprecipitation (QMI) to analyze changes in the mTOR PIN due to homeostatic scaling. QMI is an antibody-based assay that measures changes in PINs through simultaneous immunoprecipitation of multiple protein targets on flow cytometry beads. Fluorescently labeled “probe” antibodies that bind different

epitopes on target protein are applied, followed by analysis with flow cytometry. The median fluorescent intensity (MFI) of IP_Probe pairs quantify the magnitude of the interaction between the IP antibody target and probe antibody target. The simultaneous measurement of binary interactions allows the use of network level statistical approaches like weighted gene correlated network analysis (CNA) to model the behavior of sets of interactions and identify groups of protein interactions that correlate to experimental variables (Langfelder and Horvath 2008).

We first evaluated PIN differences between TTX, BIC, and DMSO treated neurons using principal component analysis (PCA) (Figure 2.1C). PCA analysis indicated that the mTOR PINs of DMSO and TTX treated neurons are more alike than the BIC PIN. Additionally, the difference in the mTOR PIN due to BIC treatment peaked after forty-eight hours of treatment. CNA identified three clusters, hereafter referred to as modules, of protein interactions whose behavior is correlated with different traits of interest (Figure 2.1D). The yellow module was most significantly and negatively correlated with BIC treatment regardless of timepoint (correlation coefficient = -0.45, p = 0.001). The blue module was most significantly correlated with any treatment, indicating that the interactions are uniformly effected after either TTX or BIC treatment compared to DMSO (correlation coefficient = 0.62, $p = 3*10^{-6}$). The turquoise module, like the yellow module, was most significantly and negatively correlated with BIC treatment regardless of timepoint (correlation coefficient = -0.79, $p = 4*10^{-11}$).

We used adaptive, nonparametric statistical test corrected for multiple comparisons (ANC) to ensure that only high-confidence interactions are reported. Interactions that were identified as significant by both ANC and CNA were considered high confidence.

These interactions were visualized as a row-normalized heatmap (Figure 2.1E) and organized by their module membership.

Interactions in the blue module are comprised mostly of EIF4E/EIF4G related interactions and responded to both TTX and BIC treatment, with their maximum response occurring after forty-eight hours of treatment. EIF4E and EIF4G are proteins crucial to the formation of the ribosome around RNA and the initiation of translation. We took the average row-normalized values for interactions in a module to describe its behavior. The mean scaled value for all interactions in the blue 'translation related' module indicates that both up and down scaling produced a similar change in the translation related proteins that are downstream of mTOR signaling (Figure 2.1F). The turquoise module, comprised of many mTORC1 and mTORC2 related interactions, specifically responded to BIC treatment at either timepoint. The module was reduced relative to DMSO after BIC treatment and did not change in response to TTX treatment Figure (1G). The yellow module is comprised of an eclectic mix of intermediary interactions, though they are mostly TSC1 and FMRP related. This FMRP-TSC1 module is significantly reduced after BIC treatment. TTX treatment caused yellow module interactions to trend downward after twelve hours of treatment, but these interactions move back toward baseline after forty-eight hours (Figure 2.1H).

We expected that the response of the mTOR PIN would be bidirectional in a manner that is like observations made in the synaptic interaction network and to patterns observed in RPS6 phosphorylation (Heavner et al., 2021) (Figure 2.1A). The behavior of the mTOR interaction modules may reflect a mechanism of signal specificity that differs from the synaptic protein network. The behavior of the blue translation module may be

reflective of the fact that both up and downscaling are translation dependent. The similarity of the module behavior after either treatment could be broadly indicative of this shared feature. The turquoise mTORC1/2 module is unique to BIC treatment and is not significantly affected by TTX treatment. This is unexpected as it is not reflective of the phosphor-western blot data. The yellow FMRP-TSC1 module is similar to the turquoise module with subtle differences in the time course, where TTX treatment trends downward at twelve hours before returning to baseline. These results indicate homeostatic scaling events will recruit different combinations of mTOR interaction modules depending on the direction of scaling. Both up and down-scaling may share modules that indicate a shared feature, but the total module combination will differentiate the direction of scaling.

The loss of Shank3 disrupts the response range of the mTOR PIN during homeostatic scaling.

We aimed to observe whether the loss of Shank3 disrupts signaling through the mTOR protein interaction network during homeostatic scaling. Previous research indicated that Shank3 deficient neurons synaptic PIN behaved as if they were ‘pre-scaled’ (Heavner et al., 2021). We sought to determine if this could be observed in the mTOR protein interaction network. We treated primary cortical cultures from wildtype and Shank3-deficient mice with TTX and BIC for forty-eight hours to induce homeostatic scaling.

Phospho-western blots of RPS6 indicate that the loss of Shank3 may dysregulate the response of the mTOR cascade, as S6 phosphorylation merely trends upward due to BIC treatment instead of being significantly different (Figure 2.2A-B). We performed QMI analysis on cultured cortical neurons after BIC/TTX treatment for forty-eight hours

as described in Figure 2.2.1. PCA analysis indicates that wildtype neurons clustered based on treatment (Figure 2.2C). However, mutant neurons did not separate to the same degree that wildtype neurons did and are closer to BIC-treated wildtype group along dimension 1. We would expect this if the mTOR PIN is pre-scaled in Shank3 deficient neurons.

CNA analysis identified three interaction modules correlated with traits of interest. The blue module, like in the previous figure, is comprised of translation related protein interactions, and is correlated with treatment (correlation coefficient = -0.43, p = 0.004) and genotype (correlation coefficient = -0.39, p = 0.01). This indicates that the interactions in the blue module responded to both TTX and BIC treatment. However, blue module interactions fromShank3-deficient neurons were decreased relative to their wildtype counterparts. The turquoise module is made of mTORC1/2 interactions and is negatively correlated with our hypothesis of 'pre-scaling' (correlation coefficient = -0.71, $p = 1*10^{-7}$). The interactions in the turquoise module from untreated mutant neurons behaved like interactions from wildtype neurons treated with BIC but have an overactive response to BIC treatment themselves. Additionally, turquoise module interactions from Shank3 deficient neurons displayed a greater response to BIC treatment than wildtype. The brown interaction module is most correlated with BIC treatment (correlation coefficient = -0.49, $p = 9*10^{-4}$) and responds to BIC treatment regardless of genotype. Visualization of the ANCxCNA significant interactions for all three modules were visualized as a row-normalized heatmap (Figure 2.2E) and organized by their module membership.

The previously observed blue translation related module comprised of interactions such as EIF4G_FMRP and EIF4G_EIF4E was recapitulated in this experiment. Quantification of the mean scale value indicates that treatment with BIC and TTX produced dissociations in the wildtype interactions as they had in the previous experiment. However, interactions from Shank3-deficient neurons were more severely decreased in all conditions relative to their wildtype counterparts (Figure 2.2F).

Additionally, we performed a puromycin incorporation assay and a proteasome activity assay. Acute slices from the prefrontal cortex of P21-P23 wildtype and Shank3B knockout mice were used to assess protein synthesis and degradation (Figure S1). Shank3 knockout slices did not display difference in puromycin incorporation, indicating that protein synthesis was normal in the Shank3 knockout mice (Figure S1A). Shank3 deficient neurons displayed a tendency toward increased protein degradation, but the difference was not statistically significant.

The turquoise module, made up of mTORC1/2 signaling interactions, was also recapitulated in this experiment. Turquoise module interactions were pre-emptively decreased in the Shank3-deficient DMSO treated neurons (Figure 2.2G). Like in the previous experiment, the turquoise module responded specifically to BIC treatment in wildtype neurons. However, unlike the blue module, the turquoise module response from Shank3 deficient neurons did not exceed the wildtype response (Figure 2.2G). This indicates that the loss of Shank3 may cause dysregulation in mTOR cascades' response range instead of simply pre-activation.

The brown module contains a variety of intermediary interactions that include GSK3B_TSC1 and FMRP_Rictor; and is reminiscent of the previous experiment's

yellow module. In wildtype neurons, these interactions responded specifically to BIC treatment. However, interactions from the brown module did not respond in Shank-deficient neurons (Figure 2.2H). We have observed that the loss of Shank3 dysregulates signaling through the mTOR PIN. However, the three mTOR modules that respond to homeostatic scaling are dysregulated in different ways. While all three modules are pre-emptively dissociated at baseline in Shank3 deficient neurons, their responses to scaling are not equally dysregulated. The blue module is hyperactive, the turquoise module is at wildtype levels, and brown module does not respond to homeostatic scaling in mutant neurons. The mTOR signaling networks range of response is dysregulated asymmetrically by the loss of Shank3.

The effect of NV5138 and Rapalink treatment on Shank3-deficient neurons

Next, we aimed to characterize how the mTOR network responds to targeted stimulation and inhibition of mTOR in Shank3 deficient neurons. We attempted to stimulate cultured cortical neurons with a brain specific mTORC1 activator NV5138, a small molecule activator derived from the amino acid leucine. We also inhibited mTOR signaling in cultured neurons with the third generation Rapalink-1. Western blot analysis of AKT and S6 indicates that treatment with NV5138 did not produce robust stimulation of mTOR signaling while Rapalink-1 treatment did inhibit the mTOR cascade (Figure 2.3A). Phospho-AKT was not significantly changed by NV5138 treatment. As expected, Rapalink treatment did not affect levels of AKT phosphorylation (Figure 2.3B). NV5138 treatment did not affect S6 phosphorylation in either wildtype or Shank3 deficient neurons. Rapalink-1 treatment did significantly inhibit pS6 in mutant neurons, but only trended towards inhibition in wildtype neurons (Figure 2.3C). We then performed QMI

analysis on wildtype and Shank3 deficient neurons with Rapalink and NV5138 treated neurons. PCA analysis indicates that only Rapalink treated neurons separate from the samples. Additionally, wildtype and mutant neurons treated with Rapalink show some amount of separation (Figure 2.3D).

CNA analysis revealed two modules (Figure 2.3E). The brown module was most significantly and negatively correlated with Rapalink treatment (correlation coefficient = -0.88, $p = 2*10^{-8}$). The interactions associated with the brown module were decreased in Rapalink treated neurons relative to those treated with NV5138 and DMSO. The turquoise module was most significantly and positively correlated with Rapalink treatment (correlation coefficient = 0.61, p = 0.002), indicating that turquoise associated interactions increased in response to Rapalink treatment. The heatmap that visualizes brown module interactions significant by both ANC and CNA analysis indicates that while Shank3 deficient neurons respond similarly to wildtype neurons, the response to Rapalink is significantly more severe in mutant neurons (Figure 2.3G). Interactions within the brown module are predominantly made up of mTOR complex associated proteins. The turquoise module is comprised of a variety of proteins involved in the mTORC1/2, TSCs, and EIF4 complexes. Rapalink treatment caused an increase in these interactions in both modules relative to DMSO and NV5138 treated neurons (Figure 2.3H). Shank3 deficient neurons displayed an attenuated response to inhibition with Rapalink (Figure 2.3H). Shank3 deficient neurons have a dysregulated response range during inhibition with Rapalink like the dysregulated response range observed during homeostatic scaling.

Discussion:

We sought to characterize how the mTOR protein interaction network responds to neuronal signaling events and how that process is disrupted by the loss of Shank3. Previous research documenting the behavior of mTOR network used a serum starvation +refeed method to induce signaling in mouse embryonic fibroblasts. The mTOR PIN was found to respond as a whole module of interactions that could be broken up into discreet modules by pathway inhibitors (Wehle et al., 2023).

Here, we find that the mTOR network in neurons differentiates stimuli through the recruitment of unique combinations of modules. Initial experiments characterizing synaptic scaling at different timepoints in wildtype neurons indicate that there are two major modules of interactions that respond to scaling. The ‘blue’ module was found to be comprised of protein interactions whose members are involved with RNA translation, such as EIF4G_EIF4E. The involvement of such proteins could be indicative of changes in translation that occur during homeostatic scaling. Interestingly, we did not observe any bi-directional trends in any interaction module. We expected that up- and down-scaling would illicit reciprocal changes in affected modules, but we did not observe this. In the case of the blue translation module, BIC treatment was differentiated from TTX by the timepoints affected. BIC treatment significantly differed from control treatment at both 12 and 48 hours, while TTX only differed at 48 hours. At that 48-hour timepoint, both BIC and TTX treatment produce similar changes in blue module interactions. Additionally, BIC treatment’s effect on the module peaked at 48 hours rather than 12 hours. These kinetic differences between up and down scaling could be representative

of the nuanced differences between up and down-scaling. However, the data suggests that up- and down-scaling act upon a shared translation module.

The fact that this module is shared by both up and down scaling is not entirely unexpected and is reflective of trends in protein synthesis observed in previous work. Both up- and down-scaling require intact translation (Schanzenbacher et al., 2016). BONCAT analysis of neurons treated with TTX or BIC revealed that neither treatment induced a global bidirectional change in protein regulation, but instead induced up or down regulation of specific sets of proteins. Additionally, the fraction of uniquely regulated proteins was enhanced at twenty-four hours of treatment, indicating a long time-course is required to achieve peak activity (Schanzenbacher et al 2018). This pattern of behavior is in accord with our observations of the translation module's kinetics and lack of specificity. The translation module is not unique to either up- or down-scaling and reaches peak activation at 48 hours of treatment (Figure 2.1F). This observation is to be expected based on previous research. . SILAC labeling mass spectrometry experiments after twenty-four hours of TTX/BIC treatment revealed that the largest groups of proteins were regulated by decreased synthesis in both up- and down-scaled neurons (Dorrbaum et al 2020). This is in line with the observation that TTX and BIC treatment induced dissociations in the protein-protein interactions that facilitate translation initiation, such as EIF4G_EIF4E. So, the similarity between TTX and BIC treatments' module effect is most likely because both up- and down-scaling decrease protein synthesis, which would entail the protein-protein interactions in the translation module to dissociate.

In contrast, the ‘turquoise’ module is composed mostly of interactions involved with mTORC1/mTORC2 and other central mTOR signaling regulators such as TSC1/2. This module was unique to BIC treatment regardless of treatment time (Figure 2.1G). Similarly, the yellow module is unique to BIC treatment and was comprised of a mix of regulatory interactions, including those involving FMRP and TSC1. The specificity of the turquoise and yellow modules may be representative of signaling mechanisms that differentiate between up- and down-scaling. While both up- and down-scaling share common modulation and signaling changes through pathways such as the CaMKK/CaMKIV pathways, other signaling elements like brain-derived neurotrophic factor (BDNF), Arc, and PSD95 that are essential for up-scaling are dispensable for down-scaling (Turrigiano 2012). Characterization of the phospho-proteome during homeostatic scaling with liquid chromatography-tandem mass spectrometry revealed reciprocal changes in phosphorylation events when comparing up- and down- scaling. However, phospho-events that were specific to up- and down-scaling were identified (Desch et al 2021). This indicates that up- and down- scaling may recruit signaling pathways unique to the direction of scaling.

Homeostatic scaling and chemical LTP are both dependent on mTOR signaling but have been shown to regulate mTORC1 through different mechanisms. Homeostatic up-scaling through AMPA receptor blockade induces phospholipase D (PLD) dependent synthesis of phosphatidic acid while cLTP does not. PLD inhibition or disruption of PA(phosphatidic acid)_mTOR interactions eliminates mTORC1 activity and presynaptic compensation induced by AMPAR blockade. However, mTORC1 activation and cLTP driven synaptic changes are not altered by either PLD inhibition or PA_mTOR

interaction disruption (Henry et al., 2018). Multiple types of neuronal plasticity converge on similar sets of signaling pathways like the mTOR cascade, but they can be differentiated by activating different pathways or engaging convergent pathways in alternative ways.

Our observations seem to reveal an example of alternative activation of a convergent pathway. Rather than homeostatic scaling directionality being differentiated by the bidirectional changes in protein interactions, as observed in the synaptic interaction network (Heavner et al., 2021), the mTOR network seems to distinguish scaling events by the combination and intensity of module activation. Downscaling is specified by the activation of the blue, turquoise, and yellow modules. Upscaling is specified by blue module activation and a lack of activation in the turquoise and yellow module. While both directions of scaling converge on the translation module, they are differentiated by alternative mTOR signaling. This is indicated by the engagement of protein modules unique to downscaling. To better understand homeostatic scaling and synaptic plasticity, future research must work to characterize which signaling pathways are truly convergent, unique to plasticity types, and feature alternative patterns of signal transduction.

After characterizing how the mTOR signaling pathway responds to homeostatic scaling in a neurotypical model, we wanted to determine how the loss of Shank3 affects such signaling. Previous research into Shank3-deficient signaling using QMI revealed that the loss of Shank3 causes the synaptic PIN to form a ‘pre-scaled’ state, meaning that the untreated Shank3 mutant PINs were in a confirmation that resembled the scaled

wildtype PIN (Heavner et al., 2021). We then hypothesized that this ‘pre-scaled’ feature would be present in the mTOR network during scaling events.

The ‘blue’ translation module appears in this experimental set and is shared by both BIC and TTX treatment as it was in the previous experiment. However, Shank3-deficient-DMSO control neurons displayed a blue module PIN that was significantly decreased when compared to wildtype (Figure 2F). In addition, mutant neurons displayed a significantly more severe protein network response during BIC and TTX treatment compared to wildtype. Interactions in the ‘turquoise’ mTORC1/2 module also displayed this genotype driven effect. Like in the previous experiment, the turquoise module was specific to BIC treatment. The median scaled value for the turquoise module of Shank3 deficient neurons treated with DMSO was significantly lower relative to wildtype neurons. However, BIC treatment did not elicit module behavior in mutant neurons that was significantly different than wildtype neurons. Unexpectedly, TTX treatment did not rescue deficits in the module driven by the loss of Shank3. The turquoise mTORC1/2 signaling module remained unresponsive to TTX treatment in Shank3-deficient neurons. Like the yellow module in the previous experiment, the brown module was BIC specific and comprised of a mix of intermediary interactions. However, this module was unresponsive to homeostatic scaling in Shank3 deficient neurons.

This indicates that the loss of Shank3 causes asymmetrical dysregulation of signaling through the protein interaction network. The behavior of the mTOR network does resemble patterns one may expect of a pre-scaling hypothesis and CNA analysis confirmed this (Figure 2D). This pre-scaling behavior did not manifest in the three modules equally. In the blue module, mutant neurons were pre-scaled before treatment

and their response exceeded the wildtype during treatment. The whole response range of the blue translational module was shifted toward a pre-scaled state with a higher ceiling. The functional implication of this observation in the translation module may be indicative of dysregulated translation.

There are conflicting reports regarding protein synthesis deficits in the Shank3 mouse model. One group looked for protein synthesis deficits in striatal slices from 4-week-old Shank3Δe4–22 deficient mice with puromycin incorporation but did not observe differences in protein synthesis (Lee et al., 2019). Another group used the L-[1-14C] leucine quantitative autoradiographic method to measure rates of cerebral protein synthesis (rCPS) in Shank3Δe4–9 deficient adult mice and found every brain region examined exhibited increased protein synthesis (Torossian et al 2021). The contradictions in reported protein synthesis deficits could be explained by key differences between the reported experiments. The group that reported increased protein synthesis used adult mice while experiments using juvenile mice did not observe protein synthesis deficits. The pathology of Shank3 deficiency changes over development. Analysis of Shank3ΔC dependent deficits in behavior, neurotransmission, and spine morphology at 10-, 20-, and 40-weeks old reveal age dependent alterations in observed deficits over development (Thabault et al., 2023). Furthermore, Shank3B deficient pups (P5) display reduced mRNA expression levels for key neuronal markers in the frontal cortex, but by adulthood the expression of many markers is either normalized or overexpressed (Bukatova et al., 2021). One reason that we may not have observed deficits in protein synthesis or degradation is due to the age of the mice. Future work ought to analyze the developmental trajectory of Shank3-mutant pathology.

It has been reported that the loss of Shank3 causes hypoactive mTOR signaling (Bidinosti et al 2016; Mossa et al 2020). However, Shank3 overexpression also causes hypoactivation of the mTOR cascade (Lee et al 2017). We fail to observe any deficits in S6 phosphorylation (Figure 2.2A-B). We do observe mTOR PIN deficits, but they are not necessarily associated with hypoactivation. The manner that Shank3 modulates signaling does not appear to be linear, which may explain why the deficits we observe in the mTOR PIN do not conform to hypoactivity and why hypoactivity has been observed in cases of Shank3 deficiency and overexpression.

Shank3 deficiency affects the modules of the mTOR PIN in an asymmetrical manner. We summarize this asymmetrical dysregulation in Figure 2.4. We portray the blue and turquoise interaction modules as units that begin at point 0 at baseline and move positions during treatment. Shank3-deficiency appears to dysregulate this process in different ways. In the case of the translation module, the module starts at position 1 and moves to position 4 instead of position 3 creating a shifted response range. However, in the mTORC1/2 interactions, the Shank3 knockout module begins at 1 but still ends at position 3, creating a contracted response range. The mechanism that produces these differing effects of the modules is unclear, but we can speculate based on Shank3's known roles in signaling.

Shank3 is an important scaffolding protein for the post-synaptic density, regulating the arrangement of its receptors and consequently their downstream signaling cascades (Scheefhals and MacGillavry 2018). other signaling cascades may be dysregulated by the loss of Shank3. The loss of Shank3 disrupts the mGLUR5_HOMER interaction, which impairs ERK and mTOR signaling (Moutin et al., 2021). The ERK and mTOR

pathway are parallel signaling pathways that regulate each other's activity. Our previous work determined that the inhibition of ERK signaling induces inhibitory effects on the mTOR PIN that can meet and exceed inhibition with Rapamycin (Wehle et al 2023). It is possible that the uneven application of signaling deficits through the mTOR network may be influenced by parallel signaling pathways being differentially affected. Future research should seek to better understand how Shank3 regulates other signaling cascades and to disentangle how such Shank3 related signaling deficits compound on each other.

We aimed to determine whether stimulation or inhibition would normalize signaling deficits in Shank3-deficient neurons. We expected NV5138 treatment would induce a normalizing effect on the mTOR PIN, as mTOR activators like IGF-1 have been applied to attempt treating Phelan-McDermid syndrome (Kolevzon et al 2022). It is likely that our treatment was not sufficient to produce a significant effect on the mTOR pathway. The mTOR pathway's baseline levels of activity may be high enough that NV5138 treatment could not induce detectable changes with our assays. Future experiments may need to either dampen baseline signaling or give a more severe stimulant.

Shank3 deficiency caused the mTOR PIN to have a more severe response to Rapalink. The "turquoise" module is comprised of protein involved in mTORC1/2 regulation and translation regulation. This module of proteins displayed an increase due to Rapalink treatment in both wildtype and mutant neurons. This was unexpected as these interactions were decreased after Rapalink treatment in 3T3 mouse embryonic fibroblasts (Wehle et al, 2023). However, this could be explained by protocol differences. Our previous work used twelve hours of serum-starvation with an hour of

Rapalink treatment followed by one hour of fresh media stimulation with Rapalink for an additional hour. In our current experiments, we simply added Rapalink directly to the media for three hours based on previous research (Ehinger et al., 2021; Zhang et al., 2022). Therefore, these experiments are not directly comparable. One reason that inhibition caused an increase in these interactions may be compensatory signaling mechanisms.

The loss of Shank3 dysregulated signaling through the turquoise module by displacing the response range. This contrasts with the dysregulation of the brown module, which displayed an expanded response range. Like BIC/TTX treatment, Shank3 causes asymmetrical dysregulation of mTOR modules' response range during treatment with Rapalink. Shank3 abnormalities in signaling are not linear nor evenly applied to signalosome, so potential treatments may need to be carefully titrated to achieve a desired outcome.

In conclusion, we establish that homeostatic scaling signals through the mTOR protein network through specific combinations of interaction modules. We show that Shank3-deficient neurons show asymmetrical disruptions in signaling through the mTOR cascade during both homeostatic scaling and mTOR inhibition warp the response range of mTOR modules. The deficit is reflective of Shank3's intertwined roles in regulating the structure of the synapse and in recruiting signaling pathways. Further research into Shank3's role in regulating signaling at the synapse through protein-protein interactions will be insightful into understanding synaptic plasticity and ASD.

Materials and Methods:

Animals

All work with animals was performed in compliance with the Seattle Children's Research Institute Institutional Animal Care and Use Committee under approved protocol no. 00072 and federal guidelines. CD1 and Shank3^{tm2Gfng} (stock 017688) mice were originally obtained from The Jackson Laboratory (Bar Harbor, ME).

Genotyping

Crude DNA extract (0.2 ul) (Kapa Biosystems) from ear punch tissue was used for genotyping the Shank3 allele with the following primers: 5′-GAGACTGATCAGCGCAGTTG-3′, 5′-TGACATAATCGCTGGCAAAG-3′, and 5′-GCTATACGAAGT-TATGTCGACTAGG-3′ using standard polymerase chain reaction protocols.

Cortical neuron culture and drug treatment

Primary cortical neuron cultures were prepared as described in previous works (Heavner et al., 2021). Whole cortex from P0 or P1 mouse neonates was dissociated using papain (Worthington) and plated at a $1*10^6$ cell density per well in six well plates treated with poly-D-lysine. Cells were cultured in Neurobasal medium supplemented with 2% B27 and 0.5 mM GlutaMAX (Thermo Fisher Scientific) and kept at 37°, 5% CO_2 for 17-21 days. After 3 to 5 days in vitro (DIV), 5-fluoro-2'-deoxyuridine was added to a final concentration of 5 µM to inhibit glial proliferation. For in vitro homeostatic scaling experiments, TTX (2 µM) or BIC (40 µM) (Tocris) was added directly to the culture medium, and cells were cultured as normal and then lysed after either 12 or 48 hours.

DMSO (0.4%) served as a vehicle control. Prior to mTOR stimulation and inhibition experiments, cultured neurons were given 680 µL of fresh media [400 µl] and pure water [280 µl] two days prior to experimentation. NV5138 (Working concentration: 300 µM) or Rapalink (Working concentration:10 nM) was diluted in 500 µl of Neurobasal medium that lacked any supplements and added directly to the culture medium. Neurons were cultured as normal and lysed after 3 hours. DMSO was served as a vehicle control.

Lysate Preparation

After drug treatment, neuron culture medium was removed, cells were washed twice with ice-cold dPBS, and cells were scraped in cold lysis buffer [150 mM NaCl, 50 mM Tris (pH 7.4), 1% Digitonin, 10 mM sodium fluoride, 2 mM sodium orthovanadate, protease inhibitor cocktail (Sigma-Aldrich), and phos-phatase inhibitor cocktail (Sigma-Aldrich). Lysate was transferred to a centrifuge tube, incubated on ice for fifteen minutes, and centrifuged at 15000g for fifteen minutes to remove nuclear and cellular debris. The protein concentration of the supernatant was determined using a Bradford assay (Pierce).

Western Blotting

Proteins were separated by SDS-polyacrylamide gel electrophoresis and transferred to a polyvinylidene difluoride membrane. Membranes were blocked in 4-5% milk in TBST [0.05 M tris (pH 7.2), 0.15 M NaCl, 0.1% Tween 20] for 1 hour at room temperature and incubated overnight at 4°C or for 1 hour at room temperature. Primary antibodies were detected using species-specific horseradish peroxidase-conjugated secondary

antibodies. Blots were developed using Femto Maximum Sensitivity Substrate (Pierce) and imaged using either a Protein Simple imaging system or Azur Biosystem 600.

Antibodies

The following antibodies for the purpose of western blotting were acquired from Cell Signaling Technologies: pAKT S473 (Catalog number 4060), PAN-AKT (#2920), Phospho-p44/42 MAPK (#4370), p44/42 MAPK (#4695), S6 Ribosomal Protein (#2317), Phospho-S6 Ribosomal Protein (#4858), Phospho-p70S6 Kinase Thr389 (#97596), p70S6 Kinase (#9202), Phospho-4EBP1 Thr37/46 (#2855), 4EBP1 (#9452). Antibodies against Beta-Actin were purchased from GeneTex (catalog number 109639). NV5138 (Cat# HY-114384) and Rapalink-1 (Cat# HY-111373) were purchased from MedChem Express.

Quantitative Multiplex Immunoprecipitation

QMI was performed as described previously (Brown et al., 2019). A master mix containing each antibody-coupled Luminex bead was prepared and distributed to lysates normalized for protein concentration. Samples were incubated overnight at 4°C on a rotator. The following day, samples were washed in cold FlyP buffer [50 mM tris (pH7.4), 100 mM NaCl, 1% bovine serum albumin, and 0.02% sodium azide] and distributed into twice as many wells of a 96-well plate as there were probe antibodies for technical replicates. Biotinylated probe antibodies were added, and the plate was incubated at 4°C with gentle agitation for one hour. The resulting complexes were washed three times with FlyP buffer on an automatic plate washer. The samples were then incubated for thirty minutes with streptavidin-phycoerythrin at 4°C with gentle

agitation. Samples were washed three times again and resuspended in 120 ul of cold FlyP buffer and processed with a customized refrigerated Bio-Plex 200.

Adaptive nonparametric analysis with an empirical alpha cutoff (ANC)

Statistically significant differences in bead distributions between conditions for each of ~400 individual interactions, after correcting for multiple comparisons, were identified using ANC as described in previous work (Brown et al., 2019; Smith et al., 2016). Any Interaction that was found to be significant by an ANC comparison was considered a "hit."

Correlation Network Analysis (CNA)

Modules of Interactions that covaried with experimental conditions were identified using weighted correlation network analysis (Langfelder and Horvath, 2008) as described in previous work (Brown et al., 2019; Smith et al., 2016). Bead distributions used in ANC were collapsed and the median fluorescent intensity (MFI) value was averaged across technical replicates for input into the WGCNA package for R. Interactions with an MFI less than 100 were removed as noise, and batch effects were corrected using COMBAT (Leek et al., 2012). Power values giving the approximation of scale-free topology were determined using soft thresholding with a power adjacency function, and modules were determined by the TOM matrix function in WGCNA. Modules whose eigenvectors were correlated with an experimental trait ($P < 0.05$) were of interest. Interactions whose probability of membership in a module of interest was ($P < 0.05$) were considered "hits". Interactions that were "hits" by both ANC and CNA for a given experimental condition were considered high confidence interactions affected in that condition.

Hierarchical Clustering and PCA

Post-COMBAT, log2 transformed MFI values were clustered using the hclust function in R with a correlation distance matrix and average clustering method. Approximately unbiased (AU) P values were determined using the pvclust package in R. PCA was performed using the prcomp function in R.

Acknowledgements:

This work was supported by grants MH113545 and MH121487 (SEPS). Special gratitude to all donors to Seattle Children's Research Institute who invest in breakthrough discoveries that help prevent, treat, and eliminate childhood disease. The authors declare no conflicts of interest.

Author Contributions: DTW and SEPS designed the study. DTW performed all experiments. DTW and SEPS analyzed data. DTW and SEPS wrote the manuscript. All authors read and approved the manuscript.

Data Availability Statement: All data necessary to evaluate the conclusions presented in the manuscript are contained within the manuscript and the supplementary data files. Original raw QMI data files are available upon request from Dr. Smith (seps@uw.edu).

References:

Antion, M. D., Hou, L., Wong, H., Hoeffer, C. A., & Klann, E. (2008). mGluR-dependent long-term depression is associated with increased phosphorylation of S6 and synthesis of elongation factor 1A but remains expressed in S6K-deficient mice. *Molecular and Cellular Biology*, *28*(9), 2996–3007. https://doi.org/10.1128/MCB.00201-08

Aoto, J., Nam, C. I., Poon, M. M., Ting, P., & Chen, L. (2008). Synaptic signaling by all-trans retinoic acid in homeostatic synaptic plasticity. *Neuron*, *60*(2), 308–320. https://doi.org/10.1016/j.neuron.2008.08.012

Betancur, C., & Buxbaum, J. D. (2013). SHANK3 haploinsufficiency: A "common" but underdiagnosed highly penetrant monogenic cause of autism spectrum disorders. *Molecular Autism*, *4*, 17. https://doi.org/10.1186/2040-2392-4-17

Bidinosti, M., Botta, P., Krüttner, S., Proenca, C. C., Stoehr, N., Bernhard, M., Fruh, I., Mueller, M., Bonenfant, D., Voshol, H., Carbone, W., Neal, S. J., McTighe, S. M., Roma, G., Dolmetsch, R. E., Porter, J. A., Caroni, P., Bouwmeester, T., Lüthi, A., & Galimberti, I. (2016). CLK2 inhibition ameliorates autistic features associated with SHANK3 deficiency. *Science*, *351*(6278), 1199–1203. https://doi.org/10.1126/science.aad5487

Brown, E. A., Neier, S. C., Neuhauser, C., Schrum, A. G., & Smith, S. E. P. (2019). Quantification of Protein Interaction Network Dynamics using Multiplexed Co-Immunoprecipitation. *Journal of Visualized Experiments: JoVE*, *150*. https://doi.org/10.3791/60029

Bukatova, S., Renczes, E., Reichova, A., Filo, J., Sadlonova, A., Mravec, B., Ostatnikova, D., Bakos, J., & Bacova, Z. (2021). Shank3 Deficiency is Associated With Altered Profile of Neurotransmission Markers in Pups and Adult Mice. *Neurochemical Research*, *46*(12), 3342–3355. https://doi.org/10.1007/s11064-021-03435-6

Bülow, P., Murphy, T. J., Bassell, G. J., & Wenner, P. (2019). Homeostatic Intrinsic Plasticity Is Functionally Altered in Fmr1 KO Cortical Neurons. *Cell Reports*, *26*(6), 1378-1388.e3. https://doi.org/10.1016/j.celrep.2019.01.035

Cammalleri, M., Lütjens, R., Berton, F., King, A. R., Simpson, C., Francesconi, W., & Sanna, P. P. (2003). Time-restricted role for dendritic activation of the mTOR-p70S6K pathway in the induction of late-phase long-term potentiation in the CA1. *Proceedings of the National Academy of Sciences of the United States of America*, *100*(24), 14368–14373. https://doi.org/10.1073/pnas.2336098100

Chen, J., Alberts, I., & Li, X. (2014). Dysregulation of the IGF-I/PI3K/AKT/mTOR signaling pathway in autism spectrum disorders. *International Journal of Developmental Neuroscience*, *35*, 35–41. https://doi.org/10.1016/j.ijdevneu.2014.03.006

Chowdhury, D., & Hell, J. W. (2018). Homeostatic synaptic scaling: Molecular regulators of synaptic AMPA-type glutamate receptors. *F1000Research*, *7*, 234. https://doi.org/10.12688/f1000research.13561.1

Desch, K., Langer, J. D., & Schuman, E. M. (2021). Dynamic bi-directional phosphorylation events associated with the reciprocal regulation of synapses during homeostatic up- and down-scaling. *Cell Reports*, *36*(8), 109583. https://doi.org/10.1016/j.celrep.2021.109583

Diering, G. H., Gustina, A. S., & Huganir, R. L. (2014). PKA-GluA1 coupling via AKAP5 controls AMPA receptor phosphorylation and cell-surface targeting during bidirectional homeostatic plasticity. *Neuron*, *84*(4), 790–805. https://doi.org/10.1016/j.neuron.2014.09.024

Dörrbaum, A. R., Alvarez-Castelao, B., Nassim-Assir, B., Langer, J. D., & Schuman, E. M. (2020). Proteome dynamics during homeostatic scaling in cultured neurons. *eLife*, *9*, e52939. https://doi.org/10.7554/eLife.52939

Ehinger, Y., Zhang, Z., Phamluong, K., Soneja, D., Shokat, K. M., & Ron, D. (2021). Brain-specific inhibition of mTORC1 eliminates side effects resulting from mTORC1 blockade in the periphery and reduces alcohol intake in mice. *Nature Communications*, *12*(1), 4407. https://doi.org/10.1038/s41467-021-24567-x

Ehlers, M. D. (2003). Activity level controls postsynaptic composition and signaling via the ubiquitin-proteasome system. *Nature Neuroscience*, *6*(3), 231–242. https://doi.org/10.1038/nn1013

Heavner, W. E., Lautz, J. D., Speed, H. E., Gniffke, E. P., Immendorf, K. B., Welsh, J. P., Baertsch, N. A., & Smith, S. E. P. (2021). Remodeling of the Homer-Shank interactome mediates homeostatic plasticity. *Science Signaling*, *14*(681), eabd7325. https://doi.org/10.1126/scisignal.abd7325

Henry, F. E., Wang, X., Serrano, D., Perez, A. S., Carruthers, C. J. L., Stuenkel, E. L., & Sutton, M. A. (2018). A Unique Homeostatic Signaling Pathway Links Synaptic Inactivity to Postsynaptic mTORC1. *Journal of Neuroscience*, *38*(9), 2207–2225. https://doi.org/10.1523/JNEUROSCI.1843-17.2017

Hoeffer, C. A., & Klann, E. (2010). mTOR signaling: At the crossroads of plasticity, memory and disease. *Trends in Neurosciences*, *33*(2), 67–75. https://doi.org/10.1016/j.tins.2009.11.003

Hooshmandi, M., Sharma, V., Thörn Perez, C., Sood, R., Krimbacher, K., Wong, C., Lister, K. C., Ureña Guzmán, A., Bartley, T. D., Rocha, C., Maussion, G., Nadler, E., Roque, P. M., Gantois, I., Popic, J., Lévesque, M., Kaufman, R. J., Avoli, M., Sanz, E., … Khoutorsky, A. (2023). Excitatory neuron-specific suppression of the integrated stress response contributes to autism-related phenotypes in fragile X syndrome. *Neuron*, *111*(19), 3028-3040.e6. https://doi.org/10.1016/j.neuron.2023.06.017

Hou, Q., Zhang, D., Jarzylo, L., Huganir, R. L., & Man, H.-Y. (2008). Homeostatic regulation of AMPA receptor expression at single hippocampal synapses. *Proceedings of the National Academy of Sciences*, *105*(2), 775–780. https://doi.org/10.1073/pnas.0706447105

Hu, J.-H., Park, J. M., Park, S., Xiao, B., Dehoff, M. H., Kim, S., Hayashi, T., Schwarz, M. K., Huganir, R. L., Seeburg, P. H., Linden, D. J., & Worley, P. F. (2010). Homeostatic Scaling requires Group I mGluR activation mediated by Homer1a. *Neuron*, *68*(6), 1128–1142. https://doi.org/10.1016/j.neuron.2010.11.008

Kolevzon, A., Breen, M. S., Siper, P. M., Halpern, D., Frank, Y., Rieger, H., Weismann, J., Trelles, M. P., Lerman, B., Rapaport, R., & Buxbaum, J. D. (2022). Clinical trial of insulin-like growth factor-1 in Phelan-McDermid syndrome. *Molecular Autism*, *13*(1), 17. https://doi.org/10.1186/s13229-022-00493-7

Langfelder, P., & Horvath, S. (2008). WGCNA: An R package for weighted correlation network analysis. *BMC Bioinformatics*, *9*(1), 559. https://doi.org/10.1186/1471-2105-9-559

Lee, Y., Kim, S. G., Lee, B., Zhang, Y., Kim, Y., Kim, S., Kim, E., Kang, H., & Han, K. (2017). Striatal Transcriptome and Interactome Analysis of Shank3-overexpressing Mice Reveals the Connectivity between Shank3 and mTORC1 Signaling. *Frontiers in Molecular Neuroscience*, *10*. https://www.frontiersin.org/articles/10.3389/fnmol.2017.00201

Mossa, A., Pagano, J., Ponzoni, L., Tozzi, A., Vezzoli, E., Sciaccaluga, M., Costa, C., Beretta, S., Francolini, M., Sala, M., Calabresi, P., Boeckers, T. M., Sala, C., & Verpelli, C. (2021). Developmental impaired Akt signaling in the Shank1 and Shank3 double knock-out mice. *Molecular Psychiatry*, *26*(6), Article 6. https://doi.org/10.1038/s41380-020-00979-x

Moutin, E., Sakkaki, S., Compan, V., Bouquier, N., Giona, F., Areias, J., Goyet, E., Hemonnot-Girard, A.-L., Seube, V., Glasson, B., Benac, N., Chastagnier, Y., Raynaud, F., Audinat, E., Groc, L., Maurice, T., Sala, C., Verpelli, C., & Perroy, J. (2021). Restoring glutamate receptosome dynamics at synapses rescues autism-like deficits in Shank3-deficient mice. *Molecular Psychiatry*, *26*(12), 7596–7609. https://doi.org/10.1038/s41380-021-01230-x

Schanzenbächer, C. T., Langer, J. D., & Schuman, E. M. (2018). Time- and polarity-dependent proteomic changes associated with homeostatic scaling at central synapses. *eLife*, *7*, e33322. https://doi.org/10.7554/eLife.33322

Schanzenbächer, C. T., Sambandan, S., Langer, J. D., & Schuman, E. M. (2016). Nascent Proteome Remodeling following Homeostatic Scaling at Hippocampal Synapses. *Neuron*, *92*(2), 358–371. https://doi.org/10.1016/j.neuron.2016.09.058

Scheefhals, N., & MacGillavry, H. D. (2018). Functional organization of postsynaptic glutamate receptors. *Molecular and Cellular Neurosciences*, *91*, 82–94. https://doi.org/10.1016/j.mcn.2018.05.002

Soden, M. E., & Chen, L. (2010). Fragile X Protein FMRP Is Required for Homeostatic Plasticity and Regulation of Synaptic Strength by Retinoic Acid. *The Journal of Neuroscience*, *30*(50), 16910–16921. https://doi.org/10.1523/JNEUROSCI.3660-10.2010

Srinivasan, B., Samaddar, S., Mylavarapu, S. V. S., Clement, J. P., & Banerjee, S. (2021). Homeostatic scaling is driven by a translation-dependent degradation axis that recruits miRISC remodeling. *PLoS Biology*, *19*(11), e3001432. https://doi.org/10.1371/journal.pbio.3001432

Tatavarty, V., Pacheco, A. T., Kuhnle, C. G., Lin, H., Koundinya, P., Miska, N. J., Hengen, K. B., Wagner, F. F., Hooser, S. D. V., & Turrigiano, G. G. (2020). Autism-associated Shank3 is essential for homeostatic compensation in rodent V1. *Neuron*, *106*(5), 769-777.e4. https://doi.org/10.1016/j.neuron.2020.02.033

Thabault, M., Turpin, V., Balado, É., Fernandes-Gomes, C., Huot, A.-L., Cantereau, A., Fernagut, P.-O., Jaber, M., & Galvan, L. (2023). Age-related behavioural and striatal dysfunctions in Shank3ΔC/ΔC mouse model of autism spectrum disorder. *European Journal of Neuroscience*, *57*(4), 607–618. https://doi.org/10.1111/ejn.15919

Torossian, A., Saré, R. M., Loutaev, I., & Smith, C. B. (2021). Increased rates of cerebral protein synthesis in *Shank3* knockout mice: Implications for a link between synaptic protein deficit and dysregulated protein synthesis in autism spectrum disorder/intellectual disability. *Neurobiology of Disease*, *148*, 105213. https://doi.org/10.1016/j.nbd.2020.105213

Turrigiano, G. (2012). Homeostatic Synaptic Plasticity: Local and Global Mechanisms for Stabilizing Neuronal Function. *Cold Spring Harbor Perspectives in Biology*, *4*(1), a005736. https://doi.org/10.1101/cshperspect.a005736

Turrigiano, G. G., Leslie, K. R., Desai, N. S., Rutherford, L. C., & Nelson, S. B. (1998). Activity-dependent scaling of quantal amplitude in neocortical neurons. *Nature*, *391*(6670), 892–896. https://doi.org/10.1038/36103

Wang, Y., Lin, J., Li, J., Yan, L., Li, W., He, X., & Ma, H. (2023). Chronic Neuronal Inactivity Utilizes the mTOR-TFEB Pathway to Drive Transcription-Dependent Autophagy for Homeostatic Up-Scaling. *Journal of Neuroscience*, *43*(15), 2631–2652. https://doi.org/10.1523/JNEUROSCI.0146-23.2023

Wehle, D. T., Bass, C. S., Sulc, J., Mirzaa, G., & Smith, S. E. P. (2023). Protein interaction network analysis of mTOR signaling reveals modular organization. *Journal of Biological Chemistry*, *299*(11). https://doi.org/10.1016/j.jbc.2023.105271

Winden, K. D., Ebrahimi-Fakhari, D., & Sahin, M. (2018). Abnormal mTOR Activation in Autism. *Annual Review of Neuroscience*, *41*(Volume 41, 2018), 1–23. https://doi.org/10.1146/annurev-neuro-080317-061747

Wu, C.-H., Ramos, R., Katz, D. B., & Turrigiano, G. G. (2021). Homeostatic synaptic scaling establishes the specificity of an associative memory. *Current Biology*, *31*(11), 2274-2285.e5. https://doi.org/10.1016/j.cub.2021.03.024

Zhu, P. J., Chen, C.-J., Mays, J., Stoica, L., & Costa-Mattioli, M. (2018). mTORC2, but not mTORC1, is required for hippocampal mGluR-LTD and associated behaviors. *Nature Neuroscience*, *21*(6), Article 6. https://doi.org/10.1038/s41593-018-0156-7

Figures:

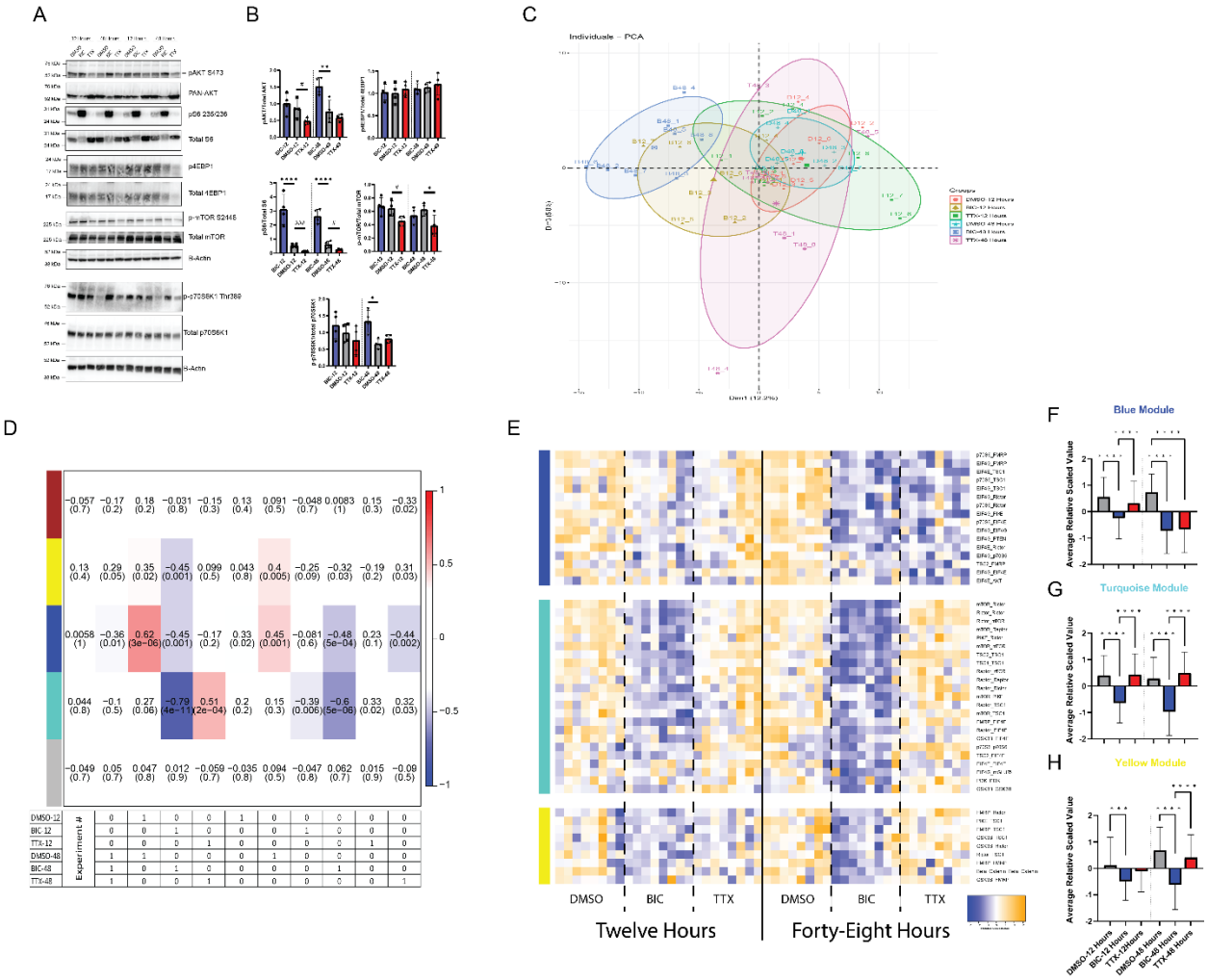

Figure 2.1: Time-course of the mTOR protein interaction network during homeostatic scaling. A) Representative western blots showing phospho- and total AKT, S6, 4EBP1, p70S6K1, and mTOR with actin for a loading control. B) Quantification of blots shown in A. * indicates significantly different from starved by ANOVA followed by Bonferroni-correction post-hoc testing, $p<0.05$. N = 4. C) Principal component graph of QMI data, N=8. D) Module-trait table showing the correlation coefficient (top number) and p-value (bottom number) between the eigenvector of each color-coded module (colored rectangles on the left) and binary-coded trait labels (“hypotheses”) shown in the

table below. E) Heatmap of the median scaled values of all significantly altered interactions. Each box represents a single interaction measurement from a single biological replicate; columns correspond to a biological replicate while rows correspond to an interaction (IP_Probe), ordered by the timepoint that the interaction first reached significance. N =8. Statistical significance calculated by ANC and CNA statistics as detailed in methods. F-H) Mean scaled value of all interactions in the blue (translation), turquoise (mTORC1/2 regulation), and yellow (middle signaling) modules which corresponds to overall module behavior. For F-H, * indicates significantly by ANOVA followed by Bonferroni-corrected post-hoc testing, $p<0.05$.

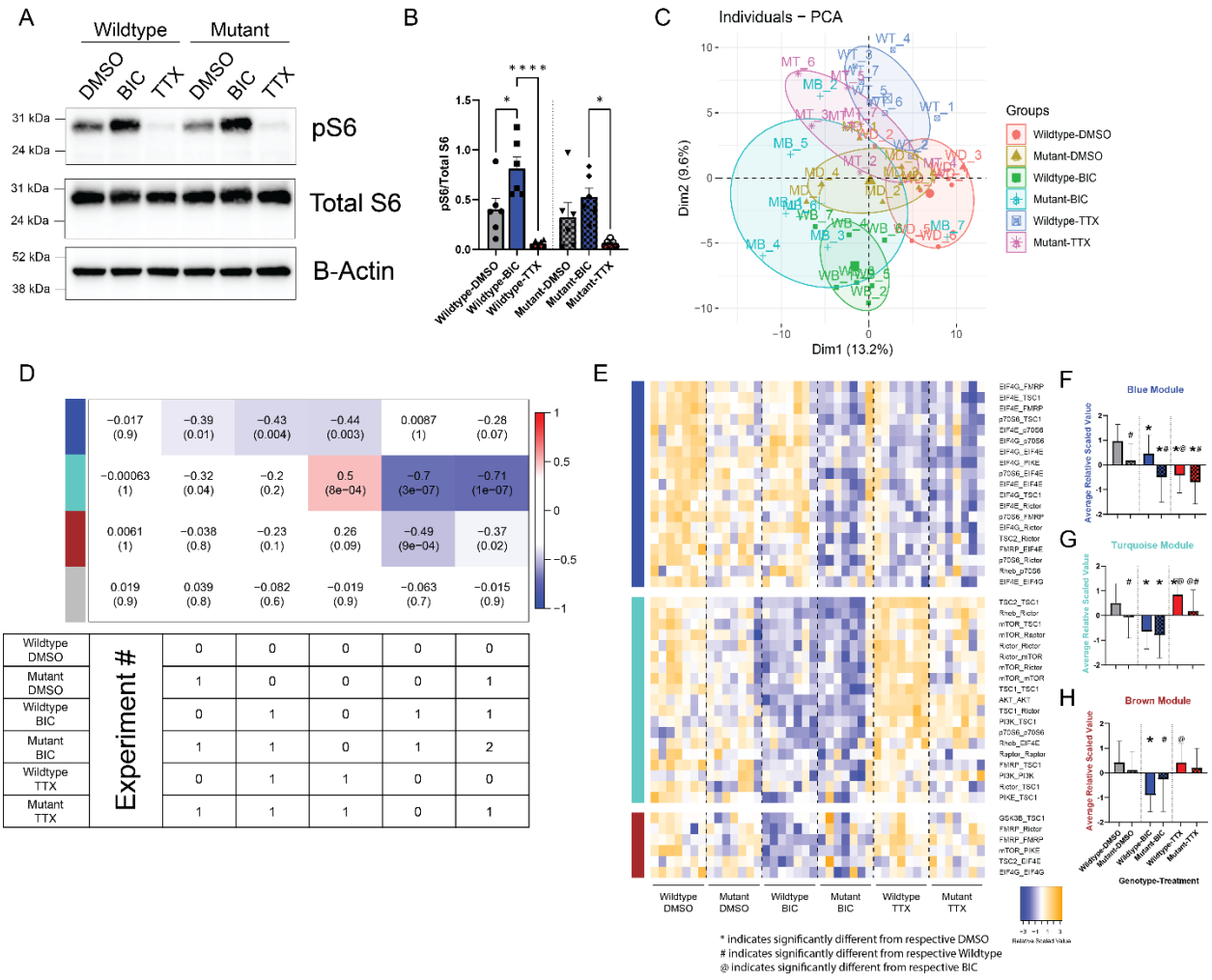

Figure 2.2: The loss of Shank3 dysregulates signaling through the mTOR protein interaction network during homeostatic scaling. A) Representative western blots showing phospho- and total S6 with actin for a loading control. B) Quantification of blots shown in A. * indicates significantly different from starved by ANOVA followed by Bonferroni-correction post-hoc testing, $p<0.05$. N =6. C) Principal component graph of QMI data, N=7. D) Module-trait table showing the correlation coefficient (top number) and p-value (bottom number) between the eigenvector of each color-coded module (colored rectangles on the left) and binary-coded trait labels (“hypotheses”) shown in the table below. E) Heatmap of the median scaled values of all significantly altered

interactions. Each box represents a single interaction measurement from a single biological replicate; columns correspond to a biological replicate while rows correspond to an interaction (IP_Probe), ordered by the timepoint that the interaction first reached significance. N =7. Statistical significance calculated by ANC and CNA statistics as detailed in methods. F-H) Mean scaled value of all interactions in the blue (translation), turquoise (mTORC1/2 regulation), and brown (mixed signaling) modules which corresponds to overall module behavior. For F-H, * indicates significantly by ANOVA followed by Bonferroni-corrected post-hoc testing, $p<0.05$.

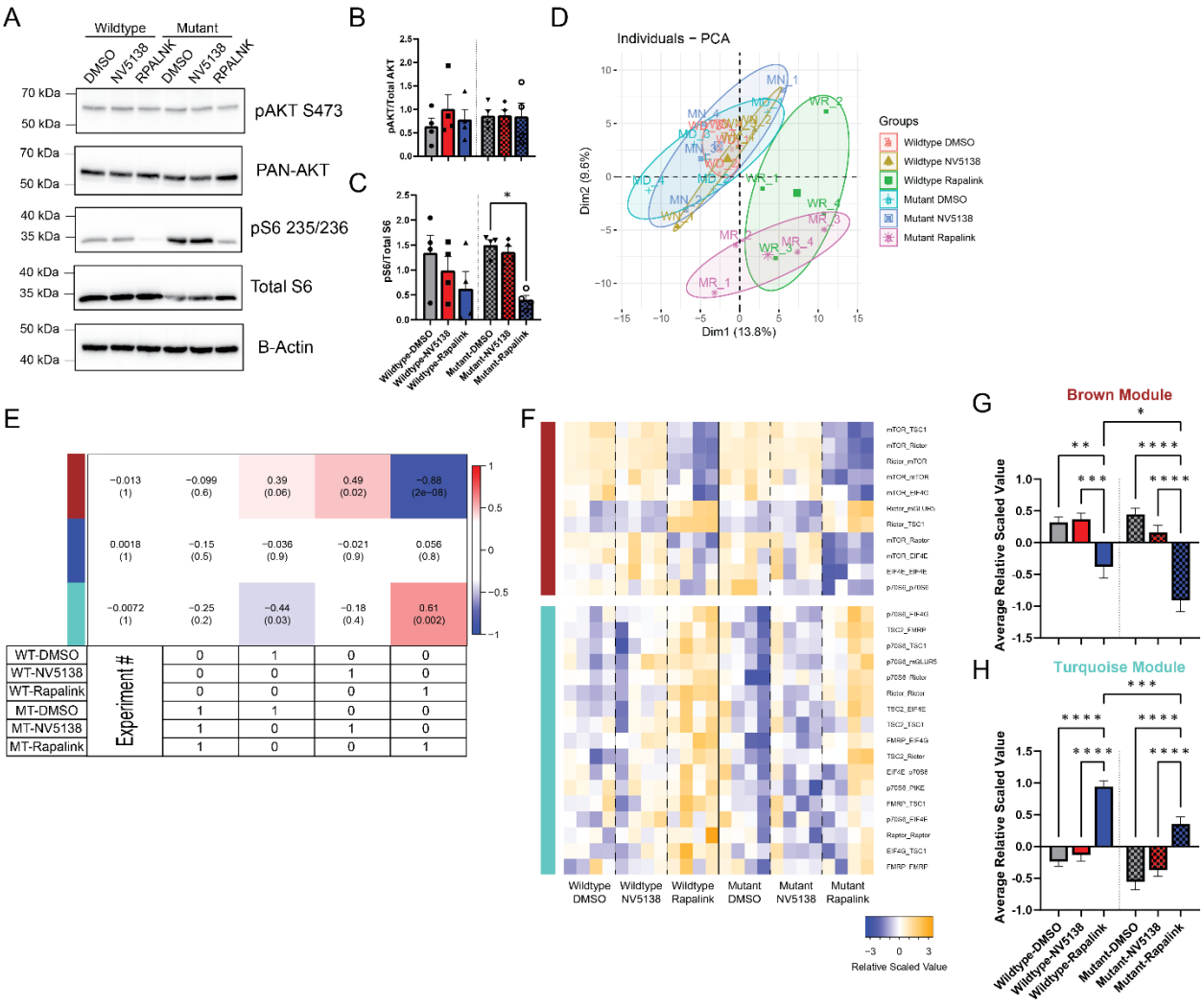

Figure 2.3: **Shank3-deficient neurons have an exaggerated response to Rapalink inhibition**. A) Representative western blots showing phospho- and total AKT and S6 with actin for a loading control. B-C) Quantification of blots shown in A. * indicates significantly different from starved by ANOVA followed by Bonferroni-correction post-hoc testing, $p<0.05$. N =4. D) Principal component graph of QMI data, N=4. E) Module-trait table showing the correlation coefficient (top number) and p-value (bottom number) between the eigenvector of each color-coded module (colored rectangles on the left) and binary-coded trait labels (“hypotheses”) shown in the table below. F) Heatmap of the median scaled values of all significantly altered interactions. Each box represents a

single interaction measurement from a single biological replicate; columns correspond to a biological replicate while rows correspond to an interaction (IP_Probe), ordered by the timepoint that the interaction first reached significance. N =4. Statistical significance calculated by ANC and CNA statistics as detailed in methods. G-H) Mean scaled value of all interactions in the brown (mTOR) and turquoise (translation/mTORC1/2 regulation) modules which corresponds to overall module behavior. For G-H, * indicates significantly by ANOVA followed by Bonferroni-corrected post-hoc testing, $p<0.05$.

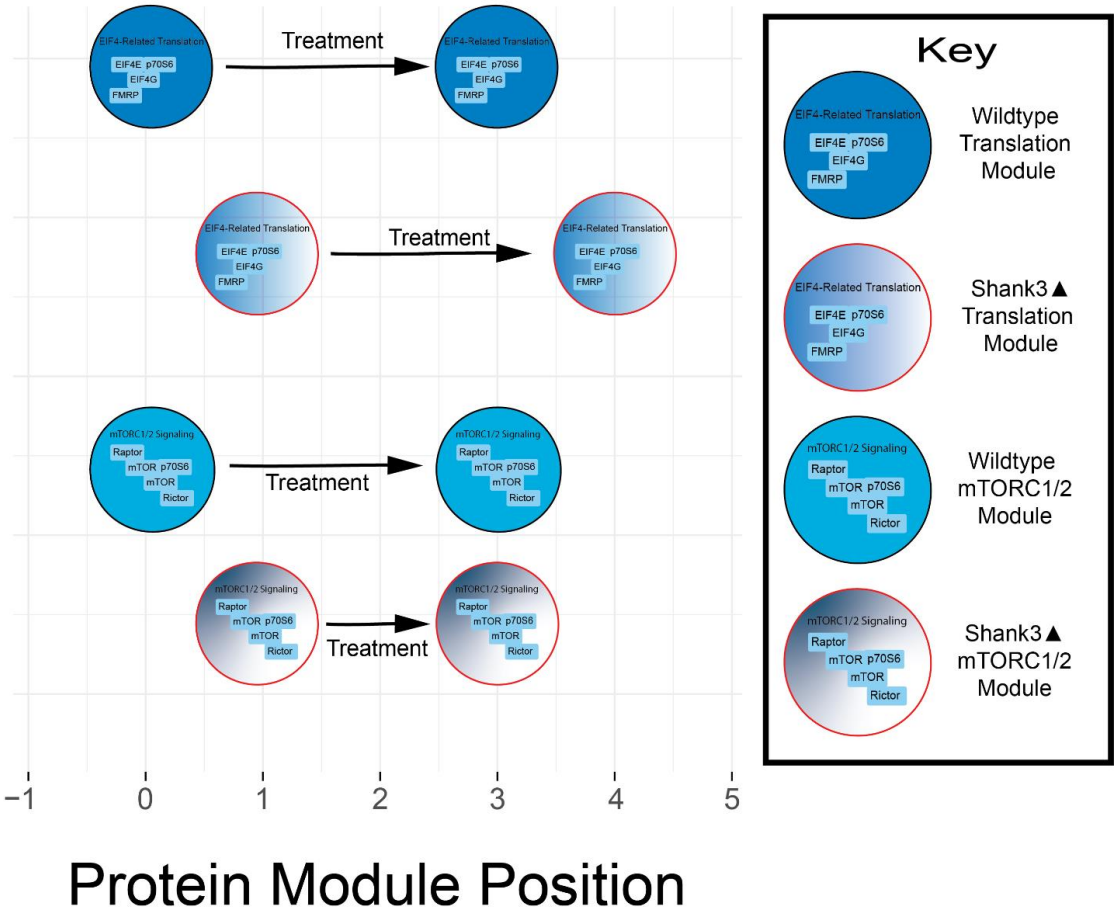

Figure 2.4: **Asymmetrical Effects of Shank3 deficiency on mTOR module behavior.** A graphical representation of the dysregulated response range of the mTOR network in Shank3 knockout neurons for the blue and turquoise modules from the homeostatic scaling experiments (Figure 2.1 and 2). The color and outline of each circle represents module membership and genotype respectively. The circles position represents the state of the interaction module while the arrows represent the new network state after treatment.

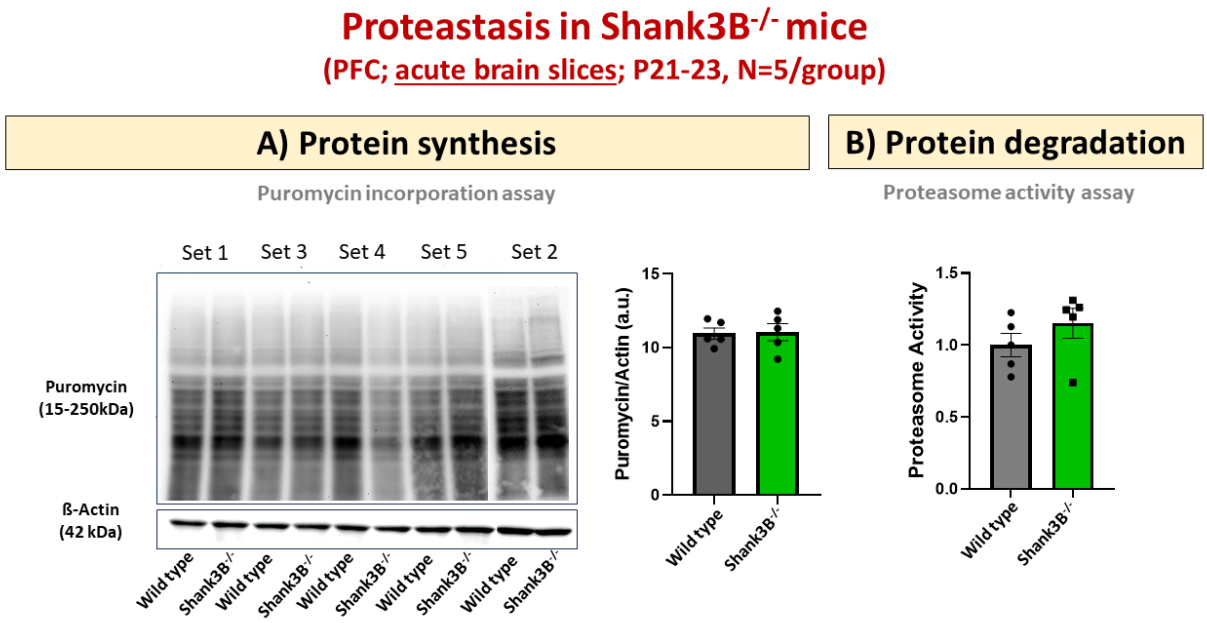

Figure S2.1: Analysis of the rate of protein synthesis and degradation in Shank3B knockout mice. A) Western blot analysis and quantification of puromycin incorporation from acute brain slices from P21-P23 mice. B) Quantification of the rate of proteasome activity comparing Shank3B knockout compared to wildtype counterparts.

Chapter 4:

Future steps in the characterization of mTOR signaling through the protein interaction network

The work described in dissertation has yielded many insights characterizing how biological signals and synaptic plasticity events are processed through the mTOR protein interaction network (PIN), and how autism related mutations disrupt that process. First, we have found that signaling through the mTOR protein interaction network occurs over longer periods of time than expected. While phosphorylation events occur within minutes of the mTOR pathway activating, robust changes to the protein interaction network take place over at least one hour. This long time-course was also observed during homeostatic scaling events, as the mTOR PINs response during scaling peaked at forty-eight hours rather than twelve. The mTOR PIN's slow kinetics were unexpected, as the glutamatergic and T-cell receptor protein interaction network responded over the course of minutes (Lautz et al., 2018; Smith et al., 2016).

Additionally, we found that various inhibitors of the mTOR pathway act on different combinations of the mTOR protein modules. Inhibition at different parts of the mTOR cascade acted on different sets of modules in a way that was not linearly related. For example, inhibition of PI3K did not also inhibit the modules that were affected by mTOR inhibition. One would not expect this as mTOR is downstream of PI3K and indicates that mTOR signaling through protein interaction networks is non-linear. This is further exemplified by the observation that ERK inhibition induced effects on the mTOR cascade that were comparable to direct mTOR inhibition.

Unexpectedly and contrary to observations made in the glutamatergic synapse, we found that the mTOR PIN does not respond to homeostatic scaling bidirectionally. Instead, we found that the direction of scaling can be differentiated by which

combination of modules are affected. Additionally, we were able to observe that the mTOR PIN of Shank3-deficient neurons was pre-scaled as hypothesized. However, we also found the response of the mTOR PIN was also warped, with some interaction modules displaying an exaggerated response during scaling and others just being pre-scaled at baseline. This indicated that the loss of Shank3 produces more complicated effects on mTOR signaling during synaptic scaling that previously expected.

There are many lines of inquiry that future research ought to undertake to better understand mTOR signaling and its role in synaptic events. However, the path that takes precedence concerns completing the characterization of mTOR protein network signaling during homeostatic scaling. While several insights were made in the experiments described in the third chapter, many important questions ought to be addressed. First, the functional relevance of the observations made during our Quantitative Multiplex Immunoprecipitation (QMI) experiments must be determined.

We have observed that the mTOR protein interaction network's behavior appears 'pre-scaled' in mutant Shank3 neurons. Specifically, we observed that Shank3-deficient neurons' baseline state resembles a downscaled network in neurotypical neurons, but mutant neurons still responded to BIC and TTX treatment. Additionally, some protein interaction modules displayed an exaggerated response despite being 'pre-scaled.' Shank3 deficient neurons also displayed an irregular response to mTOR inhibition with Rapalink. While these observations indicate that mTOR signaling during homeostatic scaling is dysfunctional in Shank3-deficient neurons, we are missing experimental observations that link mTOR network and synaptic deficiencies together.

Quantifying GluA1 surface expression during homeostatic scaling in Shank3 knockout neurons

One method to make a mechanistic connection between mTOR signaling deficits and synaptic deficits would be to use immunocytochemistry to quantify surface level GluA1 expression during homeostatic scaling. Such experiments have been performed in previous work by former laboratory members to validate the method of inducing homeostatic scaling (Heavner et al., 2021). Additionally, Shank3 mutant mice have demonstrated deficiencies in AMPA receptor expression during upscaling (Tatavarty et al., 2020). Rapamycin treatment also prevents synaptic signaling changes during homeostatic scaling (Sun et al., 2013). The immediately obvious experiment would be to quantify AMPA receptor expression in wildtype and Shank3 deficient neurons after homeostatic scaling. Additionally, we propose to observe the effect of Rapalink treatment during homeostatic scaling on both surface level AMPA receptor expression and the mTOR protein interaction network (PIN).

We propose the following experimental design. We will use immunohistochemistry and QMI to observe the relationship between scaling dependent changes in the mTOR PIN and AMPA receptor expression. Primary cultures of wildtype and Shank3-mutant mouse cortical neurons will be prepared as described in previous work in 6-well plates and on coverslips within 24-well plates. After 17 to 21 days in vitro, cortical neurons from the 6-well plates will be sorted into different treatment conditions for QMI analysis. Wildtype or Shank3B mutant cortical neurons from either genotype will be treated with TTX (2 μM), BIC (40 μM), or DMSO (0.4%) for 48 hours. Additionally, a different set of neurons will

be given Rapalink (10 nM) along with TTX, BIC, or DMSO treatment for a total of twelve conditions.

After treatment, the neurons in the 6-well plates will be lysed and analyzed with QMI. Concurrently, wildtype and mutant neurons on coverslips will be treated using the experimental conditions described above to quantify surface GluA1 expression. After 48 hours of treatment, a GluA1 antibody will be added to each culture for 20 minutes. Afterwards, each coverslip will be fixed and mounted as previously described (Heavner et al., 2021).

The aim of these concurrent experiments is to observe the relationship between scaling dependent changes in the mTOR protein network and AMPA receptor expression. Additionally, we aim to observe how Rapalink treatment interferes with both AMPA receptor expression and signaling through the mTOR protein network during homeostatic scaling. Regarding the QMI experiments, we expect to first recapitulate earlier results that showed mTOR signaling deficits in Shank3 mutant neurons during homeostatic scaling. Additionally, we expect that Rapalink treatment will prevent wildtype neurons from responding to either TTX or BIC. Specifically, we expect that profile of the mTOR network will reflect mTOR inhibition regardless of TTX or BIC treatment in wildtype neurons. In mutant neurons, we expect that the exaggerated response observed during homeostatic scaling will be dampened by Rapalink treatment, and the network profile will more strongly resemble the wildtype.

Regarding the immunocytochemistry experiments, we expect to recapitulate previous experimental observations. Surface level AMPA expression should increase and decrease following TTX and BIC treatment respectively in wildtype neurons. We also

hypothesize that Rapalink treatment in wildtype neurons will prevent either TTX or BIC treatment to induce changes in AMPA receptor expression, based on previous research (Sun et al., 2012). In Shank3 deficient neurons, we expect that TTX will fail to induce changes in AMPA expression as this has been observed previously (Tatarvaty et al., 2020). During BIC treatment, we hypothesize that AMPA expression should still decrease in mutant neurons. This is because the response to BIC treatment in the mTOR signaling network of mutant neurons is dysregulated but intact. We also expect that Rapalink treatment will reduce if not outright prevent scaling dependent changes in Shank3 deficient neurons.

Measuring Shank3 driven electrophysiological deficits and the effect of Rapalink treatment

An alternative method to provide a mechanistic insight into the relationship between mTOR signaling and synaptic scaling would be to perform electrophysiological experiments. The experimental design would utilize the same conditions outlined above and would be performed as they have been in our laboratory's previous work (Heavner et al., 2021). In wildtype neurons, we would expect that the TTX treatment would increase EPSC amplitude and frequency while BIC treatment would induce a decrease in amplitude and frequency. Rapalink treatment should abolish scaling in wildtype neurons, preventing changes in EPSC amplitude and frequency. In mutant neurons, we would expect TTX treatment to fail to induce electrophysiological changes. BIC treatment is expected to still induce a decrease in the response of mutant neurons. As previously stated, Rapalink treatment should prevent upscaling in mutant neurons and blunt the downscaling response.

These experiments would serve to directly connect observations in Shank3 deficient neurons' mTOR protein network with the outcome at the synapse. If we observe that inhibition of mTOR directly affects synaptic structure/signaling along with the mTOR protein interaction network, we can more confidently state that the mTOR protein network reflects and mediates synaptic scaling events. Additionally, we could provide a more potent link between Shank3 related deficits in both mTOR signaling and synaptic scaling to one another. These experiments would allow a much stronger conclusion to the observations made in the third chapter.

Identifying convergent ASD models through analysis of the mTOR protein interaction network

Future research ought to analyze a variety of ASD mouse models using the mTOR QMI assay. Development for the mTOR antibody panel was inspired by observations made using the glutamatergic synapse QMI panel. Previous researchers in the Smith lab analyzed seven different models of ASD using the glutamatergic synapse panel. These models included Shank3B, Shank3Δex4-9, Ube3a^{2xTG}, TSC2, FMR1, CNTNAP2, and the E12.5 VPA (maternal valproic acid injection on day 12.5 post-conception). Analysis of each models' synaptic protein network with hierarchical clustering on principal component (HCPC) analysis revealed that the TSC2, Ube3a^{2xTG}, and the VPA model clustered together. While the TSC2 and VPA models had previously described mTOR signaling deficits, such signaling deficits had not been implicated in the Ube3a model at the time. However, subsequent western blot experiments revealed a significant reduction in AKT phosphorylation in Ube3a^{2xTG} neurons. This result indicated that different models of autism could be categorized by patterns in their protein interaction

network and these patterns might reflect core molecular deficits shared amongst ASD models.

ASD is a heterogeneous neurodevelopmental disorder and variation exists in nearly all symptom domains that the disorder encompasses. This variation is a substantial barrier in creating a comprehensive, mechanistic understanding of ASD as well as in the identification of biomarkers. One solution to this challenge is to attempt to identify sub-groups of autism based on a convergent phenotype. For instance, neuroimaging has been used to characterize ASD related deficits in brain structure and function with the aim of identifying common trends that indicate subtypes (Hong et al., 2020). The most prominent efforts in subtyping ASD have been the use of genomics and transcriptomics to identify functional molecular nodes that subtypes of ASD converge upon. For example, analysis of gene expression differences between ASD and neurotypical brains revealed discrete modules of ASD related genes: one module was enriched in neuronal genes previously related to ASD while another module was enriched for immune and glial genes (Voineagu et al., 2011). Genomic analysis of rare risk variants has identified multiple points and layers of convergence. These points can include developmental time, cell type, biological pathway, and protein-protein interaction networks (Bicks and Geschwind 2024). We hypothesized that the mTOR signaling cascade is a point of molecular convergence for ASD. Deficits in mTOR signaling have been identified in a variety of models of ASD, various components of mTOR signaling are ASD risk genes, and mTOR signaling is crucial for neuronal signaling events that are implicated in ASD.

The broad aim of this proposed project would be to determine if models of autism cluster together based on patterns in the mTOR protein interaction network. Such an

observation would indicate whether the mTOR cascade is a convergent signaling node and different forms of ASD can be understood based on how each subtype affects mTOR signaling. Additionally, we may also identify deficits in ASD models not previously described based on possible deficits in the mTOR network, like how mTOR deficits were uncovered in the Ube3a^{2xTG} based on how the ASD model's glutamatergic network clustered.

To better understand how different subtypes of ASD may cluster, we propose to analyze different models of ASD with various relevance to mTOR signaling. The most obvious candidates for analysis are ASD models whose genes are directly involved in mTOR signaling. These mTOR-affected models would include FMR1, PTEN, and TSC models. The fragile X messenger ribonucleoprotein 1 (FMR1) gene encodes the protein FMRP and mutations in the CGG repeats induce methylation of the FMR1 promoters and the subsequent silencing of the FMR1 gene. This underlies Fragile X syndrome, an intellectual disability and one of the most common causes of syndromic ASD. FMRP is a regulator of translation that is downstream of mTOR signaling. mTOR signaling is also dysregulated in FMR1 deficient mice (Sharma et al., 2010). Tuberous sclerosis complex (TSC) is genetic disorder caused by mutations in either the TSC1 or TSC2 genes, whose protein products form a complex that inhibits mTORC1 activity. Like fragile X syndrome, it is a neurodevelopmental disorder that is a common cause of syndromic ASD (Mitchel et al., 2022). PTEN is an inhibitor of the mTOR pathway that dephosphorylates PIP3, resulting in inhibition of AKT and subsequently mTOR. PTEN has also been identified as a significant ASD risk gene (Satterstrom et al., 2020). Additionally, all four protein targets for each model are included on the current mTOR

antibody panel. These three models of autism are ideal to analyze with the mTOR panel as it is highly likely that they will display deficits in signaling through the mTOR protein interaction network. These three models will also serve as a point of comparison with other ASD models.

The next set of candidates include the SynGAP, Homer1, and Ube3a^{2xTG} models of ASD. These three models of ASD, though not directly part of the canonical mTOR cascade, have all demonstrated mTOR signaling deficits and we hypothesize that they are likely to display deficits in the mTOR protein interaction network. SynGAP is an abundant synaptic protein that plays many crucial roles in synaptic functions and has been identified as a strong ASD candidate gene (Hamdan et al., 2011; Satterstorm et al., 2020). SynGAP's role in the synapse also involves the regulation of translation through Erk and mTOR signaling (Wang et al., 2013). The Ube3a protein is an E3 ubiquitin ligase that is involved in protein degradation, is a highly implicated ASD risk gene, and is the cause of the neurodevelopmental disorder Angelman syndrome (Kishino et al., 1997; Nurmi et al., 2001). As mentioned previously, the Ube3a overexpression model has demonstrated deficits in ASD signaling (Brown et al., 2018). Homer1 proteins are synaptic scaffolding proteins for the metabotropic glutamate receptors. The assembly and disassembly of Homer1 scaffolding proteins with mGLUR receptors and other synaptic proteins underlie synaptic plasticity and regulate mTOR signaling in response to mGLUR5 binding (Rybchyn et al., 2019). Disruptions in the Homer1 scaffold underlie abnormal mGLUR5 signaling in the FMR1 model and Homer1 has been identified as an ASD risk gene (Kelleher RJ 3rd et al., 2012; Ronesi et al., 2012). Though these three genes are not directly part of the mTOR pathway, their

function has been linked to mTOR signaling. They may display behavior like the Shank3 model. The Shank3 gene, like the three beforementioned ASD models, is an ASD risk gene with indirect links to mTOR signaling. We did not necessarily expect to observe deficits in the mTOR protein interaction network in the Shank3 model, but we had reason to believe in the possibility. In this way, the SynGAP, Homer1, and Ube3a^{2xTG} models are promising candidates for analysis.

In contrast with any of the previously mentioned ASD models, the remainder of the chosen ASD models have tenuous connections to mTOR signaling. There is little reason to expect that these models, SCN2A, CHD8, and ARID1B, would display deficits in the mTOR protein interaction network or converge with other models like PTEN or TSC. The SCN2A gene encodes the alpha subunit of the voltage gated sodium channel. SCN2A is regarded as a very strong ASD risk gene and is also implicated in epilepsy disorder Dravet syndrome (Weiss et al., 2003; Wolf et al., 2017). While one would not expect a sodium channel to be directly linked to mTOR signaling, mTORC2 has recently been demonstrated to bind to and regulate SCN2A (Okoh et al., 2023). The chromodomain helicase DNA binding protein 8 (CHD8) is a component of the Wnt pathway that interacts with B-catenin and regulates its transcriptional activity (Kasherman et al., 2020). CHD8 is highly associated with ASD that also regulates other the transcription of other ASD risk genes (Wilkinson et al., 2015). As a component of the Wnt signaling pathway, CHD8 only has an indirect link to mTOR signaling through mutual regulation of B-Catenin and mTOR signaling (Prossomariti et al., 2020). The AT-rich DNA interacting domain containing protein (ARID1B) is a member of the chromatin remodeling complex and is strongly associated with ASD. ARID1B is also

associated with the developmental disorder Coffin-Siris syndrome (Nord et al., 2011). ARID1B also regulates mTOR expression as ARID1B knockdown increases mTOR RNA expression while ARID1B gene activation reduces mTOR RNA expression. ARID1B binds to the mTOR promoter and blocks methionine induced mTOR gene transcription (Lin et al., 2023).

These three ASD models were chosen because the proteins associated with each gene target are not traditionally connected to mTOR signaling. Though SCN2A, CHD8, and ARID1B have some connection to the mTOR cascade, we do not expect hypothetical dysregulation of mTOR signaling to be as robust as mTOR-affected ASD models. It is possible that analysis of the mTOR protein interaction network of SCN2A, CHD8, and ARID1B models could yield robust results. However, it is more likely that any deficits observed will be more modest compared to the other previously mentioned ASD models.

After each ASD model has been gathered, the first set of experiments to be done would follow the format set out by the previous ASD clustering experiments. At 60 days of age, wildtype and mutant mouse pairs for each model would be anesthetized before the removal of each brain. While day 60 was chosen previously as behavioral analysis of mouse models typically focuses on adults, additional experiments using younger mice ought to be considered. Different models of ASD may display different developmental trajectories. Specifically, a model may display a deficit at one age that is not present at another. Using mice at both day 21 and 60 may prove insightful in characterizing developmental changes in the mTOR network. Additionally, these experiments ought to

use both male and female mice to isolate any sex dependent difference between the models.

After the removal of the brain, the frontal cortex and hippocampus will be isolated, removed, and then frozen in liquid nitrogen. The frozen tissue will then be frozen at -80 degrees Celsius until all necessary samples are collected. The samples ought to be frozen instead of immediately analyzed to ensure that all samples are from mice of the same age. Once all samples are gathered, they will be homogenized with lysis buffer and analyzed using QMI.

We hypothesize that the mTOR-affected FMR1, TSC, and PTEN models will display the most robust deficits in mTOR network behavior. Additionally, the mTOR-affected models should also show patterns in protein interactions that are more alike when compared to the other models. Conversely, the SCN2A, ARID1B, and CHD8 models ought to cluster away from the mTOR-affected models because their gene targets are less associated with the mTOR cascade. The SynGAP, Homer1, and Ube3a models may cluster in several ways. One possibility is that these models may display patterns in mTOR network behavior like the mTOR-affected ASD models. This result could indicate the existence of a large ASD subtype that broadly contains types of autism with mTOR signaling deficits. Another possible result could be robust patterns of mTOR interaction deficits that are distinct from the mTOR-affected models. This hypothetical result could also appear in the SynGAP, Homer1, and Ube3a models. Such an observation may indicate that these ASD mutations converge on the mTOR pathway but split into unique subtypes that reflect how they affect the mTOR protein network. Specifically, different modules of protein interactions may be associated with different groups of ASD models.

Regardless of how these results may hypothetically come about, we expect to observe some indication that various ASD models converge on the mTOR pathway. The experiments that follow would depend on how each ASD model clusters if they do at all. Follow up experiments may include validating mTOR signaling deficits through western blotting. This would occur if an ASD model that has not yet displayed mTOR signaling deficits groups with models that have displayed deficits.

Analysis of mTOR inhibition on different models of ASD

Furthermore, each ASD model ought to be analyzed with QMI following treatment with mTOR inhibitors or activators. The mTOR cascade has been identified as a potential therapeutic target for various models of ASD (Sato 2016; Thomas et al., 2023). Inhibition of the mTOR cascade has reversed social and neurological deficits in the TSC and PTEN mutant mice models (Sato et al., 2012; Tsai et al., 2012; Schneider et al., 2017; Zhou et al., 2009). Insulin growth factor 1 (IGF-1), an activator of the mTOR cascade, has been used to potentially treat ASD (Riikonen 2016). IGF-1 has rescued synaptic deficits in neurons from patients with Phelan–McDermid syndrome (Shcheglovitov et al., 2013). However, rapamycin treatment exacerbated behavioral deficits in FMR1-deficient mice while normalizing mTOR signaling deficits (Sare et al., 2018). Unexpectedly, application of a synthetic IGF-1 analog to FMR1-deficient mice corrects behavior, synaptic, and overactive mTOR signaling deficits (Deacon et al, 2015) Additionally, IGF-1 treatment in neurons derived from idiopathic ASD patients induced heterogeneous responses in gene expression, indicating that ASD individuals may be either IGF-1 responsive or non-responsive (Linker et al., 2020). Various forms of ASD may respond differently to treatments targeting mTOR signaling. It is clinically

important to understand the effect that mTOR activation or inhibition has on different ASD models.

We propose to use Rapalink-1 and IGF-1 treatment on cortical neuron cultures derived from the nine previously identified ASD models. Primary cultures of wildtype and mutant mouse cortical neurons will be prepared as described in previous work in 6-well plates. After 17 to 21 days in vitro, cultured neurons will be sorted into different treatment conditions for QMI analysis. Cortical neurons from either genotype will be treated with Rapalink-1 (10 nM) or IGF-1 (1 μM) for 48 hours. After treatment, the neurons will be lysed and analyzed with the mTOR QMI panel. If either treatment is insufficient to induce measurable changes in the mTOR PIN, there are alternative drugs that can be used. The brain specific mTORC1 activator NV5138 or the IGF1 analog NNZ-2566 could be used as an IGF1 alternative. The rapalog RAD001 or the ATP competitive mTOR inhibitor sapanisertib could be used instead of Rapalink.

We hypothesize that different models of ASD will cluster based on which treatment normalizes deficits in the mTOR protein interaction network (PIN). We expect the TSC, PTEN, and SynGAP models will cluster together and to be normalized by Rapalink treatment because these models are either mTOR hyperactive or have been rescued by mTOR inhibition. Conversely, we expect that FMR1, Homer, and Ube3a models to cluster together and to be rescued by IGF treatment because these models are either mTOR hypoactivity or have been rescued by mTOR activation. The SCN2A, ARID1B, and CHD8 models ought to cluster away from either group as we do not expect either treatment to normalize the models' function. Alternatively, the SCN2A, ARID1B, and CHD8 models may reveal mTOR signaling deficits and cluster accordingly. Overall, we

hypothesize that different ASD models will reveal patterns of mTOR protein interactions that correspond to whether targeting the mTOR pathway pharmacologically normalizes neuronal functioning. We hope that these patterns in the mTOR PIN will also be predictive of whether the model is responsive to mTOR inhibition or activation. Categorizing different forms of ASD by which treatments are viable would not only give useful insights into the function of specific ASD models but would also aid in accurately determining which treatments would be effective in ASD patients.

Conclusions

There are many lines of inquiry that could be taken to further characterize ASD through the mTOR protein interaction network. There are dozens of possible ASD models that could be studied, drug treatments that can be characterized, and various mTOR dependent neuronal events to interrogate. As these studies are made in the future, they will hopefully provide insight into shared mechanisms that contribute to ASD. By elucidating such mechanisms, we may not only be able to better understand autism, but also answer questions at the root of synaptic and cell signaling.

References

Bicks, L. K., & Geschwind, D. H. (2024). Functional neurogenomics in autism spectrum disorders: A decade of progress. *Current Opinion in Neurobiology*, *86*, 102858. https://doi.org/10.1016/j.conb.2024.102858

Brown, E. A., Lautz, J. D., Davis, T. R., Gniffke, E. P., VanSchoiack, A. A. W., Neier, S. C., Tashbook, N., Nicolini, C., Fahnestock, M., Schrum, A. G., & Smith, S. E. P. (2018). Clustering the autisms using glutamate synapse protein interaction networks from cortical and hippocampal tissue of seven mouse models. *Molecular Autism*, *9*(1), 48. https://doi.org/10.1186/s13229-018-0229-1

Deacon, R. M. J., Glass, L., Snape, M., Hurley, M. J., Altimiras, F. J., Biekofsky, R. R., & Cogram, P. (2015). NNZ-2566, a Novel Analog of (1–3) IGF-1, as a Potential Therapeutic Agent for Fragile X Syndrome. *NeuroMolecular Medicine*, *17*(1), 71–82. https://doi.org/10.1007/s12017-015-8341-2

Hamdan, F. F., Daoud, H., Piton, A., Gauthier, J., Dobrzeniecka, S., Krebs, M.-O., Joober, R., Lacaille, J.-C., Nadeau, A., Milunsky, J. M., Wang, Z., Carmant, L., Mottron, L., Beauchamp, M. H., Rouleau, G. A., & Michaud, J. L. (2011). De novo SYNGAP1 mutations in nonsyndromic intellectual disability and autism. *Biological Psychiatry*, *69*(9), 898–901. https://doi.org/10.1016/j.biopsych.2010.11.015

Heavner, W. E., Lautz, J. D., Speed, H. E., Gniffke, E. P., Immendorf, K. B., Welsh, J. P., Baertsch, N. A., & Smith, S. E. P. (2021). Remodeling of the Homer-Shank interactome mediates homeostatic plasticity. *Science Signaling*, *14*(681), eabd7325. https://doi.org/10.1126/scisignal.abd7325

Hong, S.-J., Valk, S. L., Di Martino, A., Milham, M. P., & Bernhardt, B. C. (2018). Multidimensional Neuroanatomical Subtyping of Autism Spectrum Disorder. *Cerebral Cortex*, *28*(10), 3578–3588. https://doi.org/10.1093/cercor/bhx229

Hong, S.-J., Vogelstein, J. T., Gozzi, A., Bernhardt, B. C., Yeo, B. T. T., Milham, M. P., & Di Martino, A. (2020). Toward Neurosubtypes in Autism. *Biological Psychiatry*, *88*(1), 111–128. https://doi.org/10.1016/j.biopsych.2020.03.022

Kasherman, M. A., Premarathne, S., Burne, T. H. J., Wood, S. A., & Piper, M. (2020). The Ubiquitin System: A Regulatory Hub for Intellectual Disability and Autism Spectrum Disorder. *Molecular Neurobiology*, *57*(5), 2179–2193. https://doi.org/10.1007/s12035-020-01881-x

Kelleher, R. J., Geigenmüller, U., Hovhannisyan, H., Trautman, E., Pinard, R., Rathmell, B., Carpenter, R., & Margulies, D. (2012). High-throughput sequencing of mGluR signaling pathway genes reveals enrichment of rare variants in autism. *PloS One*, *7*(4), e35003. https://doi.org/10.1371/journal.pone.0035003

Kishino, T., Lalande, M., & Wagstaff, J. (1997). UBE3A/E6-AP mutations cause Angelman syndrome. *Nature Genetics*, *15*(1), 70–73. https://doi.org/10.1038/ng0197-70

Kolevzon, A., Breen, M. S., Siper, P. M., Halpern, D., Frank, Y., Rieger, H., Weismann, J., Trelles, M. P., Lerman, B., Rapaport, R., & Buxbaum, J. D. (2022). Clinical trial of insulin-like growth factor-1 in Phelan-McDermid syndrome. *Molecular Autism*, *13*(1), 17. https://doi.org/10.1186/s13229-022-00493-7

Lautz, J. D., Brown, E. A., Williams VanSchoiack, A. A., & Smith, S. E. P. (2018). Synaptic activity induces input-specific rearrangements in a targeted synaptic protein interaction network. *Journal of Neurochemistry*, *146*(5), Article 5. https://doi.org/10.1111/jnc.14466

Lin, G., Qi, H., Guo, X., Wang, W., Zhang, M., & Gao, X. (2023). ARID1B blocks methionine-stimulated mTOR activation to inhibit milk fat and protein synthesis in and proliferation of mouse mammary epithelial cells. *The Journal of Nutritional Biochemistry*, *114*, 109274. https://doi.org/10.1016/j.jnutbio.2023.109274

Linker, S. B., Mendes, A. P. D., & Marchetto, M. C. (2020). IGF-1 treatment causes unique transcriptional response in neurons from individuals with idiopathic autism. *Molecular Autism*, *11*(1), 55. https://doi.org/10.1186/s13229-020-00359-w

Mitchell, R. A., Mitchell, M., & Williams, K. (2022). The autism spectrum disorder phenotype in children with tuberous sclerosis complex: A systematic review and meta-analysis. *Developmental Medicine & Child Neurology*, *64*(10), 1214–1229. https://doi.org/10.1111/dmcn.15307

Nord, A. S., Roeb, W., Dickel, D. E., Walsh, T., Kusenda, M., O'Connor, K. L., Malhotra, D., McCarthy, S. E., Stray, S. M., Taylor, S. M., Sebat, J., STAART Psychopharmacology Network, King, B., King, M.-C., & McClellan, J. M. (2011). Reduced transcript expression of genes affected by inherited and de novo CNVs in autism. *European Journal of Human Genetics: EJHG*, *19*(6), 727–731. https://doi.org/10.1038/ejhg.2011.24

Nurmi, E. L., Bradford, Y., Chen, Y., Hall, J., Arnone, B., Gardiner, M. B., Hutcheson, H. B., Gilbert, J. R., Pericak-Vance, M. A., Copeland-Yates, S. A., Michaelis, R. C., Wassink, T. H., Santangelo, S. L., Sheffield, V. C., Piven, J., Folstein, S. E., Haines, J. L., & Sutcliffe, J. S. (2001). Linkage disequilibrium at the Angelman syndrome gene UBE3A in autism families. *Genomics*, *77*(1–2), 105–113. https://doi.org/10.1006/geno.2001.6617

Okoh, J., Mays, J., Bacq, A., Oses-Prieto, J. A., Tyanova, S., Chen, C.-J., Imanbeyev, K., Doladilhe, M., Zhou, H., Jafar-Nejad, P., Burlingame, A., Noebels, J., Baulac, S., & Costa-Mattioli, M. (2023). Targeted suppression of mTORC2 reduces seizures across models of epilepsy. *Nature Communications*, *14*, 7364. https://doi.org/10.1038/s41467-023-42922-y

Prossomariti, A., Piazzi, G., Alquati, C., & Ricciardiello, L. (2020). Are Wnt/β-Catenin and PI3K/AKT/mTORC1 Distinct Pathways in Colorectal Cancer? *Cellular and Molecular Gastroenterology and Hepatology*, *10*(3), 491–506. https://doi.org/10.1016/j.jcmgh.2020.04.007

Riikonen, R. (2016). Treatment of autistic spectrum disorder with insulin-like growth factors. *European Journal of Paediatric Neurology*, *20*(6), 816–823. https://doi.org/10.1016/j.ejpn.2016.08.005

Ronesi, J. A., Collins, K. A., Hays, S. A., Tsai, N.-P., Guo, W., Birnbaum, S. G., Hu, J.-H., Worley, P. F., Gibson, J. R., & Huber, K. M. (2012). Disrupted Homer scaffolds mediate abnormal mGluR5 function in a mouse model of fragile X syndrome. *Nature Neuroscience*, *15*(3), 431–440. https://doi.org/10.1038/nn.3033

Rybchyn, M. S., Islam, K. S., Brennan-Speranza, T. C., Cheng, Z., Brennan, S. C., Chang, W., Mason, R. S., & Conigrave, A. D. (2019). Homer1 mediates CaSR-

dependent activation of mTOR complex 2 and initiates a novel pathway for AKT-dependent β-catenin stabilization in osteoblasts. *The Journal of Biological Chemistry*, *294*(44), 16337–16350. https://doi.org/10.1074/jbc.RA118.006587

Saré, R. M., Song, A., Loutaev, I., Cook, A., Maita, I., Lemons, A., Sheeler, C., & Smith, C. B. (2018). Negative Effects of Chronic Rapamycin Treatment on Behavior in a Mouse Model of Fragile X Syndrome. *Frontiers in Molecular Neuroscience*, *10*. https://doi.org/10.3389/fnmol.2017.00452

Sato, A. (2016). mTOR, a Potential Target to Treat Autism Spectrum Disorder. *CNS & Neurological Disorders - Drug Targets- CNS & Neurological Disorders)*, *15*(5), 533–543.

Sato, A., Kasai, S., Kobayashi, T., Takamatsu, Y., Hino, O., Ikeda, K., & Mizuguchi, M. (2012). Rapamycin reverses impaired social interaction in mouse models of tuberous sclerosis complex. *Nature Communications*, *3*, 1292. https://doi.org/10.1038/ncomms2295

Satterstrom, F. K., Kosmicki, J. A., Wang, J., Breen, M. S., De Rubeis, S., An, J.-Y., Peng, M., Collins, R., Grove, J., Klei, L., Stevens, C., Reichert, J., Mulhern, M. S., Artomov, M., Gerges, S., Sheppard, B., Xu, X., Bhaduri, A., Norman, U., … Buxbaum, J. D. (2020). Large-Scale Exome Sequencing Study Implicates Both Developmental and Functional Changes in the Neurobiology of Autism. *Cell*, *180*(3), 568-584.e23. https://doi.org/10.1016/j.cell.2019.12.036

Schneider, M., de Vries, P. J., Schönig, K., Rößner, V., & Waltereit, R. (2017). mTOR inhibitor reverses autistic-like social deficit behaviours in adult rats with both Tsc2 haploinsufficiency and developmental status epilepticus. *European Archives of Psychiatry and Clinical Neuroscience*, *267*(5), 455–463. https://doi.org/10.1007/s00406-016-0703-8

Sharma, A., Hoeffer, C. A., Takayasu, Y., Miyawaki, T., McBride, S. M., Klann, E., & Zukin, R. S. (2010). Dysregulation of mTOR Signaling in Fragile X Syndrome. *The Journal of Neuroscience*, *30*(2), 694–702. https://doi.org/10.1523/JNEUROSCI.3696-09.2010

Shcheglovitov, A., Shcheglovitova, O., Yazawa, M., Portmann, T., Shu, R., Sebastiano, V., Krawisz, A., Froehlich, W., Bernstein, J. A., Hallmayer, J. F., & Dolmetsch, R. E. (2013). SHANK3 and IGF1 restore synaptic deficits in neurons from 22q13 deletion syndrome patients. *Nature*, *503*(7475), 267–271. https://doi.org/10.1038/nature12618

Smith, S. E. P., Neier, S. C., Reed, B. K., Davis, T. R., Sinnwell, J. P., Eckel-Passow, J. E., Sciallis, G. F., Wieland, C. N., Torgerson, R. R., Gil, D., Neuhauser, C., & Schrum, A. G. (2016). Multiplex matrix network analysis of protein complexes in the human TCR signalosome. *Science Signaling*, *9*(439), Article 439. https://doi.org/10.1126/scisignal.aad7279

Sun, H., Kosaras, B., Klein, P. M., & Jensen, F. E. (2013). Mammalian target of rapamycin complex 1 activation negatively regulates Polo-like kinase 2-mediated homeostatic compensation following neonatal seizures. *Proceedings of the National Academy of Sciences of the United States of America*, *110*(13), 5199–5204. https://doi.org/10.1073/pnas.1208010110

Tatavarty, V., Torrado Pacheco, A., Groves Kuhnle, C., Lin, H., Koundinya, P., Miska, N. J., Hengen, K. B., Wagner, F. F., Van Hooser, S. D., & Turrigiano, G. G.

(2020). Autism-Associated Shank3 Is Essential for Homeostatic Compensation in Rodent V1. *Neuron*, *106*(5), 769-777.e4. https://doi.org/10.1016/j.neuron.2020.02.033

Thomas, S. D., Jha, N. K., Ojha, S., & Sadek, B. (2023). mTOR Signaling Disruption and Its Association with the Development of Autism Spectrum Disorder. *Molecules*, *28*(4), Article 4. https://doi.org/10.3390/molecules28041889

Tsai, P. T., Hull, C., Chu, Y., Greene-Colozzi, E., Sadowski, A. R., Leech, J. M., Steinberg, J., Crawley, J. N., Regehr, W. G., & Sahin, M. (2012). Autistic-like behaviour and cerebellar dysfunction in Purkinje cell Tsc1 mutant mice. *Nature*, *488*(7413), 647–651. https://doi.org/10.1038/nature11310

Voineagu, I., Wang, X., Johnston, P., Lowe, J. K., Tian, Y., Horvath, S., Mill, J., Cantor, R. M., Blencowe, B. J., & Geschwind, D. H. (2011). Transcriptomic analysis of autistic brain reveals convergent molecular pathology. *Nature*, *474*(7351), 380–384. https://doi.org/10.1038/nature10110

Wang, C.-C., Held, R. G., & Hall, B. J. (2013). SynGAP Regulates Protein Synthesis and Homeostatic Synaptic Plasticity in Developing Cortical Networks. *PLoS ONE*, *8*(12), e83941. https://doi.org/10.1371/journal.pone.0083941

Weiss, L. A., Escayg, A., Kearney, J. A., Trudeau, M., MacDonald, B. T., Mori, M., Reichert, J., Buxbaum, J. D., & Meisler, M. H. (2003). Sodium channels SCN1A, SCN2A and SCN3A in familial autism. *Molecular Psychiatry*, *8*(2), 186–194. https://doi.org/10.1038/sj.mp.4001241

Wilkinson, B., Grepo, N., Thompson, B. L., Kim, J., Wang, K., Evgrafov, O. V., Lu, W., Knowles, J. A., & Campbell, D. B. (2015). The autism-associated gene chromodomain helicase DNA-binding protein 8 (CHD8) regulates noncoding RNAs and autism-related genes. *Translational Psychiatry*, *5*(5), e568–e568. https://doi.org/10.1038/tp.2015.62

Wolff, M., Johannesen, K. M., Hedrich, U. B. S., Masnada, S., Rubboli, G., Gardella, E., Lesca, G., Ville, D., Milh, M., Villard, L., Afenjar, A., Chantot-Bastaraud, S., Mignot, C., Lardennois, C., Nava, C., Schwarz, N., Gérard, M., Perrin, L., Doummar, D., … Møller, R. S. (2017). Genetic and phenotypic heterogeneity suggest therapeutic implications in SCN2A-related disorders. *Brain: A Journal of Neurology*, *140*(5), 1316–1336. https://doi.org/10.1093/brain/awx054

Zhou, J., Blundell, J., Ogawa, S., Kwon, C.-H., Zhang, W., Sinton, C., Powell, C. M., & Parada, L. F. (2009). Pharmacological Inhibition of mTORC1 Suppresses Anatomical, Cellular, and Behavioral Abnormalities in Neural-Specific Pten Knock-Out Mice. *Journal of Neuroscience*, *29*(6), 1773–1783. https://doi.org/10.1523/JNEUROSCI.5685-08.2009